Volume 8, No. 2

May, 1961

THE SOVIET JOURNAL OF

ATOMIC ENERGY

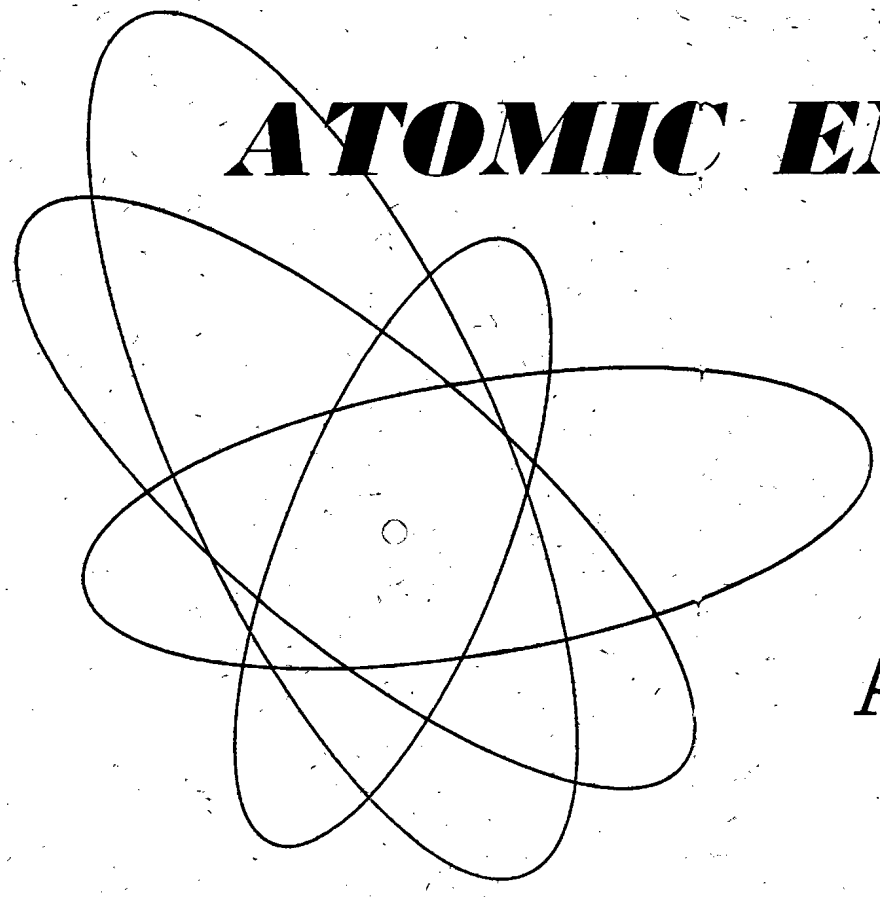

Атомная энергия

TRANSLATED FROM RUSSIAN

CONSULTANTS BUREAU

the latest Soviet techniques!

CONTEMPORARY EQUIPMENT for WORK with RADIOACTIVE ISOTOPES

A comprehensive review of the Soviet methods and technological procedures used in the production of isotopes and the preparation of labelled compounds from them. The shielding and manipulative devices are described as well as illustrated in detail. It is an excellent guide for all scientists and technologists concerned with radioactive isotopes.

CONTENTS

durable paper covers - 67 pages - illus. *$15.00*

c/b
CONSULTANTS BUREAU
227 W. 17th ST., NEW YORK 11, N. Y.

THE SOVIET JOURNAL OF

ATOMIC ENERGY

A translation of ATOMNAYA ÉNERGIYA, a publication of the Academy of Sciences of the USSR

(Russian original dated February, 1960)

Vol. 8, No. 2 May, 1961

CONTENTS

Annual subscription $ 75.00
Single issue 20.00
Single article 12.50

CONTENTS (continued)

NOTE

The Table of Contents lists all material that appears in Atomnaya Énergiya. Those items that originated in the English language are not included in the translation and are shown enclosed in brackets. Whenever possible, the English-language source containing the omitted reports will be given.

THERMAL STRESSES IN REACTOR CONSTRUCTIONS

A. Ya. Kramerov, Ya. B. Fridman, and S. A. Ivanov

Translated from Atomnaya Énergiya, Vol. 8, No. 2, pp. 101-111,
February, 1960
Original article submitted May 9, 1960

Conditions for the appearance of thermal stresses in reactors are investigated; also their magnitude and the danger they create are estimated. The influence of the form of the heat-generating elements (HGE) on the temperature drop and magnitudes of thermal stresses is analyzed; recommendations are given with the aim of decreasing the harmful effect of thermal stresses.

The methods from the theory of elasticity employed in the calculation of thermal stresses have significant limitations. In many cases when estimating the magnitude and degree of danger created by the thermal stresses, when combining such stresses with mechanical stresses, and also when seeking a way to decrease them, other effects such as fluidity, creep, initial breakdown, and microscopic processes must be taken into consideration.

INTRODUCTION

In recent years the study of thermal stress has enjoyed great attention, particularly in connection with the known framework of atomic reactors. Among the characteristics of reactors we make particular note of the following:

a) the intensive neutron and γ radiation at moderate temperatures which leads to a decrease in plasticity;

b) internal radiational heat sources;

c) high thermal current (10^6 kcal/m^2-hour) and heat production density (10^9 kcal/m^3-hour), resulting in a large temperature gradient (~100° C/mm);

d) the use of new little-studied materials (sometimes undergoing undesirable structural transformations upon heating) and combinations of materials with different coefficients of thermal expansion;

e) sharply repeated changes in the temperature resulting in a thermal shock in the structure (for example, in the case of an emergency stoppage of the reactor);

f) the use of new complex structures, for which there have been neither analogies in the usual engineering techniques, nor long-run operational tests. Significant thermal stresses also may arise in structures associated with long established areas of engineering (for example, in reactor turbine construction). However, the many variants and long operational tests which have accumulated in these areas in many cases permit by extrapolation the use of structures near to those tested in practice, and thereby some of the dangers from thermal stresses may be avoided.

The literature on theoretical questions having to do with thermal stresses is fairly large, but it consists primarily of papers treating the analytical solution of different problems in the field of eleasticity [1], and, far more rarely, in elastoplasticity [2-5]. In this literature only macroscopic stresses (of the first kind) are considered. We mention also papers [6-13].

Estimate of the magnitude of temperature stresses

Basic notation: $\sigma_\theta, \sigma_r, \sigma_z$ are the normal stresses acting in the angular, radial and axial directions respectively; α is the thermal coefficient of linear expansion; E, the modulus of elasticity (kg/cm^2); ν, Poisson's coefficient; $\Delta T = T_r - T_{init}$ the deviation of the temperature from that of the initial (T_{init}) unstressed state; $\overline{\Delta T}$, the average value of ΔT with respect to cross section; Q, the total rate of heat generation (kcal/hour); q_F the thermal flux (kcal/m^2-hr); q the density of heat generation (kcal/m^3-hr); a, b the internal and external radii of a tube; r_0 the radius of a cylindrical rod; $\rho = a/b$ the dimensionless radius of the hole in a tube; and Ψ is a form factor, equal to the ratio of stress (or temperature drop) in a body of the shape considered, to that in a circular cylinder (other conditions being equal).

The magnitude of the thermoelastic stresses of the first kind is estimated by the formula

$$\sigma = E\Delta(\alpha T) \text{ and } \sigma = E\alpha\Delta T \text{ (for } \alpha = \text{const}). \quad (1)$$

In the presence of internal heat sources in bodies with more or less smooth shapes the temperature change in a cross section is equal to

$$\Delta T = \frac{q_F \frac{1}{2} r_0}{\lambda} = \frac{1}{\lambda} \frac{Q}{F_q} \frac{V}{F_q} = \frac{q}{4\lambda} r_0^2, \quad (2)$$

where $\frac{1}{2} r_0 = \frac{1}{2} \cdot 2V/F_q$ is a quantity proportional to the mean path taken by the flow of heat in the body; V is the volume of the body (m^3); $q_F = Q/F_q$, the thermal flux; and F, the heat transfer at the surface.

If the thermal stresses reach the yield point for the material, then the body or its individual parts enter the plastic state and thermoplastic stresses arise. In the elastic region the stresses at each moment are determined by the existing temperature field, whereas in the plastic region the stresses depend also on the past history of the body.

The exact temperature field, and also the thermal stress and displacements of the first kind in the elastic region are found from a known system of equations from the theory of heat conduction and the theory of elasticity. These equations differ from the usual by the additional terms $\alpha\Delta T$ in the expression for the generalized Hooke's law. In this case only mathematical difficulties are encountered, which however limit the possibility of obtaining exact solutions in practice.

There exist approximate methods of calculating the thermoelastic stress [2, 3, 5, 14]. Methods for calculating thermal stresses of the second kind have also been little studied.

In reactor construction one often has to deal with problems relating to cylindrical bodies of revolution: housings, heat generating elements, and their casings.

In these cases in the absence of external forces the thermoelastic stresses of the first kind are determined, as is known, by the relations

$$\sigma_\theta = \frac{E}{1-\nu}\left(\frac{1}{r^2}\frac{r^2+a^2}{b^2-a^2}\int_a^b \alpha\Delta T(r)\,r\,dr + \right.$$

$$\left. + \frac{1}{r^2}\int_a^r \alpha\Delta T(r)\,dr - \alpha\Delta T(r)\right); \qquad (3)$$

$$\sigma_r = \frac{E}{1-\nu}\left(\frac{1}{r^2}\frac{r^2-a^2}{b^2-a^2}\int_a^b \alpha\Delta T(r)\,dr - \right.$$

$$\left. - \frac{1}{r^2}\int_a^r \alpha\Delta T(r)\,r dr\right) \qquad (4)$$

and

$$\sigma_z = \sigma_\theta + \sigma_r. \qquad (5)$$

Ordinarily the largest stresses occur at the inner (r=a) or outer (r=b) bounding surface [depending on the form of the function $\Delta T(r)$] and equal

$$\left.\begin{aligned}(\sigma_\theta)_{r=a} &= \frac{E}{1-\nu}\times \\ \times\left(\frac{2}{b^2-a^2}\int_a^b \alpha\Delta T(r)\,r\,dr - \alpha\Delta T(a)\right);& \\ (\sigma_\theta)_{r=b} &= \frac{E}{1-\nu}\times \\ \times\left(\frac{2}{b^2-a^2}\int_a^b \alpha\Delta T(r)\,r dr - \alpha\Delta T(b)\right).&\end{aligned}\right\} \qquad (6)$$

Thermoelastic stresses of the first kind in a thin plate with built-in edges or temperature field symmetric with respect to the mean surface may be found from the formula

$$\sigma = \frac{E}{1-\nu}\left(\frac{1}{2\delta}\int_{-\delta}^{+\delta}\alpha\Delta T(x)\,dx - \alpha\Delta T(x)\right). \qquad (7)$$

The first terms included in the parentheses in formulas (6) and (7) represent the mean (with respect to cross section) temperature difference or, more accurately, the mean value of the free thermal expansion $\overline{\alpha\Delta T}$.

Formulas (6) and (7) may be combined in the relation

$$\sigma = \frac{E}{1-\nu}(\overline{\alpha\Delta T} - \alpha\Delta T), \qquad (8)$$

which permits one to find the greatest stresses in a circular rod, thin-walled tube, in a plate with built-in edges with symmetric temperature distribution, and in certain other cases, when the principal deformations at each point are equal among themselves, or some of them are equal to zero (linear and plane stressed states) and moreover, are constant in some principal plane.* Actually under these conditions the relative stretching in the plane indicated may be determined by the formula

$$\varepsilon = \frac{\sigma(1-c\nu)}{E} + \alpha\Delta T,$$

where c is equal to 0, 1, or 2 for the one-dimensional, two-dimensional, or volume stress states respectively. Integrating over the entire cross section of the body in this plane

$$\left(\varepsilon F = \frac{1-c\nu}{E}\int_F \sigma dF + \int_F \alpha\Delta T\,dF\right)$$

and using the equilibrium condition

$$\int_F \sigma\,dF = 0,$$

we find that $\varepsilon = \frac{1}{F}\int_F \alpha\Delta T\,dF = \overline{\alpha\Delta T}$, and, finally,

we obtain the relation [8]:

$$\sigma = \frac{E}{1-c\nu}(\overline{\alpha\Delta T} - \alpha\Delta T).$$

In the cases examined, by virtue of the linearity of the heat conduction equations, the temperature distribution, and consequently the thermoelastic stresses of the first kind, may be represented in the form of a sum of a solution to the homogeneous equation (without internal heat sources) with the actual boundary conditions (index "ΔT") and the solution to the heat conduction equation

*These results for thermoelastic stresses of the first kind may be generalized to the case of variable $\alpha(r)$ by replacing the quantity $\alpha\Delta T$ by the quantity $\Delta(\alpha T)$.

with internal heat sources but zero boundary conditions (index "q"). Each of these solutions in turn may be written in the form of the product of three factors, expressing respectively the influence of the physical properties, the density of heat generation, and the dimensions (or ΔT_{bdy}) and shape of the body. Hence we have

$$\sigma = \sigma_q + \sigma_{\Delta T} = \left[\frac{\alpha E}{1-\nu}\frac{1}{\lambda}\right]\left[\frac{qr_0^2}{4}\right]\Psi_{\sigma_q} + \left[\frac{\alpha E}{1-\nu}\right]\left[\frac{\Delta T_{bdy}}{2}\right]\Psi_{\sigma_{\Delta T}}.$$

The factor $[\alpha E/(1-\nu)](1/\lambda)$ conditionally expresses the influence of the physical properties. Introducing the ratio σ/σ_T, we obtain the factor $[\alpha E/(1-\nu)](1/\lambda\sigma_T)$, conditionally characterizing the influence of the physical properties of the body, taking into consideration also the margin in attaining the yield stress.

For structural elements in the active zone, where the heat is generated by the absorption of energy from γ rays and neutrons, the complex of physical properties (first factor) will depend as well on the corresponding cross sections or coefficients of absorption. Neglecting the self-screening and the heat generation from the absorption of neutron energy, we find that the first factor is proportional to the mean coefficient of γ-ray absorption or (for elements with moderate atomic weight) the specific weight; i. e.,the expression $[\alpha E/(1-\nu)](1/\lambda)$ may depend on the expression $[\alpha E/(1-\nu)](\gamma/\lambda)$.

When using materials with high α and low λ and σ_T it is especially difficult to avoid going beyond the yield point and the resulting residual deformations. In this connection uranium and stainless steel possess undesirable properties. Thorium, black lead, and to a lesser degree zirconium and aluminum are better behaved as regards the appearance of permanent deformation, notwithstanding their comparatively low σ_B and σ_T. Even if economical considerations and estimates as to the resistance of the material to radiation, corrosion, etc., are not entered into, still the estimates and comparisons of different materials as to their resistance to thermal stress are very complex and conditional; in the corresponding complex coefficients there should enter characteristics of durability, which for many plastic materials,worked under conditions of thermal fatigue, are still unclear. The influence of the quantity σ_T,introduced into the set of coefficients, is not unique, since an increase in σ_T may cause harmful (later release of thermal stresses of plastic deformation), as well as useful effects (decrease in the accumulated plastic deformations)[12].

The comparison of materials is still further complicated in that many properties (especially σ_T, δ, σ_B, and others) strongly depend on the working and structure of the material.

Comparison of HGE of different forms

In order to have a dimensional relationship to characterize the HGE, it is useful to require for all forms considered that they have equal volumes per unit heat-transfer surface. This guarantees their approximate equivalence as regards neutron physical calculations with identical thermal conditions at the surface (for equal volume densities of heat generation q inside the HGE), i.e., among comparable forms, $r_0 = 2V_{HGE}/F_q$=idem.

Formulas are given below for the greatest temperature drop and for the high-temperature elastic stresses of the first kind for four basic shapes for the cross sections of the heat generating elements (no account taken of the casing, and for uniform heat generation). For conciseness, the temperature drop $qr_0^2/4\lambda$ at the cylinder radius r_0 is denoted by ΔT_0, and the maximal thermoelastic stress $[\alpha E/(1-\nu)](\Delta T_0/2)$in the solid cylinder is denoted by σ_0.

The expressions introduced below are obtained by substituting into relation (8) the solution of the equation of steady heat flow ($-\lambda\Delta T=q$) for suitable boundary conditions—zero or prescribed values ΔT_{bdy} (for a derivation of the most complicated case, the third, see the Appendix).

Case 1. For a tube or cylinder cooled from the outside,

$$\Delta T_{max} = \Delta T_0 \Psi^{(1)\dagger}_{\Delta T_q};\ (\sigma_\theta)_{r=b} = \sigma_0 \Psi^{(1)}_{\sigma_q}.$$

Case 2. For a tube cooled from the inside,

$$\Delta T_{max} = \Delta T_0 \Psi^{(2)}_{\Delta T_q};\ (\sigma_\theta)_{r=a} = \sigma_0 \Psi^{(2)}_{\sigma_q}.$$

Case 3. For a tube cooled from the inside and the outside (in this case the maximum temperature difference is nonlinear relative to ΔT_{bdy}),

$$\Delta T_{max} = \Delta T_0 \frac{1-\tilde{\varrho}^2(1-\ln\tilde{\varrho}^2)}{(1-\varrho)^2},$$

where

$$\tilde{\varrho}^2 = \frac{R^2}{b^2} = \frac{1}{\ln\varrho^2}\left[\frac{\Delta T_{bdy}}{\Delta T_0}(1-\varrho^2) + \varrho^2 - 1\right]$$

and R is the radius of the circle (within the limits of the tube's wall thickness $a < R < b$), on which the temperature attains its maximal value ($T=T_{max}$) in particular, for ΔT_{bdy}=T (a)—T (b)=0 we obtain

$$\Delta T_{max} = \Delta T_0 \Psi^{(3)}_{\Delta T_q};$$

$$\sigma_{max} = \sigma_0 \Psi^{(3)}_{\sigma_q} + \frac{\alpha E}{1-\nu}\frac{\Delta T_{bdy}}{2}\Psi^{(3)}_{\sigma_{\Delta T}},$$

where σ_{max} denotes the maximum stress attained on one of the bounding surfaces (r=a or r=b).

† The upper indices on Ψ indicate which case is under consideration.

TABLE 1. Influence of the Shape of the Body on the Temperatures Drop and on the Thermal Stresses (basic formulas).

Parameter	Tube or cylinder cooled from the outside (case 1)	Tube cooled from the inside (case 2)	Tube cooled from the inside and from the outside (case 3)	Plate cooled on both sides (case 4)
Exterior radius (or half-thickness) b (or δ)	$\frac{r_0}{1-\varrho^2}$	$\frac{r_0\varrho}{1-\varrho^2}$	$\frac{r_0}{1-\varrho}$	$\frac{r_0}{2}$
Inside radius a	$\frac{r_0\varrho}{1-\varrho^2}$	$\frac{r_0\varrho^2}{1-\varrho^2}$	$\frac{r_0\varrho}{1-\varrho}$	—
Dimensionless temperature drop (form factor) from internal heat sources, $\Psi_{\Delta T_q}$	$-\left(\frac{1}{1-\varrho^2}+\frac{\varrho^2\ln\varrho^2}{(1-\varrho^2)^2}\right)$	$\frac{\varrho^2}{1-\varrho^2}+\frac{\varrho^2\ln\varrho^2}{(1-\varrho^2)^2}$	$\frac{1}{(1-\varrho)^2}+\frac{1+\varrho}{(1-\varrho)\ln\varrho^2}\left[1-\ln\frac{\varrho^2-1}{\ln\varrho^2}\right]$	$\frac{1}{2}$
Dimensionless thermal stresses (form factor): from internal heat sources, Ψ_{σ_q}	$\frac{2\varrho^2}{(1-\varrho^2)^2}\left(\frac{1-\varrho^2}{2\varrho^2}-\frac{\varrho^2\ln\varrho^2}{1-\varrho^2}-1\right)$	$-\frac{2\varrho^2}{(1-\varrho^2)^2}\left(\frac{1-\varrho^2}{2}+\frac{\ln\varrho^2}{1-\varrho^2}+1\right)$	$\frac{1+\varrho^2}{(1-\varrho)^2}+\frac{1+\varrho}{(1-\varrho)\ln\varrho}$	$\frac{2}{3}$
from the temperature difference on the cooling surfaces, $\Psi_{\sigma_{\Delta T}}$	—	—	$-\left(\frac{1}{\ln\varrho}+\frac{2}{1-\varrho^2}\right)_{r=a}$ $-\left(\frac{1}{\ln\varrho}+\frac{2\varrho^2}{1-\varrho^2}\right)_{r=b}$	1

Declassified and Approved For Release 2013/02/19 : CIA-RDP10-02196R000100050002-7

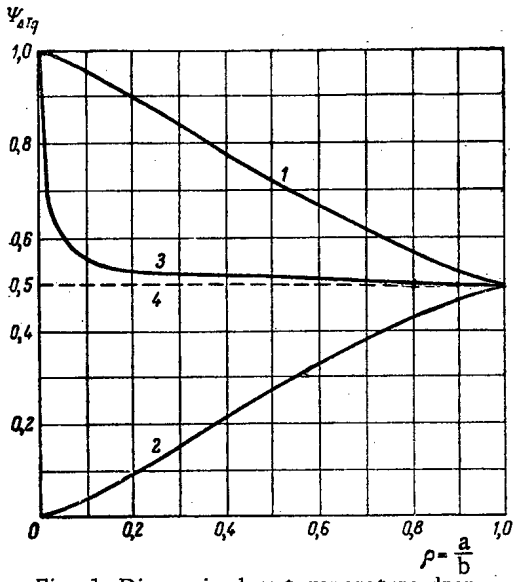

Fig. 1. Dimensionless temperature drop $\Psi_{\Delta T_q} = \Delta T_{max} / \Delta T_0$ resulting from internal heat sources, in its dependence on the dimensionless inner radius of the tube $\rho = a/b$ (for cases 1–4).

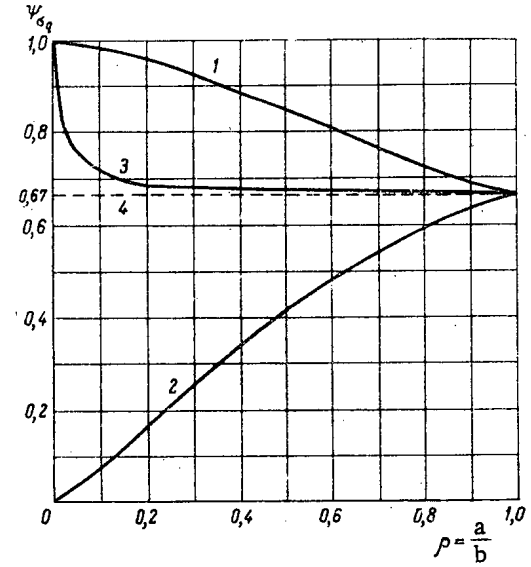

Fig. 2. Dependence of the dimensionless thermal stress $\Psi_{\sigma_q} = \frac{\sigma_q}{\sigma_0}$ (in the presence of internal heat sources) on the dimensionless inner tube radius $\varrho = \frac{a}{b}$ (for cases 1-4).

Case 4. For a plate cooled from both sides,

$$\Delta T_{max} = \Delta T_0 \frac{1}{2}\left(1 + \frac{\tilde{x}}{\delta}\right)^2,$$

where $\frac{\tilde{x}}{\delta} = \frac{1}{2}\frac{\Delta T_{bdy}}{\Delta T_0}$ and $\tilde{x}$ is the distance from the center of the plate (of thickness 2δ); to the point with maximum temperature $[T(\tilde{x}) = T_{max}]$: in particular, for $\Delta T_{bdy} = T_1 - T_2 = 0$ we have

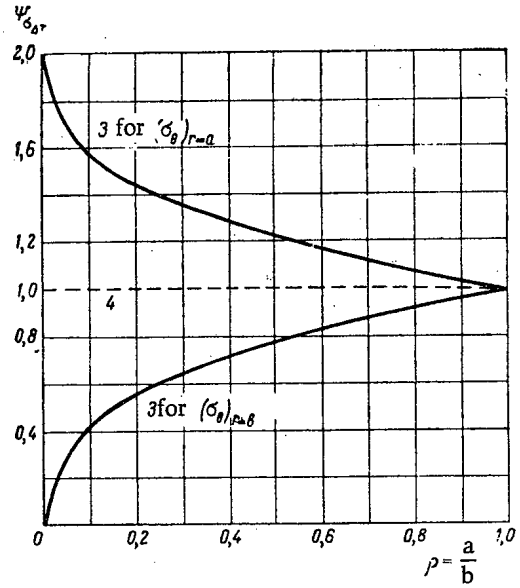

Fig. 3. The dimensionless thermal stress $\Psi_{\sigma_{\Delta T}} = \frac{\sigma_{\Delta T}}{\frac{\alpha E}{r\nu}\frac{\Delta T_{bdy}}{2}}$, arising from the temperature difference on the cooling surfaces, in dependence on the dimensionless inner tube radius $\varrho = \frac{a}{b}$ (for cases 3-4).

$$\Delta T_{max} = \Delta T_0 \Psi^{(4)}_{\Delta T_q};$$

$$\sigma_{max} = \sigma_0 \Psi^{(4)}_{\sigma_q} + \frac{\alpha E}{1-\nu}\frac{\Delta T_{bdy}}{2}\Psi^{(4)}_{\sigma_{\Delta T}}.$$

The values of b, $\Psi_{\Delta T_q}$, Ψ_{σ_q}, $\Psi_{\sigma_{\Delta T}}$ are given in Table 1 and in Figs. 1, 2, and 3 as functions of the dimensionless hole radius $\rho = a/b$.

From the figures it is evident that, other conditions being equal, (for the same densities of heat generation, material, and ratio of the volume to the heat transfer surface), the temperature drop and thermal stresses in all forms considered for the HGE is less than that in the case of the solid rod. For a plate the temperature drop is just half that for a circular rod, and the stress is one third less. In the case of a hollow cylinder cooled from the outside or from both sides, when the ratio $\rho = a/b$ increases the temperature drop and stress change from the value corresponding to a circular rod (for $\rho = 0$), to the value corresponding to a plate (at $\rho = 1$). In the case of cylinders cooled from the inside (or of massive heaters with holes for the cooling medium), the temperature drop and the stress are significantly less than in elements of other forms (for which $r_0 = 2V/F_q$).

The data from Figs. 1-3 agree with data from [4], obtained by an incomparably more complicated means for one particular case (if the comparison of the thermal stresses in the HGE of differing forms is carried out under comparable conditions; i.e., for equal specific heat generation and specific volumes), and do not confirm the deductions of [15], in which the above indicated comparison

conditions for HGE of differing forms are not fulfilled. As a consequence of the latter, the author of [15] is led to the invalid conclusion that the best shape for the HGE from a heat engineering point of view is that of a circular rod.

It should also be noted that in comparing HGE's of different shapes it is of course necessary to bear in mind technological questions concerned with obtaining qualitative HGE's with shapes which will aid the maintenance of stable cooling conditions.

Estimate of the danger in thermal stresses‡

In the case of repeated microthermal stresses (for example, with cyclic loading of a thin sample in a heated fluid), cumulative micro-and macro-residual deformations and small cracks may occur [7, 17].

For plastic materials with a small number of heat changes a stationary temperature field ordinarily does not lead to fracture (with the exception of the cases involving very high deformation concentrations), since the thermal stresses are removed or decreased. Therefore in such cases danger is ordinarily seen only with exceedingly great deformation or with damage to the metals from possible overheating. Moreover, a nonstationary character (dependence of σ on time) is less significant than a cyclically repeated loading with accumulation of residual deformations and structural changes.

The order of magnitude of the deformation ϵ which is necessary for complete removal of the thermal stresses may be estimated by the formula

$$\varepsilon = \frac{\sigma}{E} = \alpha \Delta T.$$

For example, for steel with $\alpha = 10^{-5}$ 1/°C and $\Delta T = 100$°C, $\epsilon = 10^{-3}$, or 0.1%. From this it follows that the thermal stresses (probably microscopic as well as macroscopic) are rapidly relaxed in the presence of creep or crack formation, which also results in nonelastic deformation. This explains the small influence exerted by single thermal loads (with the exclusion of very brittle materials) and in many cases the small danger of thermal (in comparison to mechanical) stresses, if the latter are weakly relaxed in the process of nonelastic deformation (the so-called "liberal loading methods" [8], for example, in the case of steam or gas pressure on a reactor housing).

The smaller number of heat changes up to breakdown for more coarsely grained materials [11] in comparison with fine-grained structures is probably connected with the large displacements at the boundaries of the grains.

Therefore the residual deformation which is a result of fluidity or creep is to a certain extent even useful in that it permits stress relaxation.**

In the case of thermal stresses, the relaxation will proceed all the faster (other conditions being equal), the less the thermal expansion; in the case of mechanical stresses, the less the elastic energy of the system, the faster relaxation proceeds [8].

Taking into consideration the existence of seams and welding stresses which are only with difficulty taken into account and controlled, and which may harmfully interact with the stresses caused by thermal and mechanical loads, the importance of plasticity is again seen to be important. With sufficient heating the residual stresses are practically eliminated (Table 2).

TABLE 2. Temperature at Which Residual Stresses are Removed for Various Materials [6].

Material	Temperature at which removal of residual stresses takes place, for example, after 1 hour, in °C
Magnesium alloy	150–170
Aluminum alloy	220–250
Iron	500–550
Carbonic small-and moderately-alloyed steel	600–650
Stainless steel	800–820

Approaches to lessening the danger of thermal stresses

The magnitude of thermal stresses of the first kind depends on the properties of the body ($\alpha E/\lambda$), it is proportional to the heat output and dimensions, and depends on the shape of the body, as well as on the other characteristics (on the yield point, for example).

There are two basic methods of decreasing the danger of thermal fracture; by decreasing the magnitude of thermal stresses arising, and by increasing the permissible thermal stresses.

A decrease in the magnitude of the thermal stresses may be attained by:

a) using materials with low value of $\alpha E/\lambda$ and joining materials with values of the thermal expansion ($\alpha \Delta T$) which are near each other;

b) choosing shapes admitting free expansion to the largest extent (compound elements, thermal expansion joints, etc.)

c) creation of sufficiently smooth shapes and uniform cooling conditions, in order to exclude the appearance of large temperature differences between connected parts of the body in the stationary and also the transitional operating stages;

‡ Phase stresses and microthermal stresses may weaken as well as strengthen each other [7, 16].

** This was noted in [18]; however in the case considered in this paper involving mechanical loading of the housing by internal fluid pressure, the stress relaxation is less significant than in the case of loading by gas or steam pressure.

d) guaranteeing operating conditions which will exclude appreciable and frequent temperature fluctuations, etc.

The stability of the materials with respect to thermal stresses may be increased by satisfying the two following conditions, which are to a known extent contradictory;

a) increasing the yield point to such a degree that dangerous residual deformations will not accumulate, resulting in fatigue damage;

b) increasing the plastic properties of the material, and the isotropicity and homogeneity of the structure, in particular by refining the grains, in order to decrease the microthermal stresses and increase the number of heat changes necessary for fracture.

It is desirable to avoid cold hardening and other processes which decrease the plasticity, in order that the structure will be able to resist temperature shifts accompanying sizeable plastic deformations [17]. Other important factors include the quality of the welding (it should be without microbrittleness, cracks, imperfections, etc.), the absence of stress concentrators, deformation concentrators, and others.

The purity of the worked surfaces is of great importance, since the largest thermal and mechanical stresses occur usually on the surface, and small defects on the surface will lead to their further growth by virtue of the concentrations. A pure surface has fewer initial defects which may serve as sources for the beginning of fracture.††

Conclusions

The methods of the theory of elasticity applied in the calculation of thermal stresses, have two significant limitations:

a) they may be used to estimate stresses of the first kind only in regions with dimensions of the order of those of the body, and they do not consider microstresses arising as a consequence of anisotropy and inhomogeneity of the individual grains. Microstresses in combination with macrostresses are especially important in the beginning stages of fracture;

b) they do not take into account the change (usually decrease) in the stresses in the elastoplastic regions [12].

The application of different approximate estimates, in particular the use of expressions of the type (8), show that the elastic thermal stresses of the first kind are proportional to the difference between the free thermal expansion (αT) and the actual expansion, near to the mean value ($\overline{\alpha T}$). Since in the majority of materials plastic deformation and fracture do not proceed immediately, but rather accumulate in time during heat changes and in the intervals between them, the danger is determined not only by the magnitude, but also by the duration of the action and the number of repetitions of the stress. Single thermal loading is ordinarily not dangerous, if the shape of the body is sufficiently smooth and does not include excessive concentrations of plastic deformations.

Therefore in estimating the magnitude and degree of danger from thermal stresses when these are taken together with mechanical stresses, and also when methods of decreasing them are sought, it is not possible to limit oneself to determining the elastic macrostresses alone, but it is necessary to estimate also the degree to which they are decreased due to fluidity, creep, and the beginning of fracture.

The choice of optimal shape plays an important role. For equal volumes of the heater per unit area of heat transfer surface, inner cooling of a tubular HGE yields the least temperature drop and magnitude of stress in comparison with external or two-sided cooling of a rod, tube, or plate.

In order to increase the resistance to thermal stresses it is necessary to tend toward fine grains, high homogeneity of the structure, to high local plasticity, increases in the resistance to fracture in the intergrain regions, and to decreases in the cold hardening and surface defects.

To establish a basis for durability calculations it is necessary to engage in systematic experiments to study the influence of the number, amplitude and sharpness of the heat changes on plastic deformations [17] and the fracture of samples of different shapes and dimensions and different surface states, and under different actions from external media, and also for changing relationships between the mechanical and thermal loads.

It is desirable to introduce characteristics for the material in order to obtain a qualitative estimate of its resistance to thermal stresses; for example, a curve of residual deformation as a function of the number of heat transfer cycles in a thin sample, up to the appearance of small cracks of certain size.

APPENDIX

Temperature drop and thermoelastic stresses of the first kind in a cylindrical body with two-sided cooling

Here a derivation of the relations determining the temperature drops and thermoelastic stresses of the first kind in the most complicated case—two-sided cooling of a cylindrical tube—is given.

From the conditions of volume equality we find the radius of the equivalent cylinder of solid cylinder:

$$r_0=\frac{2V}{F_q}=\frac{2\pi(b^2-a^2)}{2\pi(b+a)}=b(1-\varrho), \qquad (1)$$

from which

$$b=\frac{r_0}{1-\varrho} \quad \text{and} \quad a=b\varrho=\frac{\varrho}{1-\varrho}r_0. \qquad (2)$$

If we denote by r_* (or $R_*=r_*/b$) the radius of the neighborhood where a maximum in temperature $T_q(r)$ is attained under zero boundary conditions

$$T_q(a)=T_q(b)=0, \qquad (3)$$

†† We note also the possibility of significantly accelerating the fracture by the joint action of corrosive substances and stresses on the surface of the body.

then the heat conduction equation (balance of heat) under the condition of uniformity of density of internal heat sources q takes the form

$$q\pi(r^2-r_*^2)=-\lambda 2\pi r\frac{dT_q}{dr}, \qquad (4)$$

from which

$$\text{(for } \lambda=\text{const)}\ T_q=-\frac{q}{2\lambda}\int\frac{r^2-r_*^2}{r}dr=$$

$$=\frac{q}{2\lambda}\left(\frac{r^2}{2}-r_*^2\ln r\right)+C,$$

or

$$T_q=-\frac{\Delta T_0}{(1-\varrho)^2}(R^2-R_*^2\ln R^2b^2)+C, \qquad (5)$$

where

$$\Delta T_0=\frac{qr_0^2}{4\lambda}\ \text{and}\ R=\frac{r}{b}. \qquad (6)$$

If we define R=r/b, then conditions (3) may be written in the form

$$T_q(a)=T_q(R=\varrho)=0;\ T_q(b)=T_q(R=1)=0. \qquad (7)$$

Applying condition (7) to formula (5), we find

$$R_*^2=\frac{\varrho^2-1}{\ln\varrho^2}; \qquad (8)$$

$$C=\frac{\Delta T_0}{(1-\varrho)^2}(1-R_*^2\ln b^2)=$$

$$=\frac{\Delta T_0}{(1-\varrho)^2}\left(1-\frac{\varrho^2-1}{\ln\varrho^2}\ln b^2\right). \qquad (9)$$

Substituting expressions (8) and (9) into formula (5), we obtain

$$T_q(R)=\frac{\Delta T_0}{(1-\varrho)^2}\left(1-R^2+\frac{\varrho^2-1}{\ln\varrho^2}\ln R^2\right). \qquad (10)$$

The maximum of T_q is attained at $R=R_*$:

$$\max T_q=\Delta T_0\Psi_{\Delta T_q}, \qquad (11)$$

where

$$\Psi_{\Delta T_q}=\frac{1}{(1-\varrho)^2}+\frac{1+\varrho}{2(1-\varrho)\ln\varrho}\left(1-\ln\frac{\varrho^2-1}{\ln\varrho^2}\right). \qquad (12)$$

If we denote

$$T_{\Delta T}(a)=T_a,\ T_{\Delta T}(b)=T_b$$

and consider

$$T_a-T_b\neq 0,\text{but}\ q=0, \qquad (13)$$

then the heat balance equation will be

$$\frac{d}{dr}\left(-\lambda 2\pi r\frac{dT_{\Delta T}}{dr}\right)=0, \qquad (14)$$

from which

$$-\lambda 2\pi r\frac{dT_{\Delta T}}{dr}=C_1\ \text{and}\ T_{\Delta T}=\frac{C_1}{2\pi\lambda}\ln r+C_2. \qquad (15)$$

Applying condition (13) to condition (15), we obtain

$$C_1=2\pi\lambda\frac{T_a-T_b}{\ln\varrho}=2\pi\lambda\frac{\Delta T_{bdy}}{\ln\varrho};\ C_2=T_a-\frac{T_a-T_b}{\ln\varrho}a. \qquad (16)$$

Applying the condition $T_b=0$ (initial reading), we find $C_2=-T_a(\ln b/\ln\rho)$ and, according to conditions (15),

$$T_{\Delta T}=\Delta T_{bdy}\frac{\ln R}{\ln\varrho}. \qquad (17)$$

The general solution will clearly be the sum of T_q and $T_{\Delta T}$, and therefore, summing expressions (10) and (17), we shall have

$$T=\Delta T_0\frac{1-R^2+\frac{\varrho^2-1}{\ln\varrho^2}\ln R^2}{(1-\varrho)^2}+\Delta T_{bdy}\frac{\ln R^2}{\ln\varrho^2}. \qquad (18)$$

The maximum temperature T will be found at the point $R^2=\tilde{\rho}^2$, determined from the condition

$$\left(\frac{\partial T}{\partial(R^2)}\right)_{R^2=\tilde{\varrho}^2}=0, \qquad (19)$$

from which

$$R^2=\tilde{\varrho}^2=\frac{(1-\varrho)^2}{\ln\varrho^2}\left(\frac{\Delta T_{bdy}}{\Delta T_0}\frac{1+\varrho}{1-\varrho}\right). \qquad (20)$$

Substituting expression (20) into formula (18), we obtain after transformations

$$\max T=\Delta T_0\frac{1-\tilde{\varrho}^2(1-\ln\tilde{\varrho}^2)}{(1-\varrho)^2}. \qquad (21)$$

Using the approximate formula (7) of the main text to determine the thermoelastic stresses of the first kind and considering that

$$\overline{T}=\overline{T}_q+\overline{T}_{\Delta T} \qquad (22)$$

(since $T=T_q+T_{\Delta T}$), we have, for example, on the outer bounding surface ($r=b$) or on the inner bounding surface ($r=a$)

$$\sigma=\sigma_q+\sigma_{\Delta T},$$

where

$$\sigma_q=\frac{\alpha E}{1-\nu}(\overline{T}_q-T_q)=\frac{\alpha E}{1-\nu}\frac{\Delta T_0}{2}\Psi_{\sigma_q} \qquad (23)$$

and

$$\sigma_{\Delta T}=\frac{\alpha E}{1-\nu}(\overline{T}_{\Delta T}-T_{\Delta T})=\frac{\alpha E}{1-\nu}\frac{\Delta T_{bdy}}{2}\Psi_{\sigma_{\Delta T}}, \qquad (24)$$

and we find

$$\bar{T}=\frac{1}{\pi(b^2-a^2)}\int_a^b T2\pi r\,dr=\frac{1}{1-\varrho^2}\int_{\varrho^2}^1 Td(R^2);$$

$$\bar{T}_q=\frac{1}{1-\varrho^2}\int_{\varrho^2}^1\frac{\Delta T_0}{(1-\varrho)^2}\left(1-R^2+\frac{\varrho^2-1}{\ln\varrho^2}\ln R^2\right)\times$$

$$\times dR^2=\frac{\Delta T_0}{2}\left[\frac{1+\varrho^2}{(1-\varrho)^2}+\frac{1+\varrho}{(1-\varrho)\ln\varrho}\right]. \quad (25)$$

Comparing formulas (25) and (23) with account taken of (3), we come to the conclusion that the form factor for stresses on the outer and inner surfaces from internal heat sources has the form

$$\Psi_{\sigma_q}=\frac{1+\varrho^2}{(1-\varrho)^2}+\frac{1+\varrho}{(1-\varrho)\ln\varrho}. \quad (26)$$

In an analogous manner we find

$$\bar{T}_{\Delta T}=\frac{1}{1-\varrho^2}\int_{\varrho^2}^1\Delta T_{bdy}\frac{\ln R^2}{\ln\varrho^2}dR^2=$$

$$=\frac{\Delta T_{bdy}}{2}\left(-\frac{2}{\ln\varrho^2}-\frac{2\varrho^2}{1-\varrho^2}\right)$$

and the stresses on the outer surface r =b (T_b=0) and on the inner surface r =a [T(r =a)=T_a= ΔT_{bdy}]:

$$\sigma^b_{\Delta T}=\frac{\alpha E}{1-\nu}\frac{\Delta T_{bdy}}{2}\Psi^b_{\sigma_{\Delta T}} \quad (27)$$

and

$$\sigma^a_{\Delta T}=\frac{\alpha E}{1-\nu}\frac{\Delta T_{bdy}}{2}\Psi^a_{\sigma_{\Delta T}}, \quad (28)$$

where

$$\Psi^b_{\sigma_{\Delta T}}=-\left(\frac{1}{\ln\varrho}+\frac{2\varrho^2}{1-\varrho^2}\right) \quad (29)$$

and

$$\Psi^a_{\sigma_{\Delta T}}=-\left(\frac{1}{\ln\varrho}+\frac{2}{1-\varrho^2}\right). \quad (30)$$

These determine the values of the form factors for stresses on the outer (b) and inner (a) surfaces in their dependence on the temperature drop at the boundaries.

LITERATURE CITED

1. R. Dane, Materials of the Atomic Energy Comm. of the USA Nuclear Reactors. Vol. II—Nuclear Reactor Engineering [Russian translation] (IL Moscow, 1957).
2. L. M. Kachanov, Zhur. Tekh. Fiz. 10, No. 14 (1940).
3. A. E. Danyushevskii, L. M. Kachanov, Sovetskoe Kotloturbostroenie No. 6 (1945).
4. K. Merckx, Trans. ASME 80, No. 5 (1958).
5. B. Gatewood, Thermal Stresses USA, 1957.
6. L. A. Glikman, Zhur. Tekh. Fiz. 7 3, 294 (1937).
7. A. A. Bochvar et al., Doklady Akad. Nauk SSSR 112 No. 6 (1957);‡‡ 113, No. 3 (1957); 117, No. 1 (1957);‡‡ Izv. Akad. Nauk SSSR, Otdel. Tekh. Nauk 11 (1956);‡‡ Atomnaya Énergiya 2, 6, 520 (1957).***
8. Ya. B. Fridman, Collection: Theoretical Basis for MachineConstruction [in Russian] (Mashgiz, 1957)
9. V. N. Kuznetsov, Teploénergetika, No. 12 (1957).
10. A. V. Ratner, Teploénergetika, No. 10 (1957).
11. S. V. Serensen, P. I. Kotov, Zavod. Laboratoriya No. 9 (1958);‡‡ No. 10(1959);
12. B. F. Shorr, Doklady Akad. Nauk SSSR 5, 123 (1958).‡‡
13. J. Bernard et al., Report No. 1164, presented by France at the Second International Conference on the Peaceful Uses of Atomic Energy (Geneva, 1958).
14. B. N. Finkel'shtein, Tr. Mosk. In-ta Stali. (Metallurgizdat, Moscow, 1951).
15. M. A. Zimin, Collection: Physics and Heat Engineering of Reactors [in Russian] (Atomizdat, Moscow, 1958).
16. E. Schmidt and K. Linter, Z. Metallkunde No. 4 (1956); Metall No. 9-10 (1956); Schweiss-technik (Österr.) No. 5 (1957); Berg-und Hütenmann Monatsh. No 12 (1956).
17. V. A. Likhachev et al., Scientific Bulletin of Leningrad Polytechnic Institute. Physics-Mathematics Section No. 12 (1958).
18. B. Langer, Trans. ASME 77, No. 5 (1958).

‡‡See C. B. translation.

***Original Russian pagination. See C. B. translation.

THE DEFORMATION OF URANIUM UNDER THE INFLUENCE OF THERMAL CYCLES DURING THE SIMULTANEOUS ACTION OF AN EXTERNAL TENSILE LOAD

A. A. Bochvar, G. Ya. Sergeev, and V. A. Davydov

Translated from Atomnaya Énergiya, Vol. 8, No. 2, pp. 112-116,
February, 1960
Original article submitted October 8, 1959

We established the fact that cyclical thermal working of uranium (CTW) in its α-phase, under the action of a constantly applied external tensile load, leads to a significant residual deformation which exceeds by several times the total deformation occurring during CTW without the application of constant tension or due to creepage. The change in size of the samples in all of the cases which we studied occurred in the direction of action of the external force. CTW of transverse samples of sheet uranium in the temperature region of the α-phase resulted in a shrinking of the samples when a tensile load was not applied, however the application of an external tensile load not only did not prevent the lengthening of the samples but led to the appearance of a deformation in the direction of the external force which was greater than the deformation due to creepage.

We have observed in uranium in a series of definite cases a significant increase in the speed of plastic deformation. Papers [1,2] reported an increase in the creepage speed of uranium during neutron irradiation. The strong influence of the thermal cycles upon the creepage speed of uranium was also noted [3,4].

In this paper we present data regarding the effect of cyclical thermal working (CTW) of uranium under the action of an external tensile load upon the dimensional stability of uranium.

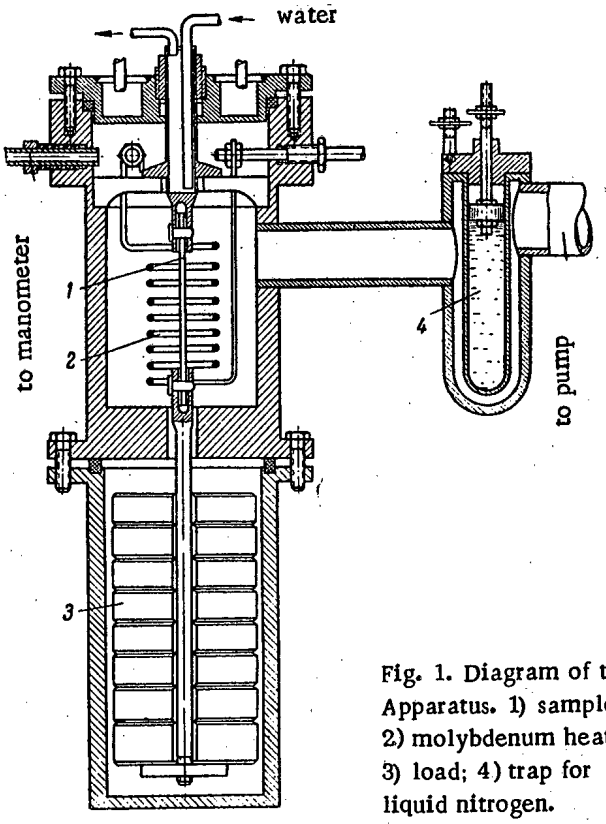

Fig. 1. Diagram of the Apparatus. 1) sample; 2) molybdenum heater; 3) load; 4) trap for liquid nitrogen.

Method of Investigation. The investigation was carried out in a vacuum of the order of 10^{-5} mm of Hg using the special experimental apparatus shown in Fig. 1. The temperature was controlled automatically. The magnitude of the residual deformation of the uranium was studied by measuring the dimensions of the samples after they had undergone three types of tests:

1) CTW without the application of an external load (lightweight samples freely suspended);

2) creepage tests at a temperature equal to the upper temperature of the cycle, this temperature being maintained for a period of time equal to the entire duration of the cycle multiplied by the number of cycles (in addition to the tests the results of which are shown in Table 1 and Fig. 2);

3) CTW under the action of a load (using the same load as for the creepage tests).

The conditions of CTW were as follows:

Thermal cycle temperatures	°C
upper	550
lower	180
1. Time, minutes:	
heating	3
cooling	4-4.5
total cycle	5.5-6
2. Time, minutes	
heating	3
cooling	4
total cycle	7

The temperature of the samples was controlled at three points of the sample by thermocouples which were welded to the samples. The drop in temperature over the

TABLE 1. Influence of a Constant Stress upon the Residual Deformation of Uranium during CTW and after Creepage Tests (Samples Cut Out in a Direction Transverse to the Direction in which the Uranium was Rolled)

Type of treatment	Constant Applied Stress σ, kg/mm²	Residual Lengthening of Samples					
		after 40 Cycles in the temperature interval 180-550°C *			after creepage tests at 550°C (without thermal cycles)**		
		sample No.	Δl, mm	δ, %	sample No.	Δl, mm	δ, %
Melt B, Rolled 60% at 300°C	0	54	−0.32	−0.8	—	—	—
	0.8	52	+0.67	+1.67	53	+0.1	+0.25
Melt A***, Rolled 70% at 300°C	0	34	−0.5	−1.25	—	—	—
	1.25	36	+1.9	+4.8	37	+0.44	+1.1
Melt A***, Rolled 70% at 300°C and Annealed at 575° for 2 hours	0	41	+2.6	−1.65	—	—	—
	1.25	40	−0.65	+6.5	39	+0.08	+0.2

*Heating time 1.5 min., cooling time 4 min
**Test continued for 3 hours; time during which the samples were kept at temperatures exceeding 350°C over the course of 200 thermal cycles
***Residual lengthening of the samples, melt A, indicated after 200 cycles

TABLE 2. Influence of a Constant Applied Stress Upon the Residual Deformation of Rolled Uranium during CTW and after Creepage Tests (Samples were Cut Out in a Direction Transverse to that in which the Uranium was Rolled)

Type of treatment	Constant applied stress σ, kg/mm²	Residual Lengthening of Samples			
		after 140 cycles*		after creepage tests at 550°C (without thermal cycles)**	
		Δl, mm	δ, %	Δl, mm	δ, %
Melt B, Rolled 85% at 500°C	0	−0.93	−2.32	—	—
	1	+0.82	+2.05	+0.5	+1.2
	2	+3.77	+9.42	+1.1	+2.7
	3	+5.32	+13.3	—	—

*Heating time 1.5 min, cooling time 4.5 min, time for a complete cycle 5.5 min
**Tests continued for 14 hours

height of the sample was 5-10 °C and was practically constant for all the samples.

We tested textured samples of sheet uranium (rolled at temperatures which were within the region of the α-phase), the samples were cut out both along and transverse to the direction in which they were rolled, and also uranium annealed at temperatures which were within the region of the α-phase (with a disordered crystal orientation).

The technological methods of preparation and the st state of the sample for the separate cases are given later.

For all of the tests listed we used flat samples of the same form having a total length of 100 mm (the length of the working portion was 40 mm, the width 8 mm) and a thickness of 2.3 mm (melt A) 2.2 mm (melt B) and 3.2 mm (melt C).

Samples Cut Out Transverse to the Direction in which the Uranium was Rolled. In Table 1 and Fig. 2 we present the results of the measurements of the dimensions of the samples after they had been subjected to the three types of tests described above.

The results of the measurement of the samples after a predetermined number of cycles shows that CTW without an applied load resulted in an insignificant change in length, CTW with a constant applied stress resulted in a significant residual deformation in the direction of application of the external load. For example, sample No. 41, melt A, shrank 1.65% after CTW over the temperature interval 180-550°C, sample No. 39 stretched 0.2% after creepage tests, while sample No. 40 not only did not shrink but stretched 6.5% after CTW under a constant stress of 1.25 kg/mm² notwithstanding the fact that the

negative effect (shrinking effect) during CTW exceeds in absolute value the positive (lengthening) creepage effect.

We made use of the transverse samples of melt B in our study of the influence of external tensile loading during CTW in the region of the α-phase upon the residual deformation of uranium. The test results are shown in Table 2. The increase in stress (tension) results in an increase in the residual deformation of the samples after CTW.

Samples Cut Out Parallel to the Direction in which the Uranium was Rolled. In Table 3 and Figs. 3 and 4 we give the results of the study of the influence of a constant applied stress upon the residual deformation of uranium during the thermal cycles and in the absence of thermal cycles.

In this case the increase due to the action of CTW and the creepage due to the influence of external tensile loading leads to a change in the dimensions of the longitudinal samples in the same direction. However, as we see from the data, CTW with a constant applied stress results in a residual deformation that exceeds by several times the total residual deformation due only to CTW (when no external tensile load is applied) or only to creepage at a temperature equal to the upper temperature of the cycle and the corresponding stress. Therefore CTW results in a 0.8% increase in creepage at 550°C and a stress of 4 kg/mm^2 for 14 hours (this corresponds to the duration time of 140 cycles) and results in a residual deformation of 8.4%, while CTW under a stress of 4 kg/mm^2 results in an increase of 63.8%. This is nearly seven times greater than the total deformation due to creepage and due to CTW without stress and almost 80 times greater than the deformation during CTW without a constant applied stress.

Samples with a Disorderly Crystal Orientation. Such samples were prepared from melt B. After being rolled 60% at 300°C the uranium was annealed at 850°C for 30 minutes. Using annealed samples we also noted that

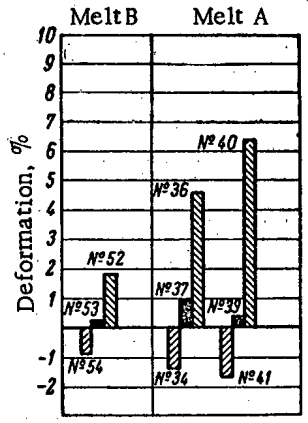

Fig. 2. Influence of a constant applied stress σ upon the residual deformation of uranium rolled in the region of the α phase during thermal cycles in the interval 180-550°C and in the absence of thermal cycles (creepage tests). Samples cut out transverse to the direction in which they were rolled. Melt A) 200 cycles, σ = 1.25 kg/mm^2; Melt B) 140 cycles, σ = 0.8 kg/mm^2.

Residual deformation of the samples after:
- Thermal cycles with a constant applied stress;
- Thermal cycles without loading;
- Creepage tests at the upper temperature of the cycle, 550°C (maintained for 3 hours).

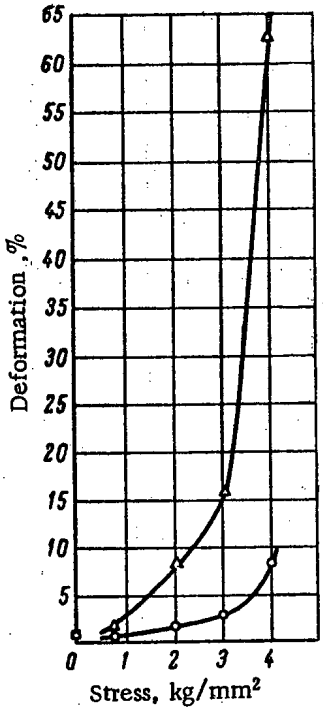

Fig. 3. Influence of a constant applied stress upon the residual deformation of uranium which was rolled in the region of the α phase during temperature cycles in the interval 180-550°C and in the absence of the temperature cycles (creepage tests). The samples were cut out parallel to the direction in which the uranium was rolled.
Residual deformation of the samples after: □-140 thermal cycles, no loading; Δ-140 thermal cycles with a constant applied load; O-creepage tests at the upper temperature of the cycle 550°C (duration 14 hours).

TABLE 3. Influen ce of a Constant Applied Stress upon the Residual Deformation of Rolled Uranium during CTW and after Creepage Tests (Samples were Cut out in a Direction Parallel to that in which the Uranium was Rolled)

Type of treatment	Constant applied stress σ, kg/mm²	Residual Lengthening of Samples			
		after 100 cycles in the temperature interval 180-550°C*		after creepage tests at 550°C (without thermal cycles)**	
		Δl, mm	δ, %	Δl, mm	δ, %
Melt B, Rolled at 300°C, with 60% Annealing	0	0.33	0.8	–	–
	0.8	0.84	2.1	0.1	0.25
	2.0	3.44	8.6	0.72	1.8
	3.0	6.31	15.8	1.2	3.0
	4.0	25.52	63.8	3.42	8.4

*Heating time 1.5 min., cooling time 4 min.
**Duration of tests: 14 hours

TABLE 4. Influence of a Constant Applied Stress Upon the Residual Deformation of Uranium Annealed in the Region of the α-Phase during CTW and after Creepage Tests

Type of treatment	Constant applied stress σ, kg/mm²	Residual Lengthening of Samples			
		after 100 cycles in the temperature interval 180-550°C*		after creepage tests at 550°C (without thermal cycles)**	
		Δl, mm	δ, %	Δl, mm	δ, %
Melt B, Rolled 60% at 300°C and Annealed at 850°C for 30 min	0	+0.17	+0.4	–	–
	1	+0.67	+1.6	+0.1	+0.25
	2	+1.22	+3.05	+0.12	+0.30
	2.7	+2.51	+6.27	+0.36	+0.9

*Heating time 3 min , cooling time 4 min , total cycle 7 min
**Duration of tests: 14 hours

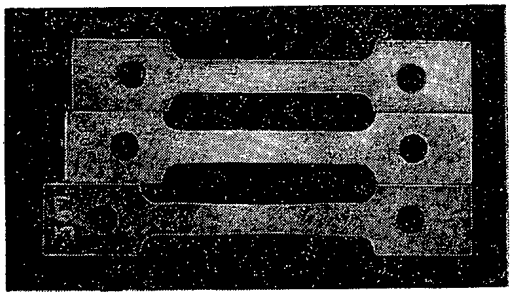

Fig. 4. Influence of a constant applied stress upon the residual deform ation of uranium rolled in the region of the α-phase in the presence of thermal cycles in the temperature interval 180-550°C and without the thermal cycles (creepage tests). Samples cut out in a direction parallel to that in which the uranium was rolled (reduced 0.77 times).
Samples: upper, before testing, middle, after creepage tests at 550°C and a stress of 3 kg/mm² (duration of tests: 14 hours); lower, after 140 cycles in the temperature interval 180-550°C with a constant applied stress of 3 kg/mm².

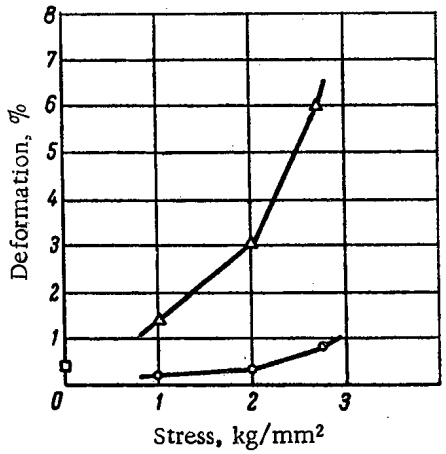

Fig. 5. The influence of a constant applied stress σ upon the residual deformation of uranium annealed in the region of the α-phase in the presence of thermal cycles in the temperature interval 180-550°C and without the thermal cycles (creepage tests): □)100 thermal cycles without loading; △) 100 thermal cycles with constant applied load; ○) creepage tests at the upper temperature of the cycle, 550°C (duration of tests: 14 hours).

the residual deformation increases several times if we apply a constant tensile stress during CTW. The results of the tests are shown in Table 4 and Fig. 5.

Thus in all cases of the simultaneous action of a tensile load and CTW, even when the effect of CTW has a different sign, there is a sharp increase in the resulting change of length of the samples as compared with the increase in length of the samples due to creepage under the action of tensile loading.

LITERATURE CITED

1. S. T. Konobeevskii, H. F. Pravdyuk, and V. I. Kutaitsev, Materials of the International Conference on the Peaceful Uses of Atomic Energy (Geneva, 1955) [in Russian] (Goskhimizdat, Moscow, 1958) Vol. 7, p. 526.
2. A. Roberts and A. Cottrell, Philosophical Magazine 1, 711 (1956).
3. R. Nichols, Nuclear Engineering 2, 18, 355 (1957).
4. A. McIntosh and T. Heal, Paper No. 49, Presented by Great Britain at the 2nd International Conference on the Peaceful Uses of Atomic Energy (Geneva, 1958).

THE SEPARATION OF Pa^{233} WITHOUT A CARRIER FROM THORIUM NITRATE PREPARATIONS IRRADIATED BY SLOW NEUTRONS

V. I. Spitsyn and M. M. Golutvina

Translated from Atomnaya Énergiya, Vol. 8, No. 2, pp. 117-120, February, 1960
Original article submitted November 13, 1959

The article gives a method for the separation of Pa^{233} without a carrier from thorium nitrate irradiated by slow neutrons. Pa^{233} was extracted from a thorium nitrate solution by absorption on a precipitate of MnO_2, amyl acetate extraction of the cupferron complex of protactinium with subsequent re-extraction by a citric acid solution and, finally, decomposition of the citric acid complex by oxidation with concentrated nitric acid. During this process satisfactory removal of α-and-β-radiation was achieved. The separated radioisotope was identified by determination of its half-life. The method developed is important for obtaining the radioactive isotope Pa^{233}, without a carrier which can be used as an indicator for studying the chemistry of protactinium and also for solving problems of the extraction of protactinium from naturally occurring raw material and the separation of Pa^{233} from thorium during the preparation of U^{233}.

Pa^{233} is obtained from thorium by the following reaction:

$$Th^{232}(n, \gamma)\, Th^{233} \xrightarrow[T_{1/2}=22{,}1\ \text{min}]{\beta^-}$$

$$\rightarrow Pa^{233} \xrightarrow[T_{1/2}=27{,}0\ \text{days}]{\beta^-} U^{233} \xrightarrow{\alpha} \ldots$$

The activation cross section of Th^{232} for neutrons is $7.33 \pm \pm 0.12$ barns [1]. Pa^{232} [2] obtained by the above-mentioned reaction is generally contaminated with thorium and various radioisotopes formed by fission of U^{233} by the action of neutrons. The literature contains a number of works on the separation of Pa^{233} from irradiated thorium [3-5].

The present work on the separation of Pa^{233} without a carrier in a radiochemically pure state from irradiated thorium nitrate was based on the method given in [6,7]. Its use was only possible after detailed investigations which made it possible to determine the conditions for carrying out the individual stages of the purification process.

To separate protactinium from thorium and zirconium its absorption on a precipitate of MnO_2—a phenomenon first described in [8]—was employed. The MnO_2 was obtained by one of the following methods:

$$2KMnO_4 + 3MnSO_4 + 2H_2O = 5MnO_2 + + K_2SO_4 + 2H_2SO_4$$

or

$$KClO_3 + 3MnSO_4 + 3H_2O = 3MnO_2 + + KCl + 3H_2SO_4.$$

Protactinium is trapped satisfactorily by MnO_2 and the conditions of the precipitation process hardly affect the sorption value of protactinium, but the fullest and most selective absorption is obtained by precipitation of MnO_2 from strongly acid solution. It should be noted that citric acid and fluorides, which form stable soluble complexes with protactinium, hinder the successful carrying out of the process.

The following experiments were carried out to investigate the absorption of Pa^{233} by a precipitate of MnO_2. Freshly irradiated thorium nitrate was dissolved in 7 N HNO_3 and the solution obtained was diluted to a specific activity of $\sim 5.10^{-4}$ counts/min · ml (the measurements were made with an end-window counter with a mica window, thickness 1.8 mg/cm^2). 0.5 ml of a 5% $MnSO_4$ solution was added to 3 ml of the solution; it was then heated on a water bath to 80°C and 0.8 ml of 0.5% $KMnO_4$ was added. The precipitated MnO_2 was coagulated by heating for 20 min and another 0.8 ml of $KMnO_4$ was then added. The precipitate was separated from the mother liquor by centrifuging and dissolved in 1 ml of 7 N HNO_3 with addition of a small amount of sodium nitrite. The experiments showed that on the average the precipitate acquires 97% of the initial activity. In these experiments 1 mg of MnO_2 was used for 1 ml of solution.

To improve the removal of impurities from Pa^{233}, the precipitate of MnO_3 was subsequently reprecipitated

TABLE 1. Extraction of Pa^{233} Cupferronate by Amyl Acetate from 6 N Solution of HCl

β-activity of the amyl acetate phase, % of the value	β-activity of the aqueous phase, % of the initial value
107	2
113	3
111	4
76	1
80	1
116	5
Mean 100	3

TABLE 2. Removal of α-Radiations from Protactinium in the Process of Separation of Pa^{233} from Irradiated Thorium Nitrate

Separated phase (MnO_2 precipitate)	α-activity of the separated phase, % of the initial value
I	43
II	14
III	8
I	42
II	10
III	5

three times. The MnO_2 content was increased to 4.4 mg per 1 ml of solution. In this case the activity acquired by the precipitate was 98% of the initial value.

To separate Pa^{233} from microimpurities retained by the MnO_2 precipitate, the cupferron complex of protactinium was extracted with amyl acetate. The experiments were carried out as follows. The MnO_2 precipitate obtained by the above-described method was dissolved in hot concentrated HCl and an equal volume of a saturated aqueous solution of cupferron containing a small amount of hydroquinone (to stabilize the solution); amyl acetate, the volume of which was equal to the sum of the volumes of the above two solutions, was also added and the mixture was shaken. The volumes of the phases were noted before and after shaking.

The results of the experiments are given in Table 1. As may be seen from the Table, protactinium cupferronate is satisfactorily extracted by amyl acetate from 6 N HCl.

To re-extract the protactinium an equal volume of a 1 M solution of citric acid was added to the amyl acetate, the mixture was shaken for 5 min and the flask with the solution was placed on a boiling water bath for 40 min. During this process the protactinium cupferronate disintegrated and the protactinium passed into the aqueous phase, in which it formed a stable complex with citric acid. After the solution had been cooled it was shaken again for 5 min, the phases were allowed to separate, their volumes were measured and the activity of each of them was determined. It was shown that 85-90% of the activity in the amyl acetate passes into the citric acid solution. Finally, the citric acid solution was repeatedly treated with concentrated HNO_3 with heating.

During the course of the work it was established that the majority of the operations of the process of separation of Pa^{233} from preparations of irradiated thorium nitrate can be successfully carried out only at a concentration of mineral acid of not less than 6-7 N. When an attempt was made to reduce the acidity to 3-3.5 N the results were markedly inferior, adsorption on the walls of the flask increased and the results could not easily be repeated.

Experiments were carried out to determine the degree of completeness of removal from protactinium of α-radiations (thorium, uranium), present in the initial solution. The activity was measured with a scintillation counter with a ZnS crystal. The data obtained are given in Table 2. From the table it is seen that the removal of α-radiations from protactinium has mainly taken place already by the third stage of reprecipitation of MnO_2 and is finally completed in the amyl acetate extraction stage. By this time the α-activity of the amyl acetate phase is zero.

As a result of the work carried out, the following method of separating Pa^{233} without a carrier from preparations of irradiated thorium nitrate was finally adopted. A 10% solution of $MnSO_4$ was added to a solution of freshly precipitated $Th(NO_3)_4$ in 7 N HNO_3, taking 0.2 ml of the former for each of the initial solution; the mixture was heated on a water bath to 80° and a 1% solution of $KMnO_4$ (0.5 ml per 1 ml of the initial solution) was then added slowly with shaking. The precipitate of MnO_2 was coagulated on the water bath for 20 min, it was separated from the mother liquor by centrifuging and then dissolved in hot concentrated HNO_3 with the addition of a small amount of sodium nitrite. An equal volume of

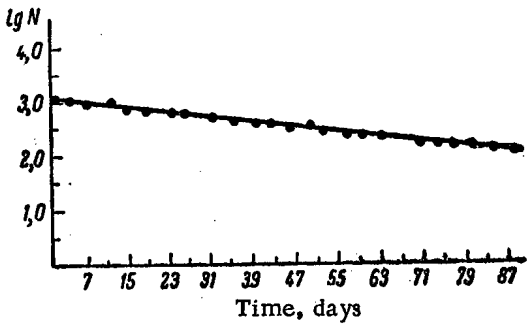

Graph of the variation with respect to time of the activity of the separated preparation of Pa^{233}

TABLE 3. Extraction of Pa^{233} from Freshly Precipitated Thorium Nitrate (Initial Solution 7 N with respect to HNO_3; 4.4 mg of MnO_2 per 1 ml of Solution)

Three-fold precipitation of MnO_2		Extraction by amyl acetate from 6 N HCl			Re-extraction by 1 M solution of citric acid		
Activity, %							
captured by the precipitate	of the mother liquid	of the amyl acetate of phase I	of the aqueous phase	left on the walls of the flask	of the citric acid phase	of the amyl acetate of phase II	left on the walls of the flask
99	1	95	2	3	112	0	0
99	1	91	3	6	81	0	19
98	2	92	2	6	83	0	17
93	—	93	—	—	89	—	—
103	—	90	—	—	86	—	—

water was added to the solution obtained and the above-described process of precipitation of MnO_2 was twice repeated. The MnO_2 obtained after the third precipitation was dissolved in hot 6 N HCl. An equal volume of a cupferron solution (7 g of cupferron and 0.2 g of hydroquinone were dissolved in 6 N HCl in such a way that the total volume of the solution was 100 ml, and the solution was filtered through a paper filter) was added to the hydrochloric acid solution. The solution was thoroughly mixed and transferred to a separating funnel of suitable volume. The flask which had contained the solution was rinsed successively with small portions of amyl acetate, the total volume of which was equal to the sum of the volumes of the hydrochloric acid and cupferron solutions, and the amyl acetate was then transferred to the separating funnel. Extraction was carried out for 5 min and the phases were allowed to separate into layers; after these had been separated the protactinium was re-extracted from the amyl acetate phase with an equal volume of a 1 M solution of citric acid. The flask containing the solution was placed on a boiling water bath for 30 min and was shaken periodically. After the indicated period the solution was cooled and the aqueous phase, containing Pa^{233}, was separated. Table 3 gives the results of the experiments obtained by the above-described method. The relative mean square-law error of the activity measurements was ± 3%. Employing this method, up to 70% of protactinium (with respect to activity) can be separated from preparations of freshly irradiated thorium nitrate. The separated protactinium was identified by the half-life. Observation of the decay of the α-activity with respect to time gave a value of 27 days for the half-life $T_{\frac{1}{2}}$ (see Fig. 1). The result obtained agrees well with literature data and confirms that the separated radioactive element is Pa^{233}.

The problem of the degree of complete separation of fission elements from protactinium was not the subject of a special investigation, but the value of $T_{\frac{1}{2}}$ obtained allows the conclusion to be drawn that if these operations are carried out appreciable capture of fission products does not take place.

LITERATURE CITED

1. Neutron Cross Sections, BNL (New York, 1958).
2. D. Strominger, J. Hollander and G. Seaborg, Rev. Mod. Phys. 30, 2, 585 (1958).
3. A. Fudge, and J. Woodhead, Analyst 81, 864, 417 (1956).
4. A. Fudge, and J. Woodhead, Chem. Ind. 33, 1122 (1957).
5. A. Goble and A. Maddock, Trans. Faraday Soc. 55, 4 591 (1959).
6. A. Maddock and G. Miles, J. Chem. Soc. Suppl. Iss. 2, 253 (1949).
7. A. Maddock and G. Miles, J. Chem. Soc. Suppl. Iss. 2, 253 (1949).
8. A. Grosse, and M. Agruss, J. Am. Chem. Soc., 57, 438 (1935).

DETERMINATION OF THE OPTIMUM YIELD OF ENRICHED ORE IN RADIOMETRIC ENRICHMENT OF URANIUM ORES

E. D. Mal'tsev

Translated from Atomnaya Énergiya, Vol. 8, No. 2, pp. 121-126
February, 1960
Original article submitted, March 9, 1959

In this article a method is presented for determining the optimum conditions of operation of radiometric ore-sorting plants with allowance for the expenditure on geological prospecting S_1, ore extraction S_2, radiometric enrichment S_3, hydrometallurgical reduction S_4; also taken into account are the ore enrichment yield γ, the uranium content in the ore α, the coefficients of uranium recovery in the radiometric enrichment of the ore ϵ and hydrometallurgical reduction ϵ'.

In order to determine the minimum cost of uranium salts S_m, an analytical method is used; S_m is represented in the form of a continuous function

$$S_m = F(S_1, S_2, S_3, S_4, \alpha, \gamma, \epsilon\epsilon').$$

The relations $\epsilon = f_1(\gamma)$ and $\epsilon' = f_2(\alpha\gamma\epsilon)$ are determined by means of approximation theory in which the experimental points are chosen in analytical form.

Since $S_m = f(\gamma)$ is an extreme function, then the optimum yield of enriched ore in a radiometric ore-sorting plant γ_{opt} corresponding to the minimum cost of the metal is determined from the equation $dS_m/d\gamma = 0$.

An example is given of the determination of the optimum yield of enriched ore.

In connection with the wide development of extraction and treatment of uranium ores, the question of lowering to a minimum the expenditure on obtaining uranium salts from the ores is of great importance. One of the most efficient processes which considerably reduces the cost of uranium salts is the enrichment of uranium ore by radiometric ore-sorting machines, permitting one to control the uranium content in the radiometric enrichment plant dumps and the enriched ore yield.

At present, the uranium content in the dumps of these plants, in most cases, is set at the level of the uranium content in hydrometallurgical plant dumps. Under the present technological possibilities of ore treatment by hydrometallurgical reduction, this meets the task of maximum recovery of uranium, but does not correspond to the lowest possible cost of uranium salts which can be obtained in the case of the optimum setting of the radiometric ore-sorting machines.

It should be noted that in a number of cases an increase of 1-1.5% in the recovery with radiometric enrichment results in an increase in the enriched ore yield of 10-15%. This considerably increases the volume of the hydrometallurgical production, the consumption of chemicals, steam, electric power, etc. Thus, a very small increase in the salt output leads to a considerable increase in the cost of the entire production.

In our opinion, the setting of the radiometric ore-sorting machines to ensure the optimum yield of enriched ore permits a lowering of the cost of uranium without decreasing the volume of its production.

The cost of uranium salts depends on the expenditure on prospecting and ore extraction, on the cost of enrichment and hydrometallurgical reduction, the recovery factors in the enrichment and hydrometallurgical processes. The relation between these factors can be represented in the form of a continuous function and expressed by the equation

$$S_m = \frac{S_1 + S_2 + S_3 + S_4\gamma}{\alpha\epsilon\epsilon'}, \qquad (1)$$

where S_m is the cost of uranium in the salts (rubles/kg); S_1 is the cost of prospecting for extractable deposits of uranium ore (rubles/ton); S_2 is the cost of extraction of the uranium ore (rubles/ton); S_3 is the cost of radiometric enrichment of uranium ore (rubles/ton); S_4 is the cost of transporting the enriched ore from the mine to the plant and its treatment in a hydrometallurgical plant (rubles/ton); γ is the ore yield after the radiometric enrichment; α is the uranium content in the ore received for radiometric enrichment (kg/ton); ϵ is the uranium recovery

factor in the radiometric enrichment of the ore; ϵ' is the uranium recovery factor in the treatment of the enriched ore at the hydrometallurgical plant.

In order to determine the optimum cost of uranium in the finished product from Eq. (1), it is necessary to determine the relation between ϵ, ϵ', and γ:

$$\varepsilon = f_1(\gamma), \quad \varepsilon' = f_2(\gamma).$$

If the points obtained experimentally are laid off on a system of rectangular coordinates (axis of abscissas: ore yield in radiometric enrichment, and axis of ordinates: the recovery factor corresponding to this yield), we then obtain the curves shown in Fig. 1.

Of course, one may construct for each type of ore a curve depending on its physical and chemical properties contrast, adopted scheme of radiometric enrichment, type of enrichment machinery, and a family of curves for the entire process of radiometric enrichment.

The equation expressing the relation between ϵ and γ, based on the main features of the enrichment process, should satisfy the following conditions: if $\gamma = 0$, then $\epsilon = 0$, i.e., a zero yield of the enriched ore corresponds to zero recovery; if $\gamma = 1$, then $\epsilon = 1$, i.e., a 100% yield of ore corresponds to 100% recovery; moreover, the curve $\epsilon = f(\gamma)$ should pass through two selected characteristic points with coordinates γ_1, ϵ_1, and γ_2, ϵ_2, obtained experimentally.

In a special case, the equation $\epsilon = f_1(\gamma)$ should transform into the equation of the bisector of the coordinate axes angle $\epsilon = \gamma$ representing the dependence between ϵ and γ for an ore which, owing to its properties, did not undergo enrichment.

Investigations showed that the most suitable form of equation satisfying the above-mentioned family of curves is

$$\varepsilon = \delta\gamma^{\varrho} - \frac{\gamma}{1+\gamma^{\nu}}, \qquad (2)$$

where δ, ρ, ν are coefficients characterizing the physical and mechanical properties of the ore and the conditions of its enrichment.

If it is assumed that $\gamma = 1$ and $\epsilon = 1$, then we obtain the first equation for determining the coefficient δ:

$$\varepsilon = \delta \cdot 1^{\varrho} - \frac{1}{1+1^{\nu}} = \delta - 0{,}5 = 1,$$

from which we find $\delta = 1.5$.

Two points on the experimentally obtained curve, i.e., two values of the enriched ore yield and the recovery corresponding to them, permit one to write the equations

$$\varrho = f_1(\nu) = \frac{\lg\left(\varepsilon_1 + \frac{\gamma_1}{1+\gamma_1^{\nu}}\right) - \lg 1{,}5}{\lg \gamma_1}; \qquad (3)$$

$$\varrho = f_2(\nu) = \frac{\lg\left(\varepsilon_2 + \frac{\gamma_2}{1+\gamma_2^{\nu}}\right) - \lg 1{,}5}{\lg \gamma_2}. \qquad (4)$$

From Eqs. (3) and (4) we determine the values ν and ρ, by a graphical–analytical method in which we construct curves whose intersections give us the values we are seeking.

In order to characterize the enrichment process by means of Eq. (2) with greater accuracy, we should have more than two experimental points. In this case, in order to determine the constant coefficients ρ and ν we may choose the most characteristic points on the curve constructed from the experimental data.

In its essentials, the hydrometallurgical process is analogous to the enrichment process, since in both cases there is a concentration of the useful constitutent. Therefore, the relation between the uranium recovered by hydrometallurgical reduction ϵ' and the uranium content in the ore β undergoing hydrometallurgical treatment can also be established from Eq. (2). It should be noted, however, that it is not necessary to investigate the relation between ϵ' and β in such wide limits (from 0 to 100%), as was done in the investigation of the relation between the recovery factor and the enriched ore yield by radiometric reduction. We shall limit ourselves to the study of the relation between ϵ' and β in the range of variation of β from α to β_0 corresponding to some given γ_0.

The amount of metal which remains in the enriched ore after radiometric reduction is equal to $\alpha\epsilon$; then the content in the enriched ore β is determined from the expression

$$\beta = \frac{\alpha\varepsilon}{\gamma} = \alpha\left(\delta\gamma^{\varrho-1} - \frac{1}{1+\gamma^{\nu}}\right) = f_0(\gamma). \qquad (5)$$

Under the conditions that the relation between ϵ' and β will be investigated in the interval from α to β_0, corresponding to γ_0, we obtain an equation for determining the extreme value of β_0:

$$\beta_0 = \alpha\left(\delta\gamma_0^{\varrho-1} - \frac{1}{1+\gamma_0^{\nu}}\right). \qquad (6)$$

The variation of the recovery factor by hydrometallurgical reduction is represented in the graph of Fig. 2.

As already indicated, we have taken the relation between ϵ' and β in the form

$$\varepsilon' = \delta_1 \beta^{\rho_1} - \frac{\beta}{1+\beta^{\nu_1}}. \qquad (7)$$

The coefficients δ_1, ρ_1, ν_1, are determined from three experimental points:

$$\delta_1 = \frac{1}{\alpha^{\rho_1}}\left(\varepsilon_1' + \frac{\alpha}{1+\alpha^{\nu_1}}\right); \qquad (8)$$

$$\rho_1 = f_1(\nu_1) = \frac{\lg\left(\varepsilon_1' + \frac{\alpha}{1+\alpha^{\nu_1}}\right) - \lg\left(\varepsilon_2' + \frac{\beta_1}{1+\beta_1^{\nu_1}}\right)}{\lg\alpha - \lg\beta_1}; \qquad (9)$$

$$\rho_1 = f_2(\nu_1) = \frac{\lg\left(\varepsilon_1' + \frac{\alpha}{1+\alpha^{\nu_1}}\right) - \lg\left(\varepsilon_0' - \frac{\beta_0}{1+\beta_0^{\nu_1}}\right)}{\lg\alpha - \lg\beta_0}. \qquad (10)$$

Constructing the curves from Eqs. (9) and (10), we obtain at their intersections the values of ρ_1 and ν_1, which we are seeking; the value of δ_1 is determined from Eq. (8).

Since, by Eq. (5), $\beta = f_0(\gamma)$, the relation between γ and ϵ' in final form is expressed by the equation

$$\varepsilon' = \delta_1 [f_0(\gamma)]^{\rho_1} - \frac{f_0(\gamma)}{1+[f_0(\gamma)]^{\nu_1}}. \qquad (11)$$

In order to determine the optimum value of γ, we insert the obtained values of ϵ and ϵ' into Eq. (1):

$$S_m = \frac{S_1+S_2+S_3+S_4\gamma}{\alpha\left[\delta\gamma^{\rho} - \frac{\gamma}{1+\gamma^{\nu}}\right]\left[\delta_1[f_0(\gamma)]^{\rho_1} - \frac{f_0(\gamma)}{1+[f_0(\gamma)]^{\nu_1}}\right]}. \qquad (12)$$

The plot of Eq. (12) is an extremum curve having a minimum at the point corresponding to the lowest cost of uranium and the optimum yield of enriched ore.

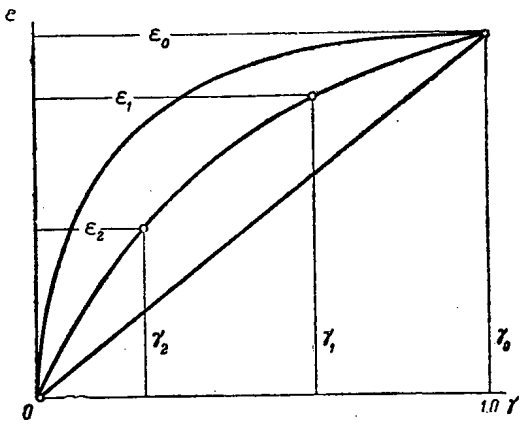

Fig. 1. Relation between yield of enriched ore γ and uranium recovery factor ϵ.

We determine the position S_m of the minimum γ_{opt} by taking the first derivative of the cost of uranium S_m with respect to γ and setting it equal to zero.

We can solve this equation for γ by a graphical–analytical method in which it is separated into two equations

$$y = \varepsilon\varepsilon' S_4; \qquad (13)$$

$$y = \left(\varepsilon' \frac{d\varepsilon}{d\gamma} + \varepsilon \frac{d\varepsilon'}{d\gamma}\right)(S_1 + S_2 + S_3 + S_4\gamma). \qquad (14)$$

The value of $d\epsilon/d\gamma$ is determined from the equation

$$\frac{d\varepsilon}{d\gamma} = \rho\delta\gamma^{\rho-1} - \frac{\gamma^{\nu}(1-\nu)+1}{(1+\gamma^{\nu})^2}. \qquad (15)$$

The value of $d\epsilon'/d\gamma$ is found from the differential equation (7):

$$\frac{d\varepsilon'}{d\gamma} = \frac{d\beta}{d\gamma}\left[\delta_1\rho_1\beta^{\rho_1-1} - \frac{1+\beta^{\nu_1}(1-\nu_1)}{(1+\beta^{\nu_1})^2}\right]. \qquad (16)$$

We find the value of $d\beta/d\gamma$ by differentiating Eq. (5):

$$\frac{d\beta}{d\gamma} = \alpha\left[\delta(\rho-1)\gamma^{\rho-2} + \frac{\nu\gamma^{\nu-1}}{(1+\gamma^{\nu})^2}\right]. \qquad (17)$$

Before radiometric enrichment, the ore was segregated by screening into classes according to size, and each class underwent enrichment separately; the relation between ϵ and γ for each class can be characterized by its constant coefficients ρ and ν.

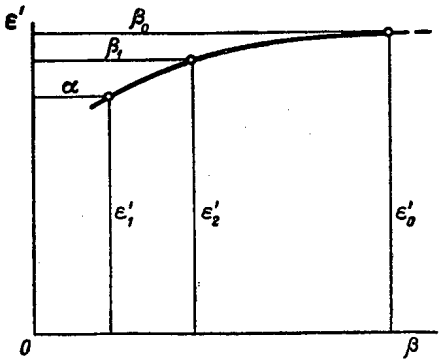

Fig. 2. Variation of the recovery factor ϵ' for hydrometallurgical reduction as a function of the uranium content in the ore β.

TABLE 1. Coordinates of the Points ρ and ν

ν	$\rho=f_1(\nu)$	$\rho=f_2(\nu)$
+2,0	0,159	0,304
+1,0	0,264	0,329
0,0	0,380	0,389
−0,5	0,447	0,424
−1,0	0,500	0,454
−3,0	0,727	0,496

In order to determine the optimum operating conditions of the machine, it is necessary to carry out the above calculation for all size classes and determine for each the optimum enriched ore yield and minimum cost of metal. Here, the cost of the ore for each size class should be determined by splitting up the total cost, including expenditure on prospecting, proportionally to the distribution of the metal according to class.

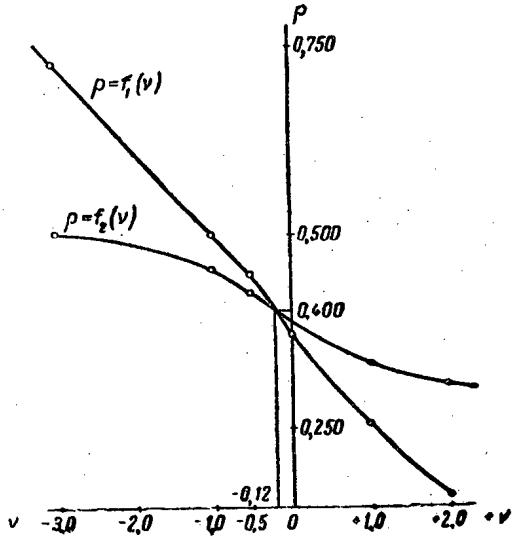

Fig. 3. Determination of the coefficients ν and ρ.

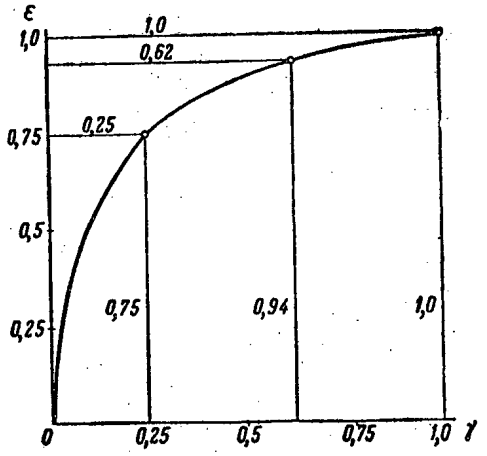

Fig. 4. Metal recovery in enriched product sorted by the radiometric method versus the product yield.

TABLE 2. Coordinates of the Points ν_1 and ρ_1

ν_1	$\rho_1=f_1(\nu_1)$	$\rho_1=f_2(\nu_1)$
$+\infty$	0,151	0,194
+1,0	0,123	0,151
0,0	0,101	0,123
−1,0	0,062	0,092
−3,0	0,040	0,046
−5,3	0,038	0,038
$-\infty$	0,038	0,038

TABLE 3. Coordinates γ and $\underline{\gamma}$

By Eq. (13)		By Eq. (14)	
γ	ν	γ	ν
0,1	80,3	0,1	195,0
0,3	110,5	0,3	92,4
0,5	124,0	0,5	58,4
0,7	131,5	0,7	35,1
0,9	134,5	0,9	16,6
1,0	135,0	1,0	7,2

The optimum yield of enriched ore for each size class should be determined from the equation

$$S_m = \frac{S_k + S_3 + S_4\gamma}{\alpha\varepsilon\varepsilon'},$$

where S_k is the cost of one ton of ore of each class size, including the expenditure on prospecting.

We assume that the ore is sorted by screening into $\underline{i}$ classes, the amount of ore in each class being $Q_1, Q_2, \ldots, Q_i$ with a metal content $\alpha_1, \alpha_2, \ldots, \alpha_i$. In this case

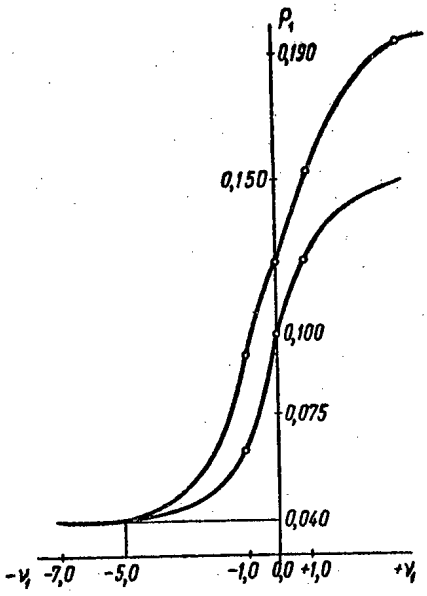

Fig. 5. Determination of the coefficients ν_2 and ρ_1.

the total optimum cost of metal as a whole for all the ore is determined by the expression

$$S_m = \frac{Q_1\alpha_1 S_{m_1} + Q_2\alpha_2 S_{m_2} + \ldots + Q_i\alpha_i S_{m_i}}{Q_1\alpha_1 + Q_2\alpha_2 + \ldots + Q_i\alpha_i}. \quad (18)$$

If one of the classes does not undergo radiometric enrichment, then the cost of the metal obtained from the ore of this class is determined by Eq. (1) for $S_3=0$ and $\gamma=1$. We shall give calculation for one class: $S_1=20$ rubles /ton; $S_2=60$ rubles/ton; $S_3=10$ rubles/ton; $S_4=150$ rubles/ton; $\alpha=1.0$ kg/ton=0.1%.

The following experimental data were obtained:

Enriched Ores	
$\gamma_1 \ldots 1.0$	$\epsilon_1 \ldots 1.0$
$\gamma_2 \ldots 0.62$	$\epsilon_2 \ldots 0.94$
$\gamma_3 \ldots 0.25$	$\epsilon_3 \ldots 0.75$

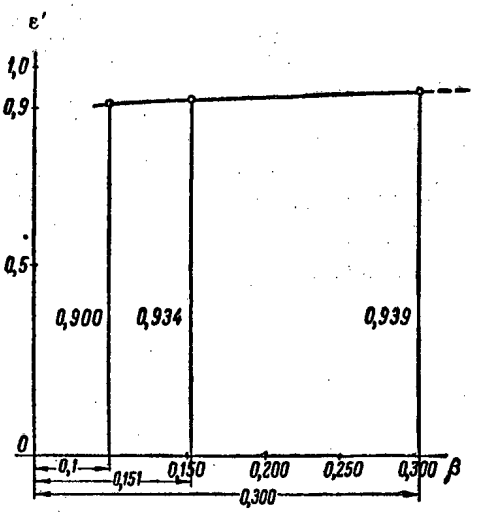

Fig. 6. Dependence of the metal recovery in the concentrate from hydrometallurgical reduction on the content of metal in the ore (rich product sorted radiometrically).

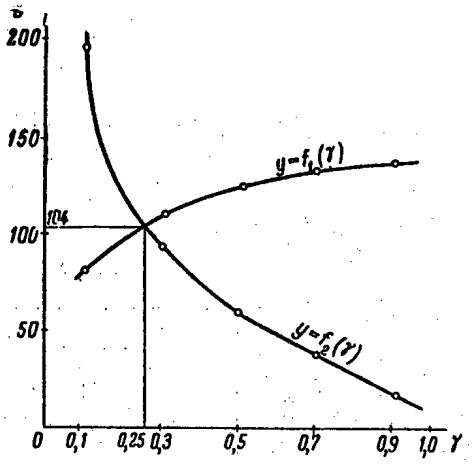

Fig. 7. Determination of the optimum yield of a rich product sorted radiometrically.

Hydrometallurgical Process	
$\beta_1 \ldots 0.1$	$\epsilon'_1 \ldots 0.900$
$\beta_2 \ldots 0.151$	$\epsilon'_2 \ldots 0.914$
$\beta_3 \ldots 0.300$	$\epsilon'_3 \ldots 0.939$

The coordinates ρ and ν calculated from Eqs. (3) and (4) are shown in Table 1. The curves in Fig. 3 were plotted to determine the values of ρ and ν.

Thus Eq. (2) takes the form

$$\varepsilon = 1{,}5\gamma^{0{,}40} - \frac{\gamma}{1+\gamma^{-0{,}12}}.$$

A plot of Eq. (2) is shown in Fig. 4.

The values ρ_1 and ν_1 determined by Eqs. (9) and (10) are shown in Table 2.

The plots of $\rho_1=f_1(\nu_1)$ and $\rho_1=f_2(\nu_1)$ are shown in Fig. 5.

The value of δ_1 calculated from Eq. (8) is 0.987. Then Eq. (7) takes the form

$$\varepsilon' = 0{,}982\beta^{0{,}04} - \frac{\beta}{1+\beta^{-5{,}0}} = f(\beta).$$

The equation for f (β) is plotted in Fig. 6.

The value of the optimum yield of enriched ore is determined from Eqs. (13) and (14). The coordinates γ and y are shown in Table 3. Plots of $y=f_1(\gamma)$ and $y=f_2(\gamma)$ are given in Fig. 7.

From Eq. (12), we calculate the coordinates of the points and construct the curve $S_m=f(\gamma)$:

γ	S_m
0,1	196,5
0,3	183,0
0,5	199,5
0,7	222,0
0,9	251,0
1 0	267,0

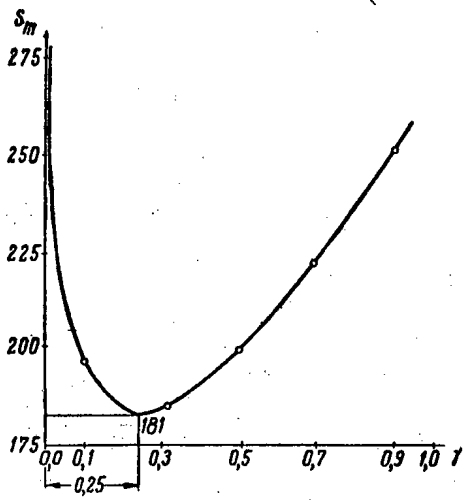

Fig. 8. Dependence of the cost of metal in the final product of hydrometallurgical reduction on the yield of enriched product sorted radiometrically.

The plot of $S_m = f(\gamma)$ is shown in Fig. 8. As seen from this figure, there is a quite distinct region of optimum yield of enriched ore characterized by minimum costs of the uranium salts.

In this case, if the economic parameters of extraction and ore processing permit one to obtain a cost of uranium in the ready product considerably lower than its mean cost in industry, then, in our opinion, it is of advantage to shift somewhat from the optimum towards a higher enriched ore yield γ and in this way increase the recovery and uranium yield in the finished product. The amount one shifts from the optimum, however, should be governed by the cost of 1 kg of additionally obtained metal, which should not exceed the mean cost of the metal in industry.

STRONG FOCUSING IN A LINEAR ACCELERATOR

P. M. Zeidlits, L. I. Bolotin, E. I. Revutskii, and V. A. Suprunenko

Translated from Atomnaya Énergiya, Vol. 8, No. 2, pp. 127-132, February, 1960
Original article submitted April 27, 1959

In this paper we consider the use of strong focusing in linear proton accelerators and carry out a detailed quantitative analysis of the motion of protons in the system. Design calculations for quadrupole lenses are given together with the experimental results obtained with the use of strong focusing in a 5.5 Mev linear proton accelerator.

In linear accelerators for protons and heavy ions it is impossible to provide simultaneous radial and phase stability without the use of supplementary focusing. At the present time, beam focusing is accomplished in a linear accelerator by means of grids, longitudinal magnetic fields, and electrostatic or magnetic quadrupole lenses.

A grid focusing system is simple and reliable but is characterized by low transmission and can be used only in short low-current accelerators.

The application of a longitudinal magnetic field for focusing a beam at the initial stage of acceleration is complicated by the fact that the large fields required in this case require the expenditure of considerable power in the accelerator. Hence, at the present time the most extensively used focusing scheme uses quadrupole lenses in an alternating-gradient focusing field.

APPLICATION OF STRONG FOCUSING IN A LINEAR ACCELERATOR

The strong focusing method was first developed in 1952 by Courant, Livingston and Snyder [1]. Blewett [2] proposed the application of this method in linear accelerators and gave a theoretical analysis of the quadrupole lens. It is found that the field required for focusing is considerably smaller than the field required by a longitudinal magnetic field system; nevertheless, the field is still quite large. In 1953 Zel'manov proposed to place a half-length lens at the beginning of the focusing system; if account is taken of the asymmetry of the capture region in terms of the initial parameter of the beam for strong focusing, we see that this naturally deforms the input beam. The half-lens and the multiple-periodicity scheme proposed by Ya. B. Fainberg, A. I. Akhiezer and K. N. Stepanov allow a considerable reduction in the field gradients required for focusing.

In focusing by quadrupole lenses the particle is subjected alternately to the effect of focusing and defocusing forces. The equation of motion of a particle in the region near the axis of the accelerating system is of the form

$$\frac{d^2x}{d\xi^2} + \Omega^2(\xi)\, x = \varepsilon f(x, \xi), \qquad (1)$$

where $\Omega^2(\xi)$ is a quasi-periodic function of variable sign; ϵ is a small parameter; $\xi = z/\beta\lambda$ is a dimensionless longitudinal coordinate; λ is the wavelength; $\beta = v/c$ is the relative velocity.

A. A. Sharshanov has developed a method for finding approximate solutions of Eq. (1) which coincide with the exact solution at the end of the period of the function $\Omega(\xi)$ for the case $\epsilon = 0$.

For a symmetric variation period for the function $\Omega(\xi)$ with an initial defocusing plane (ID) the amplitude of the periodic solution of Eq. (1) can be written in the form

$$x_m = \sqrt{x_0^2 + \left(\frac{x_0'\beta\lambda}{\Gamma_{IF}}\right)^2}\sqrt{\frac{\Gamma_{IF}^{(0)}}{\Gamma_{IF}(\xi)}}, \qquad (2)$$

where the parameter Γ_{IF} is computed numerically (values are given in Figs. 1–3) while x_0 and x_0' are respectively the initial deviations (in centimeters) and the initial angle of the particle trajectory (in radians).

We have an analogous expression for an initial focusing plane (IF). The second factor in Eq. (2) takes account of the variation of amplitude with the variation of velocity of the particle which results from the acceleration process.

In certain cases it is more convenient to use the amplitude expression which has been given in [3,4]; this expression can be written in the form

$$x_{ID} = \sqrt{(\gamma x_0)^2 + \left(\frac{x_0'\beta\lambda}{\gamma\Gamma_{IF}}\right)^2}\sqrt{\frac{\Gamma_{IF}^{(0)}}{\Gamma_{IF}(\xi)}}$$

(the value of γ is shown in Figs. 1-3).

NUMERICAL INVESTIGATION OF PARTICLE MOTION IN A STRONG-FOCUSING SYSTEM AND CHOICE OF THE OPERATING POINT

In [3,4] graphs were given for the stability regions with values of the parameters γ and Γ_{IF}. However, the formulas used for carrying out the calculations were based on very rough approximations and cannot be used in practical cases. Hence we have carried out calculations for the stability regions with the accuracy required for actual design.

In Figs. 1–3 we show the stability regions for the solutions of Eq. (1) for various combinations of focusing and defocusing lenses and the numerical values of the quantities Γ_{IF} γ computed for the case in which the function

$$\Omega(\xi) = \begin{cases} i\frac{1}{1-\alpha}Y & \text{— a) in the defocusing lens} \\ i\alpha X & \text{— b) in the acceleration gap} \\ \frac{1}{1-\alpha}Y & \text{— c) in the focusing lens} \end{cases}$$

In this case

$$X^2 = \frac{Z\alpha\pi eEG\lambda}{Amc^2\beta}\sin\varphi_s; \qquad (3)$$

for electrostatic lenses

$$Y^2 = \frac{Z(1-\alpha)^2 eVk\lambda^2}{Amc^2a^2}; \qquad (4a)$$

for magnetic lenses

$$Y^2 = \frac{300Z(1-\alpha)^2 eH'\beta\lambda^2}{Amc^2}, \qquad (4b)$$

where H' is the gradient of the magnetic field; V is the potential difference at the electrodes of the lens; K is a coefficient which depends on the electrodes; 2a is the aperture of the lens; α is the ratio of the gap length to the length of the period (α=0.25); Z, A are respectively the charge and mass number; φ_s is the synchronous phase; E is the amplitude of the accelerating field averaged over the length of the accelerator; G is the efficiency factor for the accelerating field (for α=0.25, the maximum value is G=0.9).

The focusing systems for which the stability regions are shown in Figs. 1–3 differ from each other by the number of successive lenses of the same sign which follow each other (multiple periodicity). It is apparent from these figures that with the operating point in the center of a stability region an increase in the number of successive lenses N means that the voltage applied to the lenses is reduced as $2^{-(N-1)}$.

However, as is apparent from Fig. 4 an increase in N means a considerable increase in the amplitude of the

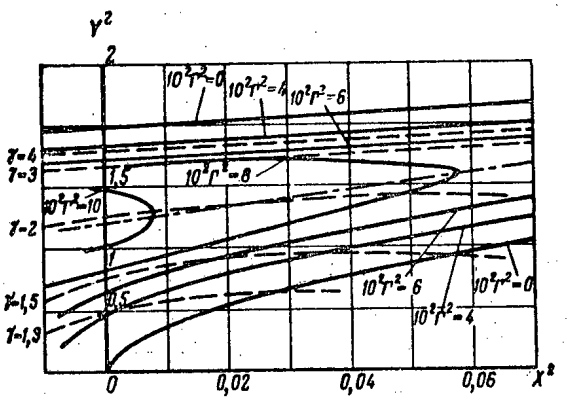

Fig. 1. Stability region for N=1.

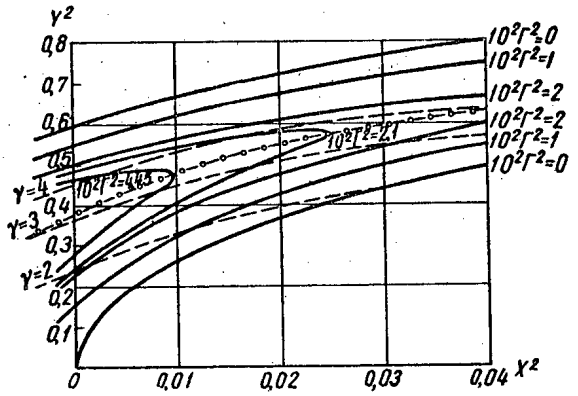

Fig. 2. Stability region for N=2.

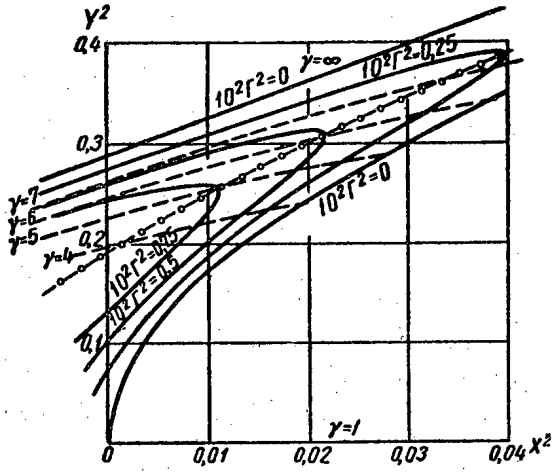

Fig. 3. Stability region for N=3.

oscillations in the defocusing plane, depending on the radius of the incoming beam; the capture region is also reduced considerably. It should be noted that the amplitude of the ion oscillations (as a function of the parameters of the incoming beam) is determined by the sign of the first lens. For an initial focusing plane the amplitude is a strong function of the angular divergence of the beam; for an initial defocusing plane the amplitude is a weak function of angular divergence but becomes a strong function of the diameter of the input beam. In Fig. 5 we show the capture region on the phase plane as a function of lens voltage for N=2. It is apparent from the figure that capture is maximized for a paraxial beam. In this case the operating point lies at the lower boundary of the stability region. As the lens voltage is increased, the capture region is sharply reduced because of the increased oscillation amplitude in the initial defocusing plane (γ grows sharply). Calculations show that the amplitude of the radial oscillations increases with increasing β since the quantity $\Gamma_{IF}(\xi)$ in Eq. (2) is reduced with an increase in ion velocity for a fixed gradient along the system. A numerical investigation of the amplitude ratio at the beginning and end of acceleration as a function of lens voltage shows that the increase in amplitude is a minimum for the voltage close to the lower boundary of the stability region. If the increase in ion velocity is accompanied by a corresponding change in lens voltage, so that the quantity $\Gamma_{IF}(\xi)$ remains constant, there is no increase in amplitude.

The mean-square increase in the amplitude of the radial oscillations due to inaccuracies in the elements can be computed approximately. As has been shown in [3], the basic effects on oscillation amplitude are due to

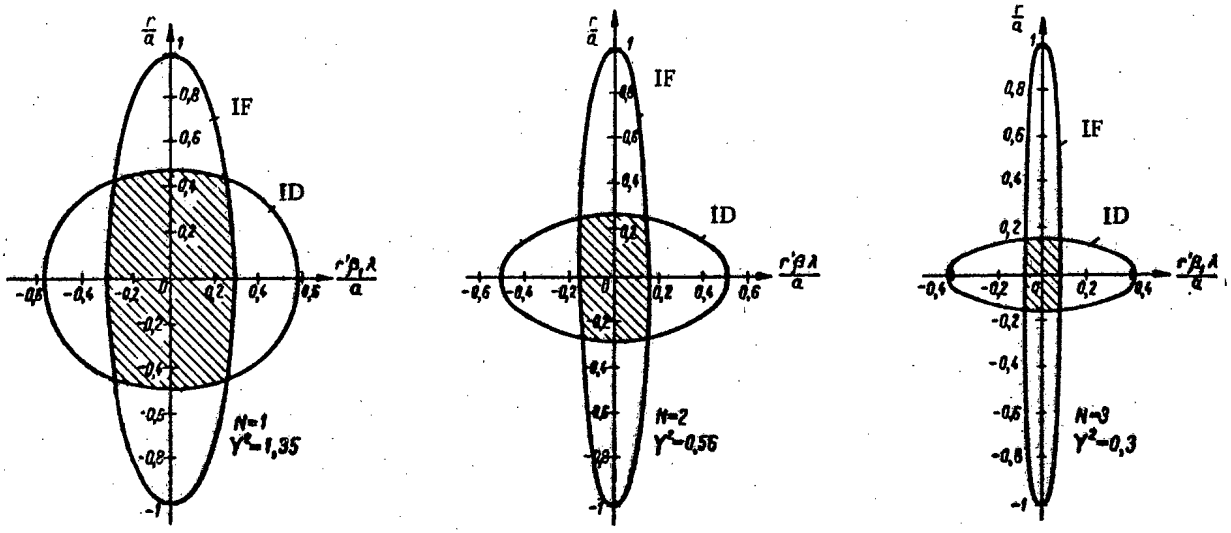

Fig. 4. Capture region as determined from the parameters of the input beam for various values of N with $X^2=0.002$.

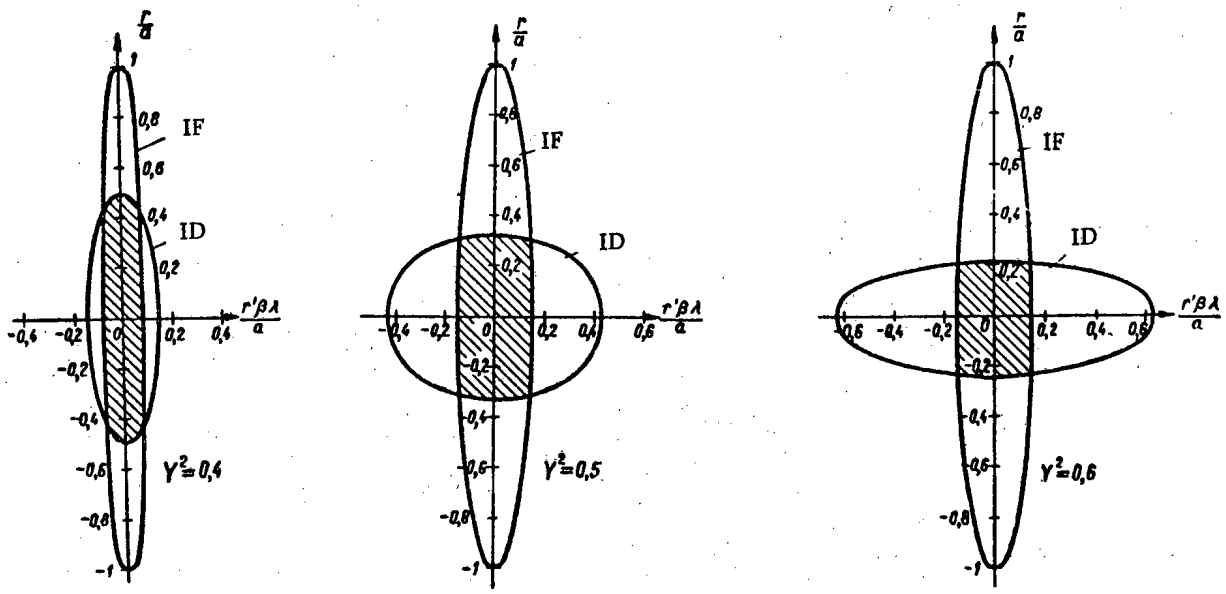

Fig. 5. Capture region from the parameters of the input beam for various lens voltages with N=2 and $X^2=0.002$.

displacement of the axis of the zeroth field, a deviation in the angle of intersection of the transverse axis from 90 deg, and fluctuations in the field distribution in the lenses.

CALCULATION OF A FOCUSING SYSTEM FOR A LINEAR ACCELERATOR

The design of a focusing system starts with the choice of the number of successive lenses of the same sign in the drift tube. Then, from the stability region (cf. Figs. 1–3) for a given value of X^2 we determine Y^2 which, for a given lens aperture, determines the required focusing voltage.

Investigations of strong focusing have been carried out in a linear proton accelerator with an energy of 5.5 Mev. The parameters are as follows: λ=2.18 m; E=20 kv/cm; β_0=0.0328; β_{fin}=0.1; φ_s=16°; K=1; G_0=0.5; X_0=0.141. We choose an aperture $2a$=1.5 cm and N=2. From the stability region we choose Y^2=0.4; γ=2, $\Gamma(0)=10^{-1}$.

The required lens electrode voltage is 8 kv. The parameters of the ellipses in the phase plane (cf. Fig. 5) are as follows: for an ID plane

$$\frac{x_m}{a}=\frac{1}{\gamma}=0{,}5;\quad \frac{x'_m}{a}=\frac{\gamma\Gamma}{\beta\lambda}=2{,}8\cdot10^{-2};$$

for an IF plane

$$\frac{x_m}{a}=1;\quad \frac{x'_m}{a}=\frac{\Gamma}{\beta\lambda}=1{,}4\cdot10^{-2},$$

where x' is the angular divergence of the input beam. Thus, the diameter of the injected beam cannot exceed 0.75 cm while the divergence cannot exceed $2.1\cdot10^{-2}$ radians. Because of inaccuracies in the fabrication of the system these parameters must be reduced.

As an example we may take the following requirements:

1) The displacements of the ends of the lens from the axis of the accelerator are 0.01 cm;

2) The inaccuracy in the alignment of the OX and OY axes is of the order of 0.02 radians;

3)The spread in the characteristic lens parameters

$$2=\frac{\Delta V}{V}=0{,}05.$$

Taking the number of drift tubes to be n=20 from Eq. (4) we obtain the mean square increase in amplitude δx=0.32 cm. Consequently, for the present tolerances the effective aperture of the lens is reduced to approximately 3mm, i.e., $2a_{eff}$=1.2 cm. From these we can determine the parameters of the input beam which can pass through the accelerator without loss: $2x_0$=0.6 cm, $2x'_0 \simeq 1\cdot10^{-2}\simeq0.5°$.

DESIGN OF THE LENS

An alternating gradient field can be produced by electrostatic or by magnetic quadrupole lenses. In order to use electrostatic quadrupole lenses in the small volume of the drift tube it is necessary to use electrodes which are at potentials of 10–20 kv.

Two lens designs have been developed: one with an aperture $2a$=1.5 cm and a voltage of 15 kv and the other with an aperture $2a$=3.0 cm and a voltage of 40 kv. The construction of a drift tube with a lens characterized by the aperture $2a$=3.0 cm for the 5.5 Mev accelerator is shown in Fig. 6. The lens electrodes are made from dural and are attached to a frame made of plexiglas. Special measures are taken to protect the inner plane of the drift tube and the lens from penetration of the accelerating radio-frequency field, which tends to reduce the electrical breakdown strength of the vacuum gap between electrodes. In the investigations of these electrostatic lenses we have used electrodes of hyperbolic shape (K=1, $2a$=1.5 cm); in the electromagnetic lenses the electrodes were of cylindrical shape.

The system for controlling the position of the axis consists of two parts: an upper unit and a lower unit. The upper unit makes use of four micrometer screws and a locking nut to align the center of the drift tube with the axis of the accelerator. The lower unit consists of a spherical joint with micrometer screws and makes it possible to align the lens axis with the accelerator axis. The position of the lens axis is monitored by means of a precision leveling instrument NA-1 and markers in the space between the electrodes. The accuracy of adjustment is ±0.1 mm. The adjustment of the gaps between the drift tubes is made by means of a mechanical indicator.

EXPERIMENTAL INVESTIGATION OF THE FOCUSING SYSTEM IN THE 5.5 MEV LINEAR ACCELERATOR

The design and construction of the system were carried out at the beginning of 1955. The first experimental results were obtained at the end of 1955.

The current at the input of the accelerator is measured by means of a Faraday cylinder, which is located directly at the input to the accelerating system. The current at the output of the accelerator is also measured by means of a Faraday cylinder, which is located at a distance of 2 m from the accelerating system. It was not necessary to provide beam focusing between the accelerator output and the cylinder. The current at the accelerator output as a function of lens voltage is shown in Fig. 7. At optimum adjustment of the accelerator, the maximum current is obtained at a lens voltage of 8 kv, corresponding to the lower boundary of the stability region, in good agreement with the calculation. It is apparent from this figure that a change of 20% in the lens voltage does not cause any substantial reduction in the current at the output of the accelerator.

With voltages applied to the lenses the current at the output of the accelerator is increased by a factor of 3 or 4 as compared with acceleration without the lenses;

the current is a strong function of the divergence of the input beam. The relatively small increase in current is explained by the small length of the accelerator. When the lenses are switched on the ratio of input current to output current is increased from 1:30 to 1:7 and depends strongly on the intensity of the accelerating field. For a lens aperture of 15 mm the diameter of the captured beam is approximately 6 mm, in good agreement with the calculations.

With grid focusing the current ratio is 1:20. Thus, the use of strong focusing requires good focusing of the beam at the input to the accelerator.

These calculations and the experimental investigation indicate the practical possibility of using strong focusing in linear ion accelerators with drift tubes. The tolerances on fabrication and assembly of the accelerating system are technically possible with appropriate choice of lens diameter. The lens voltages can be reduced considerably by using longer wavelengths (since $V \sim 1/\lambda^2$) and by reducing the mean strength of the accelerating field.

PULSED MAGNETIC LENSES FOR LINEAR PROTON ACCELERATORS

In certain cases, for example for very high currents of accelerated particles, it may be desirable to use magnetic quadrupole lenses. Calculations which have been carried out indicate that a power of approximately 250 kw is required to supply a magnetic focusing system with an alternating gradient field for a 30 Mev linear proton accelerator with an injection energy of 4 Mev. It is obvious that the installation of lenses of this kind in drift tubes together with the required cooling system would be a technically difficult problem. However, inasmuch as most linear accelerators are pulsed it is

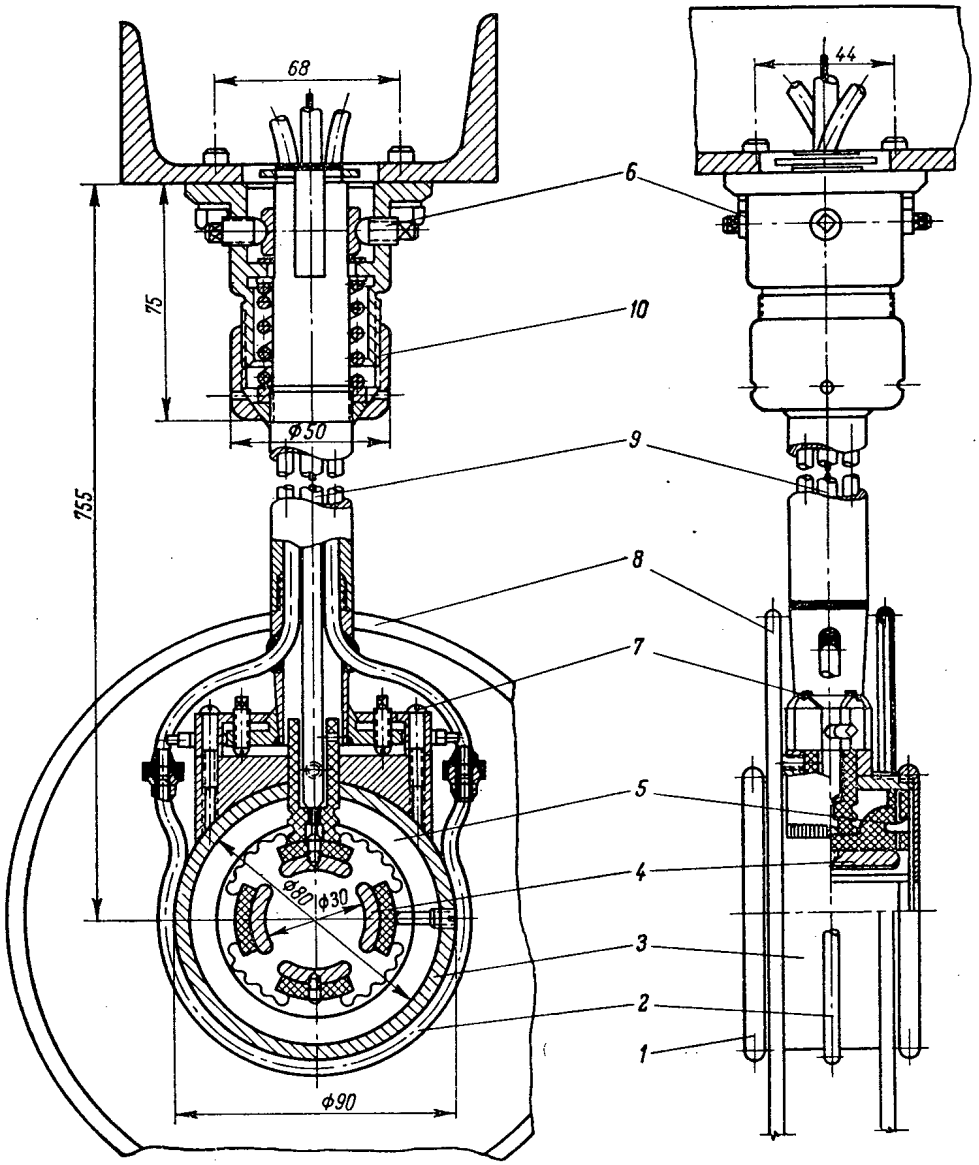

Fig. 6. Construction of the electrostatic lenses with drift tube: 1) ring diaphragm; 2) cooling turn; 3) body of the drift tube; 4) lens electrodes; 5) lens insulator; 6, 7) control screws; 8) adjustment disc; 9) cable; 10) height control nut.

feasible to use a pulsed power supply for the magnetic quadrupole lenses. Calculations for alternating-gradient systems [cf. Eq. (4b)] show that the required field gradient in the lens is determined from the relation

$$H' = \frac{Amc^2\beta_0\gamma^2}{Ze300l_{\text{lens}}}. \qquad (5)$$

In the case being considered $\gamma^2=0.4$. The induction of the magnetic field in the plane of the pole piece can be computed approximately as $B=H'a$. The number of ampere-turns on one pole piece required for producing this gradient, neglecting the magnetic reluctance of the pole pieces and the yoke, is determined from the formula

$$nI \simeq 0{,}1H'(2a)^2. \qquad (6)$$

The frame of the lens is made from transformer iron which is 0.35 mm thick. The winding is made from three turns of PÉV-2 conductor, 2 mm in diameter, covered by a layer of BF-2 cement which is inserted into grooves on the pole pieces and baked. This winding is capable of sustaining the dynamic shocks which are produced when currents of the order of 2 ka are switched on.

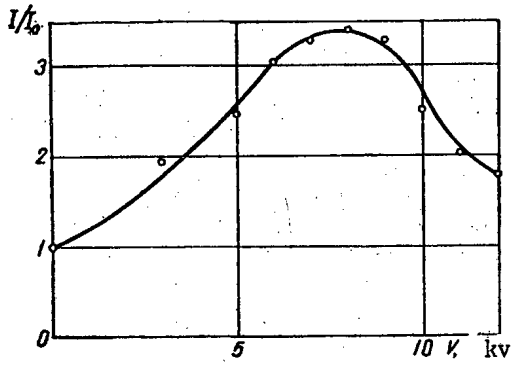

Fig. 7. The output current of the accelerator as a function of lens voltage.

In the 5.5 Mev proton accelerator the required field gradient in the first lens is $H'=1.42\cdot10^3$ oe/cm. The number of ampere-turns on the pole piece nI=1000av, i. e., for a three-turn winding a current of approximately 300 amp is required; approximately 600 amp is required for a lens with parallel-series connection of the windings and approximately 12 ka for parallel supply of twenty such lenses.

The current pulse required for exciting the windings is obtained by discharge of a line with a capacity of 60 μfd through a step-down transformer with a turns ratio of 100:1. The field gradient in the lenses is measured by means of pick-up units which make use of the Hall effect in bismuth. Measurements show that a small asymmetry in the windings does not cause any substantial disturbance of the magnetic field distribution in the lenses. The mean power consumed in the first lens at a pulse rate of one per second and a pulse length of 500 μsec is approximately 15 w; the mean power required by the entire system is approximately 250 w.

Experience with this system in a linear proton accelerator with an energy of 5.5 Mev has shown that the operation of the system is similar to the operation with electrostatic lenses.

In conclusion the authors wish to take this opportunity to thank Acad. AN SSSR K. D. Sinel'nikov and Cand. Phys.-Math. Sci. Ya. B. Fainberg for their continued interest in this work and for valuable discussions.

LITERATURE CITED

1. E. Courant, M. Livingston, and H. Snyder. Phys. Rev. 88, 1190 (1952).
2. T. Blewett. Phys. Rev. 88, 1197 (1952).
3. L. Smith, and R. Gluckstern. Rev. Scient. Instrum. 26, 220 (1955).
4. A. D. Vlasov, Atomnaya Énergiya, 5, 20 (1956).*

*Original Russian pagination. See C. B. translation

STABILITY OF PLASMA BUNCHES IN A WAVEGUIDE

M. L. Levin

Translated from Atomnaya Énergiya, Vol. 8, No. 2, pp. 134-135, February, 1960
Original article submitted June 20, 1959

In order to realize the method of accelerating plasma bunches which has been proposed in [1], it is necessary to investigate the stability of such bunches in the field produced by an accelerating wave. We shall limit our analysis to bunches which are small compared with the wavelength. In this case the field in the region occupied by the bunch is quasi-stationary and the electric field causes an electrostatic expansion of the bunch. On the other hand the magnetic field produces contraction forces in a conducting bunch. From this point of view it is desirable to accelerate a highly conducting bunch by using fields of symmetric TE modes in circular waveguide in which the only nonvanishing component at the axis of the tube is the longitudinal component of the magnetic field [2]. Having this purpose in mind we consider here the problem of deformation of an ideally conducting bunch in a quasi-stationary uniform magnetic field.

The following simple model is used. We first assume that the bunch remains a uniform sphere throughout the time considered and the axis of this sphere is parallel to the external field. As generalized coordinates we take the volume of a spheroid V and the ratio of the polar semi-axis to the equatorial axis q. Using the well-known solution of the problem of an ellipsoid in a uniform field [2] we can find the "magnetic" part $W_M(V,q)$ of the potential energy of the system. The hydrodynamic part of the potential energy $W_\Gamma(V)$ is determined from the Poisson equation $pV^\gamma = \text{const}$. Finally, making the assumption that the spheroid is uniform we can easily express the kinetic energy K in terms of V, q and $\dot{V}$, and $\dot{q}$:

$$W_M = \frac{2}{3}\frac{PV}{1-M(q)}; \quad W_\Gamma = \frac{PV_e}{\gamma-1}\left(\frac{V_e}{V}\right)^{\gamma-1};$$

$$K = \frac{m}{90}\left(\frac{3V}{4\pi q}\right)^{2/3}\left\{(q^2+2)\frac{\dot{V}^2}{V^2} + 4(q^2-1)\frac{\dot{V}}{V}\frac{\dot{q}}{q} + 2(2q^2+1)\frac{\dot{q}^2}{q^2}\right\},$$

where $P=3H_0^2/16\pi$ is the magnetic pressure averaged over the surface of the sphere (H_0 is the effective amplitude of the external field); M (q) is the diamagnetic factor (for a sphere M=1/3); $V_e = 4\pi a^3/3$ is the equilibrium volume for which p=P; m is the mass of the bunch. There is no equilibrium shape for the bunch since W_M is a monotonically decreasing function of q. The model which has been assumed is physically meaningful only as long as the velocities are small compared with the velocity of sound in plasma. Hence we can analyze only the initial stage of the deformation of the bunch. For example, let us assume that at the initial time the bunch is at rest and assumes the form of a sphere of volume V_0. Taking $q=1+\eta$, $V=V_0(1+x)$ and solving the linearized Lagrange equations for small values of η and x we have

$$\eta = \frac{3}{2}\nu\left(\frac{t}{\tau}\right)^2; \quad x = -\frac{15}{2}\nu(1-\nu^{-\gamma})\left(\frac{t}{\tau}\right)^2. \quad (1)$$

Under these conditions the radial velocities of the polar and equatorial points of the bunch are respectively

$$v_p = c\nu(5\nu^{-\gamma}-3)\frac{t}{\tau}; \quad v_e = c\nu(5\nu^{-\gamma}-6)\frac{t}{\tau} \quad (2)$$

where $c=(PV_e/m)^{\frac{1}{2}}$ is the isothermal velocity of sound; $\tau = a/c$; $\nu = V_0/V_e$. Eqs. (1) and (2) obviously apply when $t \ll \tau$. When $t \sim \tau$, acoustic oscillations are produced in the bunch and these have an important effect on stability.

Since the field in the waveguide is not uniform in the transverse direction, when the bunch is deflected from the axis, radial forces appear which act on the bunch as a whole. Let the transverse displacement r be small compared with the cross sectional radius of the waveguide but large compared with the dimensions of the bunch; then the external fields (electric and magnetic) in the region of the bunch may be assumed uniform and we find the forces which are of interest to us by the change in the quasi-static potential energy of the bunch in these fields. For a spheroid this force is

$$F_r = \frac{VH_0^2}{4\pi}\frac{\varkappa^2 + Mk^2}{1-M^2}r,$$

where k is the wave number and $\varkappa$ is the cut-off wave number. Thus, in the field of a symmetric TE mode the position of the bunch at the axis is unstable and an additional focusing field is required for radiation acceleration. At small values of r the defocusing force F_r is large compared with the focusing force F_z. For example, for a spherical

bunch of radius a, $F_r/F_z \geq 0.16\ r\bar{R}^2/\alpha^3$ (R is the waveguide radius).

We may note that in the field of a symmetric TM mode with an effective amplitude E_0 at the axis

$$F_r = -\frac{VE_0^2}{8\pi}\frac{(1+M)\varkappa^2 - 2M^2k^2}{M(1-M^2)}r,$$

so that with $k^2 < [(1+M)/2M^2]\varkappa^2$ (for a sphere $k < \sqrt{6}\varkappa$) the force becomes a focusing force. However, in this field there is an electrostatic expansion force which acts on the bunch.

LITERATURE CITED

1. V. I. Veksler, Atomnaya Énergiya 2, 5, 427 (1957)*
2. J. A. Stratton, Electromagnetic Theory [in Russian] (Moscow, Gostekhizdat, 1948).

*Original Russian pagination. See C. B. translation.

* * *

SELF-REPRODUCING SOLUTIONS OF THE PLASMA EQUATIONS

B. N. Kozlov

Translated from Atomnaya Énergiya, Vol. 8, No. 2, pp. 135-137, February, 1960
Original article submitted June 4, 1959

Electromagnetic containment of a completely ionized singly charged neutral plasma can be described by the following system of equations

$$\left.\begin{aligned}
&\operatorname{rot} \boldsymbol{E} = -\frac{\partial \boldsymbol{H}}{\partial t},\quad \operatorname{div} \boldsymbol{D} = 0,\quad \boldsymbol{D} = \varepsilon_0 \boldsymbol{E},\\
&\operatorname{rot} \boldsymbol{B} = \boldsymbol{i},\quad \operatorname{div} \boldsymbol{H} = 0,\quad \boldsymbol{B} = \mu_0 \boldsymbol{H},\\
&\boldsymbol{i} = \frac{1}{H^2}[\boldsymbol{H}\nabla P],\ \operatorname{div} \boldsymbol{J} + \frac{\partial N}{\partial t} = 0,\\
&\boldsymbol{J} = N\frac{[\boldsymbol{EH}]}{H^2} - \frac{\nu}{m\omega^2}\nabla P,\\
&P = 2NkT,\quad \nabla T = 0,\quad \boldsymbol{H}\nabla P = 0,
\end{aligned}\right\} \qquad (1)*$$

where

$$\omega = \frac{e}{m}H,\quad \nu = \frac{e^2 a}{m\mu_0}\frac{N}{T^{3/2}},$$

$$a = \frac{4\sqrt{2\pi}}{3}\frac{m^{1/2}\mu_0}{e^2 k^{3/2}}\left(\frac{e^2}{4\pi\varepsilon_0}\right)^2 \Lambda,\quad \Lambda = \ln\frac{p_{\max}}{p_{\min}} \approx 20.$$

The plasma temperature T is assumed to be a given function of the time T(t).

The boundary conditions at the plasma surface Σ are written in the form

$$N|_\Sigma = 0,\quad \boldsymbol{H}|_\Sigma = \boldsymbol{H}_1(t). \qquad (2)$$

It follows from Eq. (1) that

$$\nabla P + \nabla Q = (\boldsymbol{H}\nabla)\boldsymbol{B}, \qquad (3)$$

where

$$Q = \frac{1}{2}\boldsymbol{HB}.$$

The problem of electromagnetic containment of a plasma expressed by Eqs. (1) and (2) does not have stationary solutions or solutions with stationary density distribution, but does have self-reproducing solutions. Generally speaking, there are self-reproducing solutions for the system in (1) for a cylindrical plasma pinch. However, the most interesting case is the one in which the field is concentrated in a thin surface layer of the plasma so that the thickness of the electromagnetic surface layer is much smaller than the radius of the pinch. Under these conditions the curvature of the field is unimportant and the problem can be formulated as follows. We consider a plasma semi-space $x \leq l$, which is in contact with a vacuum at the plane $x = l$ and is contained by an electromagnetic field which partially penetrates the surface layer of the plasma and vanishes at $-\infty$ inside the plasma. All quantities depend only on the coordinate x. We wish to find the distribution of plasma and field as a function of time. This problem reduces to the single equation

$$\left[\left(\frac{a}{T^{3/2}}\frac{\psi''}{\psi'} - \frac{\dot{\psi}}{\psi'}\right)(H_1^2 - \psi'^2)\right]' + T\left(\frac{H_1^2 - \psi'^2}{T}\right)^{\cdot} = 0 \qquad (4)$$

*The meaning and notation of the vectors H and B are reversed as compared with the usual meaning: in a medium the intensity H is the average value of the microscopic intensity.

with the boundary conditions

$$\psi(-\infty, t)=0,\ \psi'(-\infty, t)=0,\ \psi'(l, t)=H_1(t) \quad (5)$$

(H_1 is the given value of the magnetic field H at the plasma surface).

We use the function $\psi=\int_{-\infty}^{x} H(x,t)\,dx$ ("quasi-potential of the field") to express all quantities which characterize the plasma and the field:

$$\left.\begin{aligned} &H_y=h_y(t)\,\psi'(x,t),\ H_z=h_z(t)\,\psi'(x,t),\\ &E_y=-(h_z(t)\,\psi(x,t))^{\cdot},\\ &E_z=(h_y(t)\,\psi(x,t))^{\cdot},\ h_y^2(t)+h_z^2(t)=1,\\ &E_\perp=-\psi^{\cdot},\ S=-\mu_0\psi'\psi^{\cdot},\ i=\mu_0\psi''. \end{aligned}\right\} \quad (6)$$

The primes are used to denote differentiation with respect to x while the dots denote differentiation with respect to t; S is the x-component of the Poynting vector.

The solution of Eq. (4) is written in the form

$$\psi(x,t)=f(t)\,\varphi\left(\frac{x}{l(t)}\right)\equiv f(t)\,\varphi(\xi),$$

where $\xi=x/l(t)$ while $l(t)$ is the coordinate of the plasma boundary, which varies with time.

There are self-reproducing solutions if the plasma temperature T and the magnetic field at the plasma surface H_1 vary according to a power law (p.l.) or an exponential law (e.l.):

$$\left.\begin{aligned} &T=C_T t^{\gamma_T},\quad H_1=C_H t^{\gamma_H},\quad (\text{p.l.})\\ &T=C_T e^{\lambda_T t},\quad H_1=C_H e^{\lambda_H t}.\quad (\text{e.l.}) \end{aligned}\right\} \quad (7)$$

In these cases the dependence of l and f on t is expressed by the formulas

$$\left.\begin{aligned} &l=C_l t^{\gamma_l},\qquad f=C_l C_H t^{\gamma_f},\\ &\gamma_l=\frac{1}{2}-\frac{3}{4}\gamma_T,\quad \gamma_f=\frac{1}{2}-\frac{3}{4}\gamma_T+\gamma_H, \end{aligned}\right\} \quad (\text{p.l.})$$

$$\left.\begin{aligned} &l=C_l e^{\lambda_l t},\qquad f=C_l C_H e^{\lambda_f t},\\ &\lambda_l=-\frac{3}{4}\lambda_T,\quad \lambda_f=-\frac{3}{4}\lambda_T+\lambda_H, \end{aligned}\right\} \quad (\text{e.l.}) \quad (8)$$

while the function $\varphi(\xi)$ is defined by the equation

$$(1-\varphi'^2)\,\varphi'\varphi'''-(1+\varphi'^2)\,\varphi''^2+b(1-\varphi'^2)\,\varphi'^2+ c(1+\varphi'^2)\,\varphi\varphi''=0, \quad (9)$$

where

$$\left.\begin{aligned} &b=(\gamma_H-\gamma_T)\frac{C_T^{3/2}C_l^2}{a},\\ &c=\left(\frac{1}{2}-\frac{3}{4}\gamma_T+\gamma_H\right)\frac{C_T^{3/2}C_l^2}{a}, \end{aligned}\right\} \quad (\text{p.l.})$$

$$\left.\begin{aligned} &b=(\lambda_H-\lambda_T)\frac{C_T^{3/2}C_l^2}{a},\\ &c=\left(-\frac{3}{4}\lambda_T+\lambda_H\right)\frac{C_T^{3/2}C_l^2}{a}, \end{aligned}\right\} \quad (\text{e.l.}) \quad (10)$$

with the boundary conditions

$$\left.\begin{aligned} &\varphi_0\equiv\varphi(-\infty)=0,\ \varphi_1\equiv\varphi(1)\equiv\alpha,\\ &\varphi_0'\equiv\varphi'(-\infty)=0,\quad \varphi_1'\equiv\varphi'(1)=1. \end{aligned}\right\} \quad (11)$$

The subscript "0" denotes values of the quantities inside the plasma for $\xi=\xi_0=-\infty$ while the subscript "1" denotes values at the surface of the plasma with $\xi=\xi_1=1$.

The following expressions are obtained for the quantities which characterize the plasma and the field

$$\left.\begin{aligned} &H=C_H t^{\gamma_H}\varrho,\ E_\perp=C_l C_H t^{\gamma_f-1}(\gamma_l\xi\varrho-\gamma_f\varphi),\\ &i=\mu_0\frac{C_H}{C_l}t^{\gamma_H-\gamma_l}\varrho',\\ &S=\mu_0 C_l C_H^2 t^{\gamma_H+\gamma_f-1}(\gamma_l\xi\varrho-\gamma_f\varphi)\varrho, \qquad (\text{p.l.})\\ &P=\frac{1}{2}\mu_0 C_H^2 t^{2\gamma_H}(1-\varrho^2),\\ &N=\frac{1}{4}\mu_0\frac{C_H^2}{C_T}t^{2\gamma_H-\gamma_T}(1-\varrho^2),\\ &J=\frac{1}{4}\mu_0 a\frac{C_H^2}{C_l C_T^{5/2}}t^{2\gamma_H-\frac{7}{4}\gamma_T-\frac{1}{2}}\times\\ &\quad\times\left[\frac{\varrho'}{\varrho}+\left(\gamma_l\xi-\gamma_f\frac{\varphi}{\varrho}\right)\frac{C_l^2C_T^{3/2}}{a}\right](1-\varrho^2);\\ &H=C_H e^{\lambda_H t}\varrho,\quad E_\perp=C_l C_H e^{\lambda_f t}(\lambda_l\xi\varrho-\lambda_f\varphi),\\ &i=\mu_0\frac{C_H}{C_l}e^{(\lambda_H-\lambda_l)t}\varrho',\\ &S=\mu_0 C_l C_H^2 e^{(\lambda_H+\lambda_f)t}(\lambda_l\xi\varrho-\lambda_f\varphi)\varrho,\\ &P=\frac{1}{2}\mu_0 C_H^2 e^{2\lambda_H t}(1-\varrho^2),\\ &N=\frac{1}{4}\mu_0\frac{C_H^2}{C_T}e^{(2\lambda_H-\lambda_T)t}(1-\varrho^2), \qquad (\text{e.l.})\\ &J=\frac{1}{4}\mu_0 a\frac{C_H^2}{C_l C_T^{5/2}}e^{(2\lambda_H-\frac{7}{4}\lambda_T)t}\times\\ &\quad\times\left[\frac{\varrho'}{\varrho}+\left(\lambda_l\xi-\lambda_f\frac{\varphi}{\varrho}\right)\frac{C_l^2C_T^{3/2}}{a}\right](1-\varrho^2). \end{aligned}\right\} \quad (12)$$

Here we have introduced the function

$$\varrho(\xi)=\varphi'(\xi). \quad (13)$$

A qualitative analysis of Eq. (9) and the boundary conditions in Eq. (11) verifies that the functions φ and ρ are monotonic. In the vicinity of $\xi=1$ we have the only

regular solution of Eq. (9) which, with the boundary conditions given in (11), is expressed by the following expansion:

$$\varphi=\alpha-(1-\xi)+\frac{1}{2}\alpha c\,(1-\xi)^2+\frac{1}{12}(b-c)(1-\xi)^3-$$
$$-\frac{1}{288}\frac{b^2-c^2+2\alpha^2c^2(5b-c)}{\alpha c}(1-\xi)^4+\ldots$$
$$\ldots \text{ for } c\neq 0, \qquad (14a)$$

$$\varphi=\alpha-(1-\xi)+\frac{1}{18}b(1-\xi)^3-$$
$$-\frac{b^2}{540}(1-\xi)^5+\ldots \text{ for } c=0. \qquad (14b)$$

The special class of solutions given in Eq. (14b) can be written in exact form by means of quadratures. These solutions describe the expansion of the plasma in the case in which the following condition is satisfied:

$$l^*=\frac{1}{\mu_0}\frac{S_1}{H_1^2}, \qquad (15)$$

which means that particles at the surface of the plasma move with the electromagnetic drift velocity. From Eqs. (8), (12) and (15) (with $\xi=1, \rho=1$) it follows that $\gamma_f=0$, $\lambda_f=0$; this result together with Eqs. (8) and (10) leads to the condition $c=0$.

Under these conditions Eq. (9) becomes a condition in the equation for $\rho=\varphi'$:

$$(1-\varrho^2)\varrho\varrho''+(1+\varrho^2)\varrho'^2+b(1-\varrho^2)\varrho^2=0, \qquad (16)$$

where

$$\left.\begin{aligned} b&=\frac{1}{3}(\gamma_f-2)\frac{C_l^2C_T^{3/2}}{a} \quad \text{(p.l.)}\\ b&=\frac{1}{3}\lambda_l\frac{C_l^2C_T^{3/2}}{a} \quad \text{(e.l.)}\end{aligned}\right\} \qquad (17)$$

We introduce the variables $z=\rho^2$, $y=(1/b)\cdot\rho'^2$ and Eq. (16) is transformed into the equation

$$(1-z)z\frac{dy}{dz}-(1+z)y+(1-z)z=0. \qquad (18)$$

The points $z=1$, $y\neq 0$ become ordinary points for this equation and the single solution $z\equiv 1$ passes through these points; it has no physical significance. The solution being sought passes through the singularity point $z=1$, $y=0$ (saddle point) where one of the solutions is $z=1$ and is devoid of physical meaning. The solution of the Eq. (18) which passes through the point $z=1$, $y=0$ is the function

$$y=-\frac{z}{(1-z)^2}\left(\ln z-2z+\frac{1}{2}z^2+\frac{3}{2}\right), \qquad (19)$$

whence

$$\frac{d\varrho}{d\xi}=\sqrt{b}\,\frac{\varrho}{1-\varrho^2}\sqrt{2\varrho^2-\ln\varrho^2-\frac{1}{2}\varrho^4-\frac{3}{2}}. \qquad (20)$$

Here we take the positive sign in front of the radical because from the boundary conditions and the fact that ρ is a monotonic function it follows that the derivative $d\rho/d\xi$ is always positive. Since the function $2\rho^2-\ln\rho^2-\rho^4/2-3/2$ is positive over the whole range of variation of ρ

$$(0\leqslant\varrho\leqslant 1)$$

it follows that $b>0$. Together with Eqs. (8), (10) and (17) this result gives

$$\gamma_l>2,\ \gamma_H<-2,\ \gamma_T<-2,\ \gamma_f=0 \quad \text{(p.l.)},$$
$$\lambda_l>0,\ \lambda_H<0,\ \lambda_T<0,\ \lambda_f=0 \quad \text{(e.l.)}.$$

The special solution in Eq. (14b) thus describes the expansion of the plasma with a reduction of the magnetic field and cooling of the plasma.

The solution of Eq. (20) is of the form

$$\xi=1-\frac{1}{\sqrt{b}}I(\varrho), \qquad (21)$$

$$I(\varrho)=\frac{1}{2}\int_0^{1-\varrho^2}\frac{x\,dx}{(1-x)\sqrt{-\ln(1-x)-x-\frac{1}{2}x^2}}. \qquad (22)$$

The values of $I(\rho)$ are given in the table. The integral in Eq. (22) is given approximately by the expression

$$I(\varrho)\simeq\sqrt{6(1-\varrho)},$$

which gives a fairly accurate dependence for $I(\rho)$ up to $\rho=0.5$, and, in conjunction with Eq. (21), gives the value $\varrho\simeq\frac{1}{6}b(1-\xi)^2$, which is in agreement with the expansion in Eq. (14b). A comparison of the expansion in Eq. (14a) with the results of an accurate numerical calculation shows that it gives an accurate solution of Eq. (9) up to $\rho=0.5$.

I am happy to thank V. N. Klimov for a number of valuable discussions and N. I. Kozlov for help in the mathematical calculations.

Values of the Function $I(\rho)$

ϱ	1	0,9	0,80	0,70	0,60	0,50	0,40	0,30	0,20	0,10
$I(\varrho)$	0	0,70	1,02	1,26	1,53	1,76	2,00	2,25	2,55	2,96

* * *

COMPLEX FISSION OF URANIUM BY 2.5-MEV NEUTRONS

Z. I. Solov'eva

Translated from Atomnaya Énergiya, Vol. 8, No. 2, pp. 137-138,
February, 1960
Original article submitted June 29, 1959

Complex fission of heavy nuclei with the formation of a long-range α-particle under the effect of slow or thermal neutrons has been studied by a number of authors. However, complex fission due to high-energy neutrons is essentially unstudied. The negative result obtained in [1] has been taken as an indication of the fact that this fission is characteristic of U^{235} and is related to the low-lying excitation levels of the fissionable nuclei. However, more recently complex fission has been observed in uranium under bombardment by 2.5-Mev neutrons [2] and 14-Mev neutrons [3].

In the present note we investigate complex fission of uranium nuclei by 2.5-Mev neutrons.

A P-9 emulsion (with good discrimination for different charged particles) was saturated with uranium salt [4% water solution of $UO_2Na(C_2H_3O_2)_3$ — with a natural isotopic abundance] and exposed to neutrons. In order to eliminate the slow-neutron background the plates were placed in a cadmium cylinder with a boron cover. The exposure time was chosen to make the background of secondary particles easy to scan.

In scanning the plates we recorded cases of complex fission in uranium and the total number of binary fission events. In all, fifty cases of ternary fission were found for approximately 30,000 binary fission events, i.e. the probability for complex fission with the formation of a long-range α-particle is 1:600 with respect to binary fission.

Comparing the value with the corresponding values for complex fission of uranium by thermal neutrons (approximately 1:350) and for 14-Mev neutrons (approximately 1:1100) [3] it may be concluded that an increase in excitation energy causes a reduction in the probability for this rare process. It should be kept in mind, however, that U^{235} fissions under the effect of thermal neutrons and in the experiments with fast neutrons the fissioning nucleus is principally U^{238}.

A control experiment was carried out to determine whether there is any change in the probability for ternary fission with a change in the isotopic composition of the uranium. The plate was saturated with uranium salt containing U^{235} in an amount approximately five times smaller than in a natural isotopic mixture and was exposed to 2.5-Mev neutrons. No noticeable difference in the probability for ternary uranium fission was found for a different U^{235} content; from this result it may be concluded that the cases of ternary fission which were observed are due to U^{238}.

The general data for the complex fission process for 2.5-Mev neutrons is not essentially different from the data for neutrons with other energies:

a) The fission is asymmetric; the mean range ratio for the heavy and light fragments is $R_L/R_H = 1.3$;

b) The angular distribution of the α-particles with respect to the direction of emission of the light fragment shows a small departure from 90° in the direction of the light particle (Fig. 1);

c) The distribution of α-particles in range in the emulsion shows a wide maximum at $R_\alpha = 130\,\mu$ (Fig. 2) corresponding to an energy of 16 Mev.

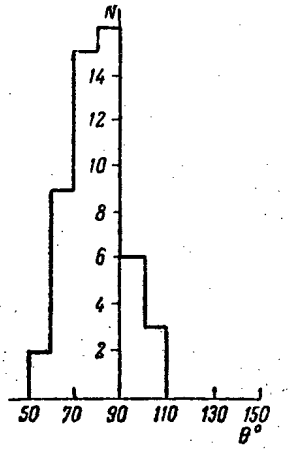

Fig. 1. Angular distribution of α particles with respect to the direction of emission of the light fragment.

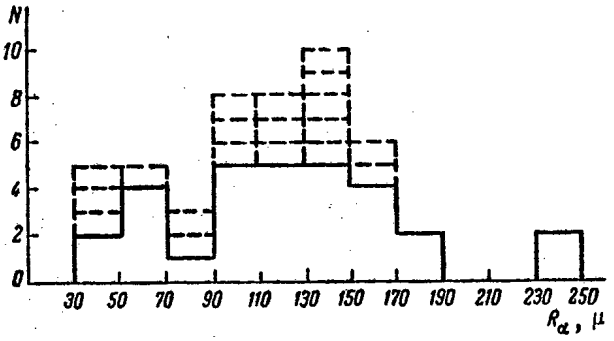

Fig. 2. Range distribution for α particles formed in fission of uranium by 2.5-Mev neutrons: ___) tracks which end outside the emulsion.

In conclusion the author wishes to thank N. A. Perfilov for his interest in this work.

LITERATURE CITED

1. Tsien San-tsiang, R. Chastel, Ho Zah-wei, and L. Vigneron, J. phys. et radium 8, 165 and 200 (1947).
2. E. Titterton. Phys. Rev. 83, 673 (1951).
3. N. A. Perfilov and Z. I. Solov'eva, Atomnaya Énergiya 5, 2, 175 (1958). *

*Original Russian pagination. See C. B. translation.

* * *

FISSION CROSS SECTIONS FOR Th^{230}, Pu^{240}, Pu^{241}, and Am^{241} BY NEUTRONS WITH ENERGIES OF 2.5 AND 14.6 MEV

M. I. Kazarinova, Yu. S. Zamyatin, and V. M. Gorbachev

Translated from Atomnaya Énergiya, Vol. 8, No. 2, pp. 139-141,
February, 1960
Original article submitted August 8, 1959

Measurements of fast-neutron fission cross sections carried out in recent years have made it possible to establish an empirical dependence for the relative probability of fission for a nucleus $f=\sigma_f/\sigma_c$ as a function of the parameter Z^2/A [1,2]. This empirical relation indicates that f falls off monotonically as the mass number A increases for each of the fissioning elements, and increases rapidly with increasing Z.

However, the dependence of f on A (for constant Z) has been investigated in adequate detail only in uranium. For this reason we still do not have a complete picture of the dependence of f on Z. We have reason to believe that the relation of f on Z is weaker than a function of the form Z^2/A [1,3]. In order to investigate this question and in order to obtain a more accurate dependence of f on A for thorium and plutonium, we have carried out measurements of the fission cross sections in Th^{230}, Pu^{240}, Pu^{241} and Am^{241} for fission induced by neutrons with energies of 2.5 and 14.6 Mev. These neutrons were obtained from deuterium and tritium targets which were bombarded by a deuteron beam with an energy of 150-200 kev. The fission events were recorded by means of a fission chamber with electron collection.

The isotopic composition of the thorium and americium was determined by a mass-spectrometer method while the content of the Pu^{239} isotope in the Pu^{240} layer was determined by "weighing" the layer in a thermal neutron flux. The amount of Am^{241} formed in the Pu^{241} layer as a result of β decay was determined by the known accumulation time. There were no other isotopes present in the Am^{241} layer.

The amount of the isotopes Th^{230}, Pu^{240} and Am^{241} in the layers was determined by counting the α particles emitted by these isotopes. In addition, the Pu^{240} content in the layer was determined by the number of spontaneous fission events while the Pu^{241} content was determined by counting the α particles from Am^{241}. Pu^{241} layer was also "weighed" in a thermal neutron flux. In this case the cross section for fission of Pu^{241} by thermal neutrons was taken as 1025 ± 10 barns. The results of the measurements of the weight of Pu^{240} and Pu^{241} by both methods coincided to within the limits of the experimental accuracy. The isotopic composition of the layers and the values of the weights are shown in Table 1 where we also give the values of the decay periods which were used in determining the weights.

The cross sections for fission by 14.6-Mev neutrons were measured by an absolute method. In this case the neutron flux was determined by counting the α particles produced in the T (d,n) He^4 reaction and the scattered neutron background was measured by carrying out measurements at various distances between the chamber and the neutron souce. All measurements were carried out several times; a statistical accuracy of at least 2–3% was obtained in each measurement.

Absolute measurements of the cross sections for fission by 2.5 -Mev neutrons could not be carried out because of the slow counting rate. Relative measurements were carried out in a double fission chamber in which, in addition to the layer of material being investigated, there was a layer with a known cross section for fission by neutrons with this energy. The measurement of the cross sections for fission in Th^{230} were carried out with respect to that for Th^{232}, the measurements of the cross sections for Pu^{240}, Am^{241} and Pu^{241} were carried out with respect to U^{238}. For control purposes, measurements were also made of the Am^{241} cross section with respect to U^{235}.

A long counter was used to monitor the 2.5-Mev neutron flux.

The values of the cross sections for the 2.5-Mev neutrons were also determined with respect to the known fission cross section for a given isotope for fission by 14.6-

TABLE 1. Characteristics of the Layers of the Investigated Isotopes

Isotope	Effective weight, micrograms	Half-decay period, years	Isotopic composition
Th^{230}	(1870±40)	$8 \cdot 10^4$ [4]	(35±1)% Th^{230}; (65±1)% Th^{232}
Pu^{240}	(345±15)	$6,6 \cdot 10^3$ [4]; $T_{1/2}$spont = $= 1,2 \cdot 10^{11}$ [5]	15% Pu^{239}; 85% Pu^{240}
Pu^{241}	(50,6±1,6)	13,2 [6]	12% Am^{241}; 88% Pu^{241}
Am^{241}	(89±2)	458±0,5 [6]	100% Am^{241}

TABLE 2. The Fission Cross Section σ_f for Neutrons with Energies of 2.5 and 14.6 Mev, barns.

Isotope	2,5 Mev		14,6 Mev		
	results of the present work	data reported by other authors	results of the present work	data reported by other authors	** σ_{f_1}
Th^{230}	0,41±0,08	—	0,72±0,15	—	0,90
Pu^{240}	1,6 ±0,3	1,5±0,15 [7]	2,4 ±0,3	2,6 ±0,2* [7]	2,55
Pu^{241}	1,2 ±0,2	—	2,05±0,1	—	2,15
Am^{241}	1,95±0,2	1,35 [4]	2,95±0,15	2,35±0,15 [8]	2,85

* Fission cross section for 15–Mev neutrons.

** Fission cross section at the second plateau computed from Eq. 1.

Mev neutrons. In these measurements use was also made of the ratio of the fission cross sections for the material and the monitor for neutrons with energies of 2.5 and 14.6 Mev in which case the fission cross section for Th^{232} was taken as 0.13 and 0.34 barns while the fission cross section for U^{238} was taken as 0.58 and 1.1 barns respectively [4].

The cross sections for fission by 2.5-Mev neutrons as obtained by both methods were found to be the same within the limits of experimental error for all the isotopes which have been investigated. The cross sections are shown in Table 2 (the measurements of the fission cross sections for Pu^{240} were carried out in conjunction with I. M. Izrailev). This table also contains the results of the measurements of σ_f carried out by other authors.

In estimating the accuracy of the measurements, special attention was given to an analysis of possible errors in the determination of the fission cross sections for Am^{241}, which do not agree with the results obtained by other authors. However, no significant measurement errors were found.

Discussion of the results. A comparison of the fission cross sections for Th^{230}, Pu^{240} and Pu^{241} for fission by 2.5 Mev neutrons with the analogous cross sections for other isotopes of the same elements verifies the tendency which has been observed earlier for a reduction in the fission cross section and the ratio of f with an increase in mass number of the isotope (for fixed Z). This variation in the relative fission probability is associated with a reduction in the neutron binding energy in the nucleus and corresponds to an increase in the probability for neutron evaporation in the compound nucleus; this process competes with the fission process. From this point of view it is somewhat strange that there is no noticeable odd-even effect in the funtion f (A) since it is known that the binding energy E_b depends on whether A is even or odd.

The values of the cross sections which have been obtained show also that f is not a unique funtion of the parameter Z^2/A since the values of f for each element lie on their own curve (cf. Figure). Attempts to choose another parameter of the type Z^n/A which would be a weaker function of Z than Z^2/A in order to obtain a

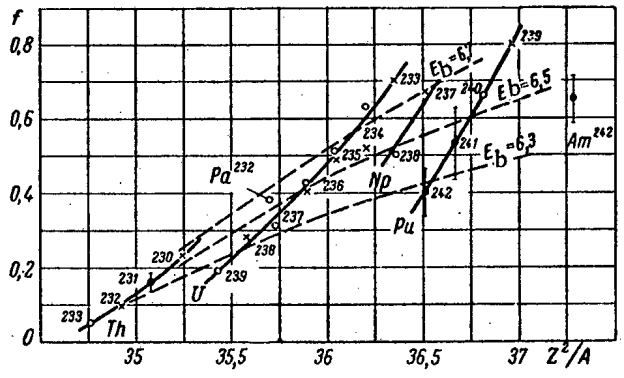

Dependence of the relative probability for fission f on the parameter Z^2/A: O) Neutron fission; x) photofission (the points O and x are taken from [1] and are corrected for newly published data on fission cross sections); ⧫ is data of the present work. The dashed line shows measurements of f (Z^2/A) for various values of the binding energy.

TABLE 3. Dependence of Neutron Binding Energy in the Nucleus on Z for a Given Z^2/A, Mev.

Z^2/A							
35,25		35,5		36,2		36,5	
—	—	Th^{228}	7,0	—	—	U^{232}	7,1
Th^{230}	6,7	Pa^{233}	6,6	U^{234}	6,7	Np^{237}	6,7
Pa^{235}	6,3	—	—	Np^{239}	6,3	Pu^{242}	6,2
—	—	U^{238}	6,0	—	—	—	—
U^{240}	5,8	—	—	—	—	—	—

single dependence for all isotopes of all elements have not been successful. It is found that different elements require different values of n. For example, in order to get the same curves for thorium, protactinium and uranium the index n must have the value 1.7; to get agreement between uranium, neptunium and plutonium a value of 1.2 is required while to get the same values of f for Am^{242} and plutonium a value of 0.8 is required.

It should be noted that the weak dependence of f on Z is apparently due to the fact that f, which is a function of Z^2/A, which characterizes the fission process is affected by the probability for neutron evaporation from the compound nucleus which, in turn, depends on the neutron binding energy. For a given value of Z^2/A and a given odd (even) nuclide an increase in Z causes a reduction in binding energy (Table 3) and consequently an increased probability for neutron evaporation; the relatively small relative probability for fission of isotopes of elements with large Z thus becomes understandable. Whence it follows that by considering nuclides with the same values of E_b we can eliminate the effect of neutron evaporation and the dependence of $f(Z^2/A)$, is determined only by the fission process (cf. Figure).

The values of the fission cross sections for 14.6-Mev neutrons obtained in this work can be compared with the expected magnitude of the fission cross section at the second plateau [1]:

$$\sigma_{f_1} = \sigma_{f_0}\left[1+\frac{(1-f_0)f_{-1}}{f_0}\right]$$

The values of σ_{f_1} computed from this formula are given in Table 2. If in making this comparison, we take account of the possibility of the appearance of a new channel which leads to fission of the nucleus, the (n, 2nf) reaction, whose energy threshold lies somewhat below 14 Mev, and the possibility of slope in the plateau because of a different rate of increase of the fission with Γ_f and the neutron with Γ_n with energy, the agreement may be considered quite good. The more marked difference in the case of Th^{230} may be attributed to the lower accuracy in the determination of the fission cross section for this case.

We wish to express our gratitude to B. V. Kurchatov, M. I. Pevzner, G. N. Yakovlev, E. P. Dergunov and S. K. Sokolov for furnishing the isotopes and for fabrication of the layers; I. A. Tishchenko and G. M. Kukavadze for carrying out the mass-spectrometer analysis; Yu. A. Vasil'ev and E. I. Sirotin for making the measurements at the accelerator. The authors are also indebted to M. S. Shvetsov, Yu. A. Barashkov and E. D. Beregovenko for help in carrying out the measurements.

LITERATURE CITED

1. Yu. S. Zamyatin, Physics of Fission Supp. No. 1, Atomnaya Énergiya, (Moscow, Atomizdat, 1957) p. 27.
2. J. Huizenga, Phys. Rev. 109, 484 (1958).
3. R. Leachman, U. S. Reports to Second International Conference on the Peaceful Uses of Atomic Energy (Geneva, 1958), Report No. 2467.
4. D. Hughes and R. Schwartz, Neutron Cross Sections (New York, BNL, 1958).
5. M. Studier and J. Huizenga, Phys. Rev. 96, 545 (1954).
6. D. Hall and T. Markin, J. Inorg. and Nucl. Chem. 4, 137, (1957).
7. V. G. Nesterov and G. N. Smirenkin, Zhur. Éksp. Teoret. Fiz. 35, 532 (1958).
8. A. N. Protopopov, Yu. A. Selitskii and S. M. Solovev, Atomnaya Énergiya 6, 1,67 (1959). •

• Original Russian pagination. See C. B. translation.

* * *

ANALYSIS OF NEUTRON INTERACTION WITH He^4, C^{12}, AND O^{16} NUCLEI USING AN OPTICAL NUCLEAR MODEL

É. Ya. Mikhlin and V. S. Stavinskii

Translated from Atomnaya Énergiya, Vol. 8, No. 2, pp. 141-143
February, 1960
Original article submitted May 30, 1959

The analysis of low-energy neutron interactions with He^4, C^{12}, and O^{16} nuclei holds great interest not only from the point of view of light-nucleus theory, but also because it has great practical value in calculating the transport properties of the most effective moderators for certain heavy nuclei.

The first application of the optical model using low energies and a complex potential was limited to heavy

TABLE 1. Values of R_0, V_0, α_l

Compound nucleus	Wave state	R_0, $cm \cdot 10^{-13}$	V_0, Mev	α_l, Mev	Experimental data used
He^5	s	2,46	38,5		For low energies σ_t=0.8 barn, phase analysis
	$p_{3/2}$ / $p_{1/2}$	3,2	22,5 / 15,0	5,0	$P_{3/2}$-resonance for E = 1.15 ± 0.05 Mev; Γ = 1.4 ± 0.2 Mev / Phase analysis
C^{13}	s	2,75	70		For low energies σ_t=4.7 barns, binding energy of the 2s-state 1.86 Mev
	$p_{3/2}$ / $p_{1/2}$	3,0	37,5 / 33,0	3,0	Level $^3/_2^-$ with excitation energy 3.69 Mev considered as an "unfilled gap" / Binding energy of the ground state $p_{1/2}$ 4.95 Mev; phase analysis
	$d_{5/2}$ / $d_{3/2}$	3,3	43 / 35	3,2	Binding energy of the $d_{5/2}$-level 1.09 Mev / $d_{1/2}$-resonance for E = 3.65 Mev; Γ = 1.2 Mev
	$f_{7/2}$	3,7	29		Position and shape of the cross section maximum for 20 Mev
O^{17}	s	4,0	37,6		Binding energy of the 2s-level 3.27 Mev; for E≤0.1 Mev; σ_t=3.5 barns; s-resonance for E=2.44 Mev
	$p_{3/2}$ / $p_{1/2}$	4,0	29,6 / 24,4	3,5	Level $^3/_2^-$ with excitation energy 7.6 Mev considered as an "unfilled gap"; phase analysis / Level $^1/_2^-$ with excitation energy 3.06 Mev considered as an "unfilled gap"; phase analysis
	$d_{5/2}$ / $d_{3/2}$	4,0	34,01 / 25,88	3,25	Binding energy of the ground state $d_{5/2}$ 4.14 Mev / $d_{3/2}$-resonance for E = 1.00 Mev, Γ = 0.1 ± 0.01 Mev
	$f_{7/2}$	4,7	33,2		Binding energy of the $f_{7/2}$-level 0.29 Mev, maximum in the cross section for 20 Mev

and intermediate nuclei [1]. In the present work we have tried to use the optical model for a detailed description of elastic neutron scattering by the light nuclei He^4, C^{12} and O^{16} for energies up to ~20, ~10, and ~6 Mev, respectively. The smallness of the incident neutron absorption cross section in the energy region under investigation permits us to use actual potentials.

The average potential acting on the neutron from the target-nucleus direction appears as a function decreasing smoothly toward the nuclear boundary. Within the energy interval under investigation we can replace the actual average potential with an effective rectangular potential function in order to simplify the calculations. This substitiution is justified because the wave length of the incident neutron is long with respect to the dimensions of major potential changes in this energy region. Furthermore, the spin-orbital interaction was accounted for as a constant term $a_l(\vec{l}, \vec{S})$ which increased the depth of the rectangular potential well.

In using such a simplified calculation scheme one must bear in mind two important circumstances. Firstly, the average potential may not be identical for various partial waves. Secondly, within the region of the centrifugal force barrier the neutrons having large angular momentum l will tend to be displaced toward the outer edge of the nucleus, and will thus spend a greater portion of their time in the potential "tail." This leads to decrease of the depth of the effective rectangular potential well with increasing l, and to increase of the radius. The latter circumstance is however only valid for light nuclei, whose dimensions are comparable to the region of rapid potential change. One of the main results forthcoming from our analysis is the fact that for a satisfactory description of elastic neutron scattering by the nuclei mentioned above it was necessary to abandon the idea of a single rectangular potential valid for all partial waves involved in the scattering phenomenon.

The rectangualr potential parameters for each partial wave were selected in such a way as to give not only the position and width of the single-particle resonances observed in the total cross section*, but also the binding energy of the corresponding single-particle bound states.

For the case of a rectangular potential well (radius R_0, depth V_0) the scattering phase is a known function of R_0 and V_0: $\delta_{l\pm1/2} = \delta_{l\pm1/2}(x, X)$,

*We shall denote by the designation "single-particle" those states of the compound nucleus which correspond to motion of the external nucleon in the central field of the residual nucleus in its ground state. The reduced width of such a level must be of the order of a Wigner single-particle range.

where

$$x=\sqrt{\frac{2ME}{\hbar^2}}R_0;\quad X=\sqrt{\frac{2\mu}{\hbar^2}(E+V_0)}R_0;$$

μ is the reduced mass of the system neutron-target nucleus; E is the kinetic energy of this system in the center-of-mass coordinate system.

On the other hand, the width of a single-particle state is likewise a function of x and X: $\Gamma_{l\pm\frac{1}{2}}=\Gamma_{l\pm\frac{1}{2}}(x,X)$. By knowing the position and width of the observed single-particle resonances, we can obtain two conditions needed to determine the two parameters V_0 and R_0. Futhermore we can easily obtain additional information regarding the values of V_0 and R_0 from the known magnitude of the cross section at low energies and from the position of the bound single-particle levels, since both these quantities depend in a simple manner on the parameters of the rectangular potential well.

Table 1 gives the values obtained for V_0, R_0 and a_l and also the experimental data [2,3] used to obtain these values. These values of R_0 and V_0 were used to calculate the scattering phases, and further to calculate the total cross sections and the angular distribution for elastic neutron scattering by the nuclei under investigation. The Breit-Wigner formula was used to calculate the contribution due to non-single-particle resonances.

The calculation reproduces the general run of total cross sections quite well. The angular distribution shows certain deviations from the distribution measured for carbon and oxygen. This deviation is attributed to inaccuracy in determining V_0 and R_0 for the p-wave, since in the absence of other information these parameters were determined from the positions of the corresponding "unfilled gap" levels [4]. In such a case there could be large deviations for individual particles from our model, thus causing errors in the determination of these parameters.

As can be seen from Table 1, the values of the parameters V_0 and R_0 differ greatly for various partial waves. Furthermore, each pair of values of V_0 and R_0 permits us to describe both the position of the bound states and also the scattering within a wide energy range.

The latter circumstances permitted us to calculate the angular distribution of elastic neutron scattering by C^{12} and O^{16} for those neutron energies for which experimental data is lacking. On the basis of the angular distribution there was obtained the mean cosine of the scattering angle ($\langle\cos\theta\rangle$) and the mean logarithm of the energy loss ξ, shown in Table 2.† Calculations of the distance required in water for neutron deceleration, made on the basis of the data in this table, agree satisfactorily with the experimental results of [5].

Thus, the above analysis shows that the optical model using the effective potential does satisfactorily describe elastic scattering of neutrons of sufficiently low energy by the light nuclei He^4, C^{12}, and O^{16}. This is obviously related to the unusual stability of the nuclei in question.

TABLE 2. Values of $\langle\cos\theta\rangle$ and ξ

O^{16}			C^{12}		
E_n, Mev	$\langle\cos\theta\rangle$	ξ	E_n, Mev	$\langle\cos\theta\rangle$	ξ
0,41	−0,09	0,136	0,55	0,11	0,148
0,435	0,276	0,091	1,0	0,13	0,145
0,48	0,49	0,064	1,5	0,19	0,135
0,7	0,15	0,106	2,0	0,16	0,140
0,9	0,079	0,115	2,07	0,09	0,151
1,03	0,059	0,118	2,5	0,16	0,140
1,1	0,037	0,120	2,9	0,18	0,137
1,32	0,42	0,073	3,0	0,27	0,122
1,41	0,16	0,105	3,3	0,13	0,145
2,0	0,12	0,111	3,66	0,06	0,156
2,4	0,14	0,108	4,1	0,30	0,117
2,9	0,19	0,101	4,5	0,49	0,085
3,1	0,25	0,094	5,0	0,54	0,077
3,3	0,18	0,103	6,0	0,69	0,052
3,5	0,27	0,091	6,3	0,75	0,042
3,8	0,39	0,077	6,6	0,5	0,083
4,1	0,35	0,081	7,2	0,15	0,141
4,4	0,51	0,061	7,4	0,32	0,113
4,7	0,37	0,079	8,0	0,50	0,083
7,0	0,23	0,096	9,0	0,50	0,083
14	0,37	0,079	10	0,51	0,082
			14	0,21	0,132

In fact, the nucleon binding energy in any of these nuclei is greater than the binding energy of the extra neutron in He^5, C^{13} or O^{17}. Therefore the incident neutron being scattered by He^4, C^{12}, and O^{16} interacts with these nuclei relatively weakly and deforms them only slightly. Thus we can speak of the interaction of an incident neutron with the target-nucleus as an interaction with the whole nucleus; this justifies the assumption of an optical potential for these nuclei.

The authors wish to express their thanks to A. S. Davydov, L. N. Usachev, and V. N. Neudachin for the interest they have shown in our work, and for their critical comments.

†It must be noted that the values of $\langle\cos\theta\rangle$ for oxygen calculated in [6] on the basis of experimental data in [7] are in obvious disagreement with these. In fact, the curve in [6] showing dependence of $\langle\cos\theta\rangle$ on E_n gives a negative value of $\langle\cos\theta\rangle$ for $E_n\simeq 2$-2.5 Mev, while it follows from [7] that $\langle\cos\theta\rangle$ cannot be negative for these energies.

LITERATURE CITED

1. H. Feshbach, C. Porter and V. Weisskopf, Phys. Rev. 96, 448 (1954).
2. F. Ajzenberg and T. Lauritsen, Rev. Mod. Phys. 27, 77 (1955).
3. D. Hughes and J. Harvey. Neutron Cross Sections. USA BNL-325 (1955).
4. R. Adair, Phys. Rev. 92, 1491 (1953).
5. V. P. Kochergin and V. V. Orlov, Atomnaya Énergiya 6, 1, 34 (1959).‡
6. P. Zweifel and H. Hurwitz, J. Appl. Phys. 25, 1241 (1954).
7. E. Baldinger, P. Huber and W. Proctor. Helv. Phys. Acta 25, 142 (1952).

‡Original Russian pagination. See C. B. translation.

* * *

EXPERIMENTAL INVESTIGATION OF HEAT TRANSFER IN SLIT-TYPE DUCTS WITH HIGH HEAT-TRANSFER RATES

Yu. P. Shlykov

Translated from Atomnaya Énergiya, Vol. 8, No. 2, pp. 144-145
February, 1960
Original article submitted May 21, 1959

Heat-exchange equipment with narrow slit-type ducts (plane or annular) enjoy wide application in the various branches of technology. Among such types of equipment are found, for example, water—water reactors with plate-or tube-type heat-withdrawal elements. The abundance of experimental and theoretical papers on heat transfer in plane ducts is well known. The majority of these are devoted to studying heat exchange in relatively broad channels with small heat-transfer rates.

In nuclear reactors and reaction technology the heat-transfer rates can attain a value of $5 \cdot 10^6$ kcal/m^2·hr and higher. Calculation of high-energy reactor equipment with narrow ducts according to the familiar equations for convective heat exchange in round tubes, using the equivalent diameter d_e as dimensional criterion, without appropriate experimental verification does not yield any convincing results.

The problem of dimensional criterion, i.e., the possibility of applying the indicated equations to narrow ducts, has been discussed in any variety of ways, but still stands unresolved. In a number of experimental papers on heat transfer in narrow annular ducts [1-4], containing generalizations with the application of d_e, equations were obtained, which differed from the equations for round tubes. In this light a reduction was noted in the heat transfer in an annular gap as compared with the heat transfer in a round tube. With the generalization of the experimental data on heat exchange in plane ducts a contradiction was also found in the choice of a dimensional criterion. Taken together, these facts encouraged the work of the present paper, the purpose of which was to verify the applicability of the usual equations for convective heat exchange to the analysis of plane narrow ducts with high heat-transfer rates and to more precisely define the problem of a dimensional criterion.

The procedure of the investigation was based on application of direct heating with a low-voltage current of the working section of the duct (1Kh18N9T steel), which is water-cooled. The principal arrangement of the experiment is shown schematically in Fig. 1, the structure of the experimental assembly in Fig. 2. The tests were carried out on narrow ducts made from flattened tubes. A series of tests were performed on the apparatus whose cross section is shown in Fig. 2.

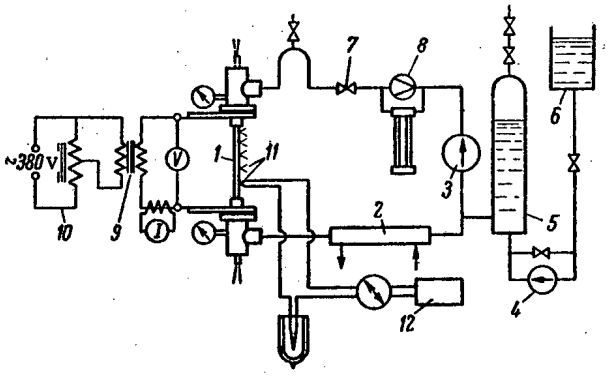

Fig. 1. Diagram of experimental setup: 1) working section; 2) heat exchanger; 3) circulation pump; 4) feed pump; 5) volume compensator; 6) deaerator; 7) flow valve; 8) discharge metering disk; 9) step-up transformer; 10) control transformer; 11) hot junctions of thermocouples; 12) potentiometer.

The experimental conditions were varied by changing the water flow rate in the duct and the heat-transfer rate. The flow velocity of the water was varied from 5 to 12 m/sec, the heat-transfer rates from 3.6 to $5.7 \cdot 10^6$ kcal/m^2·hr. The water temperature at the inlet to the duct was varied within the limits 45-80°C. A pressure of 50 atm was maintained in the loop.

A total of 65 tests were made on the heat-transfer to nonboiling water, from which 35 of the tests were performed on a duct with a gap width of 1 mm, the rest on a duct with gap width of 1.5 mm, with a constant duct width of 23 mm. The length of the working section of the duct was 200 mm. In view of the completely identical nature of the results of the measurements under the same or nearly identical working conditions, the results of 17 tests were processed.

The following formulas were used:

$Nu_1 = 0{,}027\, Re_1^{0,8}\, Pr_1^{0,33} \left(\frac{\mu_1}{\mu_{st}}\right)^{0,14}$ Zider and Tate formula for a round tube; (1)

$Nu_1 = 0{,}023\, Re_1^{0,8}\, Pr_1^{0,33} \left(\frac{\mu_1}{\mu_{st}}\right)^{0,14}$ the same formula with the coefficient corrected [3] for an annular gap; (2)

$Nu_1 = 0{,}023\, Re_1^{0,8}\, Pr_1^{0,4}$ Mc Adams formula for a round tube; (3)

$Nu_1 = 0{,}021\, Re_1^{0,8}\, Pr_1^{0,43} \left(\frac{Pr_1}{Pr_{st}}\right)^{0,25}$ Mikheev's universal formula; (4)

$Nu_1 = 0{,}0274\, Re_1^{0,8}\, Pr_1^{0,36} \left(\frac{Pr_1}{Pr_{st}}\right)^{0,11}$ Yakovlev's [5] formula for a round tube. (5)

The averaged (over duct length) heat-transfer coefficients, processed according to the dimensionless criteria from the various formulas in the form of dependences

$$k_i = \frac{Nu_1}{A_i} = f(Re_1),$$

where A_i represents the right-hand sides of Eqs. (1)-(5) without the factor $Re_1^{0.8}$, are shown in Figs. 3 and 4.

In every case the equivalent diameter $d_e = 4F/\pi$ was taken as the dimensional criterion (F is the cross section of the duct, π, the perimeter wetted).

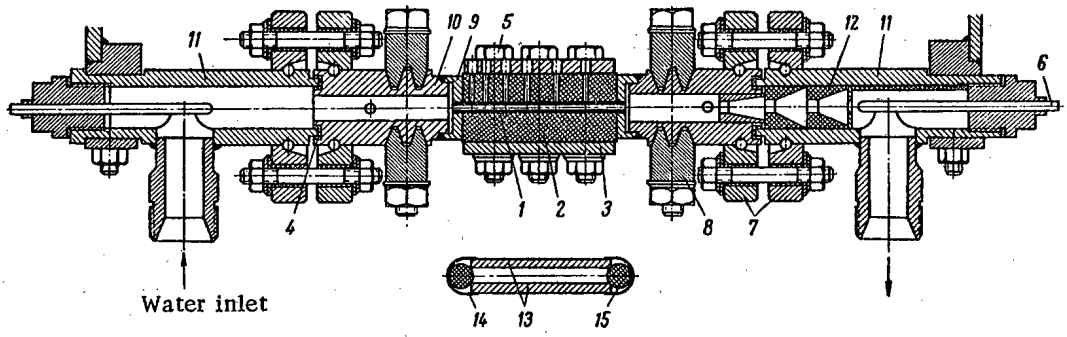

Fig. 2. Experimental assembly and cross section of the working section: 1) working section; 2) thermoelectric insulator inserts; 3) pressure relief plates; 4) electrical insulator inserts; 8) current-conducting busses; 9) contact sockets; 10) current-conducting sleeves; 11) inlet and outlet chambers; 12) mixer; 13) calibration plates; 14) steel foil; 15) displacer.

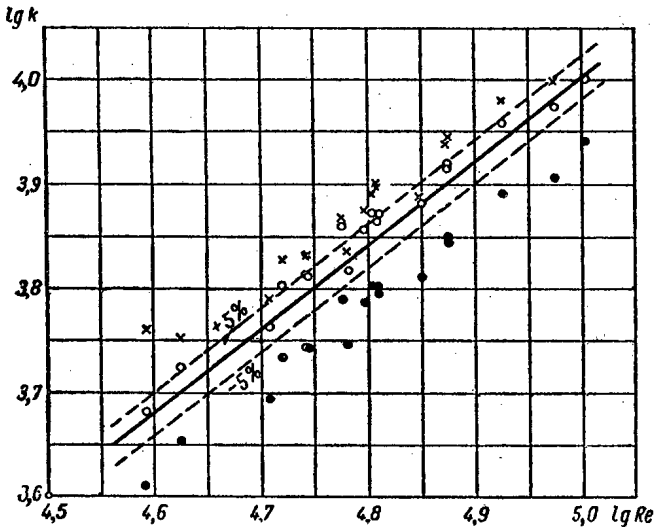

Fig. 3. Dependence $k=f(Re_1)$. According to the formulas: • —(1); o —(2); × —(3).

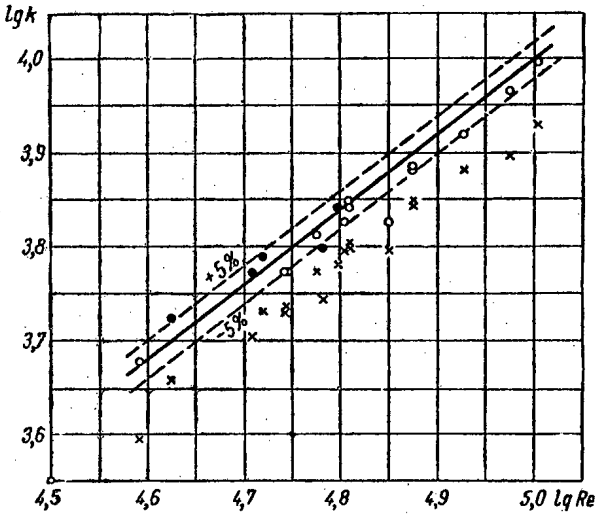

Fig. 4. Dependence $k=f(Re_1)$. • and o according to the formula (4) for ducts with 1- and 1.5-mm gaps, respectively; × according to (5).

The experimental results are generalized best (with a ±5% spread) by Eq. (4), which was verified with $4 \cdot 10^4 \leq Re_1 \leq 10^5$, a heat-transfer rate up to $5.7 \cdot 10^6$ kcal/m²·hr, and with $1.8 \leq Pr_1/Pr_{st} \leq 3$.

Close results are also given by Eq. (2), which is assumed for annular ducts [3].

The author expresses his indebtedness to Z. P. Medvedev and A. I. Evstaf'eva for the great assistance they rendered in conducting the experiments.

LITERATURE CITED

1. V. L. Lel'chuk, Izvest. VTI 4, 18 (1952).
2. V. E. Doroshchuk, Teploenergetika 1, 14 (1956).
3. F. Carpenter, A. Colburn, E. Schoenborn and A. Wurster, Trans. AIChE 42, 165 (1946).
4. W. Mc Adams, W. Kennel, and J. Addoms, Trans ASME 72, 4, 421 (1950).
5. V. V. Yakovlev, Atomnaya Énergiya 11, 2, 179 (1957).*

*Original Russian pagination. See C. B. translation.

* * *

AN INVESTIGATION OF THE ALLOYS OF THE URANIUM-GERMANIUM SYSTEM*

V. S. Lyashenko and V. N. Bykov

Translated from Atomnaya Énergiya, Vol. 8, No. 2, pp. 146-148
February, 1960
Original article submitted October 7, 1959

Manufacture and heat treatment of the alloys. There are no data available in the literature on the structure of alloys belonging to the uranium-germanium system. Some information on the existence of an intermetallic compound UGe_3 [1,2] has been since confirmed by one of the present authors and others [3].

Source materials for the alloys in our study of the phase diagrams of the uranium-germanium system were 99.86% pure uranium and 99.99% pure germanium in ingot form. A melt was produced in a vacuum induction furnace in beryllium oxide crucibles at a pressure of 10^{-3} to 10^{-4} mm Hg. Agitation of the melt and subsequent decantation eliminated any possibility of liquation. To facilitate the investigation of the phase diagram for the uranium-germanium system, 30 alloys of differing compositions were prepared, and the high-temperature region of the phase diagram was furthermore studied by using alloys obtained by extrusion. The composition of all of the alloys was monitored through chemical analysis. Any deviations from the desired compositions were insignificant. Prior to the tests, all of the alloys were subjected to a homogenization anneal in a vacuum furnace for 150 hours at 900°C. Alloys with 40-75 at.% germanium were annealed further at 1350° for 25 hours, followed by standing at 1000°C for 100 hours.

The alloy specimens were oil-quenched from temperatures of 720, 950, 1200, and 1300°C in a cooled oil bath, in investigating the high-temperature regions of the phase diagram, and the solubility limits of the components.

Methods used in the investigation, and results obtained. Thermal analysis of the alloys was conducted in a vacuum furnace with a tungsten heating unit. A thermocouple was inserted in the centrally placed bottom tube of a specially shaped crucible (Fig. 1) i.e., actually inside the alloy ingot, thus enhancing the sensitivity of the technique. A molybdenum cap was used to protect the junction of the platinum to rhodium-platinum thermocouple. A vanadium ingot subjected to conditions equi-

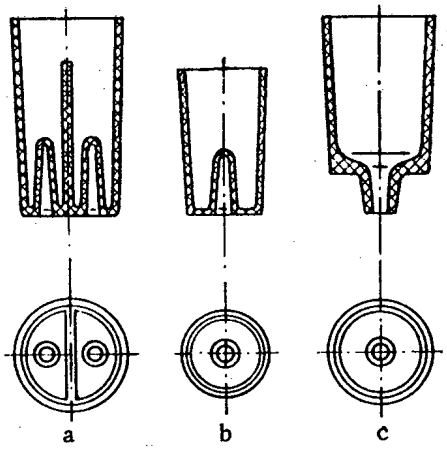

Fig. 1. Beryllium oxide crucibles used in the investigation. a,b) for thermal analysis; c) for pouring off alloys.

*Study completed in 1955.

valent to those affecting the alloy test ingot was used as a control.

A tracing of the simple and differential cooling curves was obtained on a self-recording pyrometer by N. S. Kurnakov. The simple curve was recorded concurrently on an EPP-09 recording compensation potentiometer. The potentiometer scale was calibrated to match the melting points of the pure metals and was employed for automatic calibration of a sheet of photographic paper in the pyrometer at the exact moment that the data was recorded, by moving the potentiometer scale divisions up with the aid of a flying light spot. Heating in the course of thermal analysis was accompanied by constant evacuation to keep the pressure down to 10^{-4} mm Hg. The alloy was allowed to stand at maximum temperature for 10 min, after which the furnace was filled with purified argon to a pressure of 350-500 mm Hg. The curves were recorded only during the cooling phase, with the rate of cooling set at 15°C/min by a compensation control device.

The cooling curves of alloys having melting points above 1450°C were recorded by means of a tungsten-molybdenum alloy thermocouple on a high-sensitivity Speedomax self-balancing unit. Average solidification temperatures and phase transformation temperatures of the alloys are indicated by horizontal lines in the phase diagram (cf. Fig. 3).

Dilatometric analysis was carried out using a dilatometer similar to one described earlier [4], with a sensitivity of $2 \cdot 10^{-6}$ cm. Readings were taken at temperature intervals of 2-3°C while the specimen was being heated at a rate of 4-5°C/min. The values of the thermal coefficient of linear expansion of the alloys are entered in the table below.

As-cast, annealed, and quenched alloy specimens were analyzed microscopically. The microstructure was revealed by electroetching and chemical etching in the reagents commonly employed for treating uranium alloys. A study of the microstructure with microhardness measurements taken made it possible to find out the single-phase

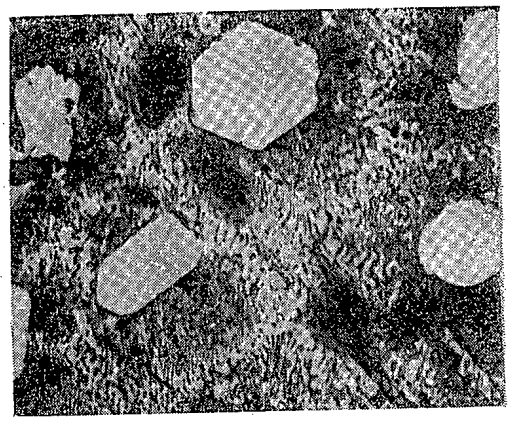

a

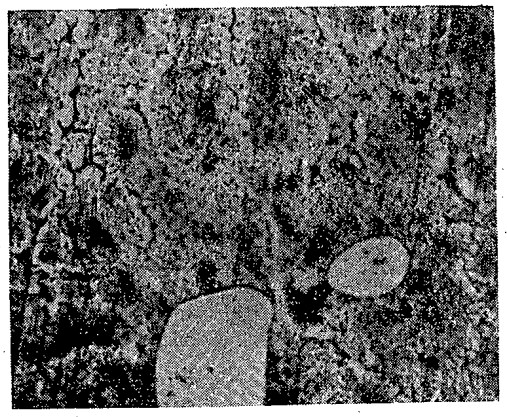

b

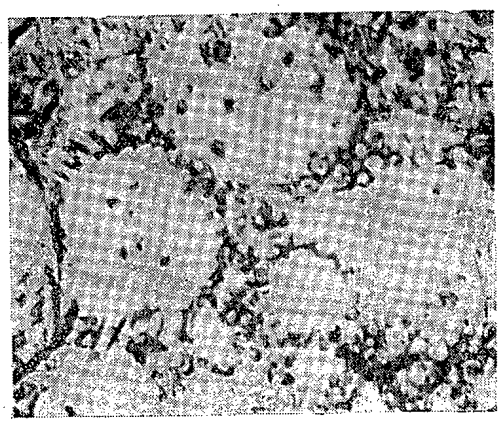

c

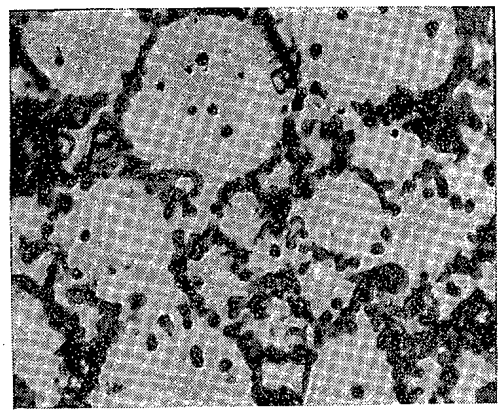

d

Fig. 2. Microstructure of alloy, 12.5 at.% germanium: a) quenched from 1000°C, left to stand 6 hr ; b) quenched at same temp°, left to stand for 126 hr ; c) quenched at same temp°, left to stand for 366 hr , d) quenching and standing same (sintered alloy).

Values of the Coefficient of Thermal Expansion ($\alpha \cdot 10^6$) of Some Alloys Belonging to the System Uranium-Germanium.

Composition of alloy, at.% Ge	Temperature range, °C				
	300—400	400—500	500—600	600—700	700—800
Uranium	—	22,6	34,0	76,5	26,2
1,0	27,0	29,0	33,0	79,0	33,0
5,0	21,0	22,5	29,0	60,5	27,5
12,5	24,0	23,0	22,0	34,0	21,0
37,5	21,8	19,5	19,5	21,5	21,0
57,14	10,2	10,5	10,0	10,0	10,0
66,6	12,0	12,0	12,0	11,0	11,0
75,0	21,0	19,0	23,0	23,0	26,0
Germanium	7,5	7,7	7,3	7,3	7,3

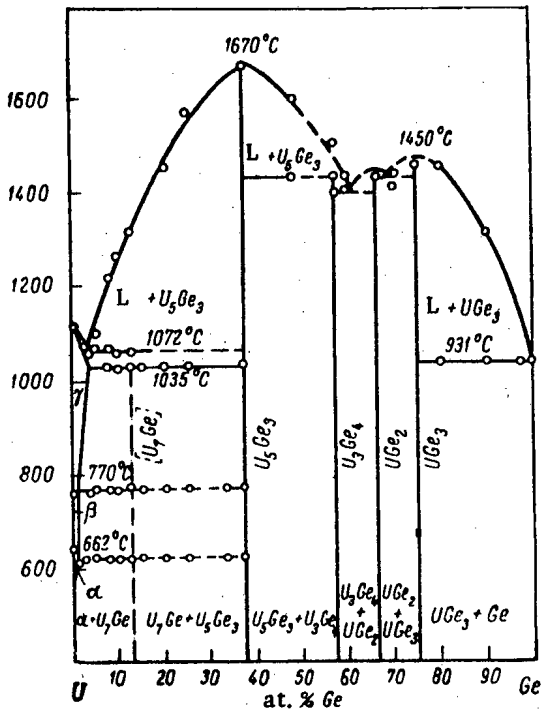

Fig. 3. Phase diagram of alloys belonging to the uranium-germanium system.

composition of alloys having 37.5, 57.14, 66.6, and 75 at.% germanium, which were assigned the formulas U_5Ge_3, U_3Ge_4, UGe_2, UG_3. Furthermore, an investigation of the microstructure of the alloy with 12.5 at.% germanium, quenched from 1000°C and left standing for 6, 126, 246, 366 hours, respectively prior to quenching, revealed a successive dissolution of high-melting grains U_5Ge_3 in the eutectic with 3.5 at.% germanium, with the subsequent formation of a chemical compound to which was tentatively assigned the formula U_7Ge. An alloy of the same composition (12.5 at.% germanium) was obtained by sintering and a quench from 1000°C, with a similar single-phase microstructure resulting (Fig. 2).

An x-ray phase analysis based on the powder method with a breakdown of x-ray diffraction photographs and evaluation of line intensities provided confirmation of the existence of the intermetallic compounds in this system. The x-ray structural analysis made it possible to ascertain the crystalline structures of four compounds [3].

On the basis of data secured by the above methods, a phase diagram was plotted for alloys in the uranium-germanium system (Fig. 3). It is readily seen from the phase diagram that uranium forms five chemical compounds with germanium, of which two crystallize out of the melt, one forms by the peritectoid reaction; congruence and the peritectoid reaction were tentatively assumed for the remaining two intermetallic compounds.

From a study of changes in the lattice constant and in the microstructure of the quenched alloys, it was learned that the solubility limit of germanium in α-uranium and β-uranium is ~1%; up to 3% germanium goes into solution in γ-uranium. Uranium is virtually insoluble in germanium.

The investigation thus filled out the overall picture of the interaction of uranium with elements in the fourth group of the Mendelevian periodic table, manifesting a remarkable similarity between the phase diagram of the uranium-germanium system and the phase diagrams of the systems uranium-silicon and uranium-lead [5].

LITERATURE CITED

1. A. Iandelli and R. Ferro, Ann. Chimica (Rome) 42, 598 (1953).
2. B. Frost and J. Maskrey, J. Inst. Metals 82, No. 4 (1953).
3. E. S. Makarov and V. N. Bykov, Kristallografiya 4, 2, 183 (1959).
4. P. G. Strelkov, G. I. Kostousov and V. M. Samoilov, Izvest. Akad. Nauk SSSR, Ser. Fiz. 17, No. 3 (1953).
5. F. Rough and A. Bauer, Constitution of Uranium and Thorium Alloys. Report BMI-1300 (1958).

* * *

COPRECIPITATION OF Pu (IV) WITH ORGANIC COPRECIPITANTS

V. I. Kuznetsov and T. G. Akimova

Translated from Atomnaya Énergiya, Vol. 8, No. 2, pp. 148-150
February, 1960
Original article submitted September 24, 1959

Organic coprecipitants have proved feasible as collectors for the coprecipitation of many elements [1-3]. The theoretical tenets elaborated enable one to choose combinations of ingredients of coprecipitants suitable for the coprecipitation of almost any element, with no special difficulties.

Coprecipitation of plutonium from highly dilute solutions of plutonium with simulaneous separation from other elements may be realized by any of several available techniques.

The "nitrate" method. In acidic solutions containing the nitrate ion, Pu (IV) forms a characteristic weakly ionized complex ion, $Pu(NO_3)_6^{2-}$ [4]. As a result, plutonium may be coprecipitated in the form of salts of this nitrate anion $Pu(NO_3)_6^{2-}$ with precipitates of the nitrates of heavy organic cations, as, e.g., with the butyl ester of rhodamine B (butyl rhodamine):

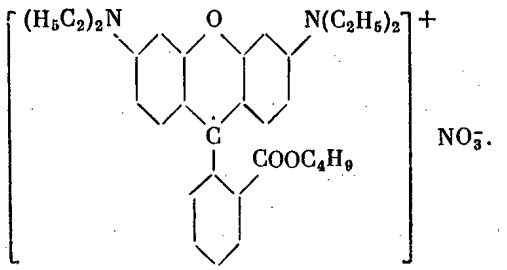

Since similar weakly ionized nitrate anions are formed by only a very few elements aside from Pu(IV), viz., U(IV), Th[5], Ce(IV), coprecitation of plutonium in the form of salts of this anion is a highly selective process.

To bring about the coprecipitation, we add, to 200 ml of a 3N solution of HNO_3 containing Pu(IV), the following: ~130 g NH_4NO_3, 1 g of powdered phenolphthalein (the latter to facilitate filtration of the precipitate, which evinces a tendency to adhere to the walls of the flask) and 40 ml of a gently heated 1% solution of butyl rhodamine. The crimson-colored precipitate which settles out collects the plutonium, and is filtered off and washed with a ~50% solution of NH_4NO_3 in ~1.8 N HNO_3, to which is added a solution of butyl rhodamine in the amount required for the formation of a small but rather appreciable precipitate, which is placed together with the paper filter in a crucible. Following this, 2 ml of saturated $(NH_4)_2SO_4$ is added (as aphlegmatizer), the specimen is lightly dried and ashed, with the temperature raised slowly to 500°C. (Ashing of a precipitate containing nitrates without the addition of $(NH_4)_2SO_4$ may be accompanied by explosions.) The coprecipitated plutonium is contained within the residue. The completeness of coprecipitation of the plutonium may be appreciated from Table 1. Results of coprecipitation of plutonium with simultaneous separation from other elements are given in Table 2 (the other elements, other than those indicated, were introduced in nitrate form, 100 mg for each element; a single element or the sum of the elements involved was taken in each run).

TABLE 1. Coprecipitation of Pu(IV) with Nitrate of Butyl Rhodamine

Dilution of Pu	Pu coprecipitated, %
$1 : 2 \cdot 10^8$	100
$1 : 1 \cdot 10^9$	100
$1 : 2 \cdot 10^9$	97; 100
$1 : 1 \cdot 10^{10}$	89; 90
$1 : 2 \cdot 10^{10}$	76; 82

It may be readily seen that the nitrate method assures rather complete coprecipitation of the Pu(IV) even when it is diluted $1:1 \cdot 10^{10}$, with separation from all elements except thorium, for practical purposes. Precipitation of Ce(IV) may be eliminated with ease by first effecting the conversion Ce(IV)→Ce(III). The conversion U(IV)→U(VI) has the effect of greatly reducing the amount of uranium carried down. Plutonium may be separated from U(VI) by repeated precipitations. For example, four successive coprecipitations produce a yield of 80% plutonium, with only 0.0025% of the original amount of uranium present carried down from the original mixture of plutonium and uranium in the ratio Pu(IV): U(VI)=1:10^7.

Coprecipitation of Pu(IV) in the form of cyclic salts. At appropriate pH values, Pu(IV) forms soluble cyclic salts with many organic reagents which contain sulfo groups. In this form, the plutonium may be coprecipitated with low-solubility precipitates formed by the organic reagents used and by basic dyes. These precipitates are organic salts in which the cation is provided by the organic cation of the basic dye, while the anion is the anion of the reagent employed. The latter must bind the plutonium in a stable complex compound.

TABLE 2. Coprecipitation of Pu(IV) with Simultaneous Separation from Other Elements

Other elements present		Weight of ashed residue, mg	Pu coprecipitated, %
No other elements added		—	99; 100
Me (I):	Li + Na + K + Rb + Cs	1	95
Me (II):	Cu; Be ($BeSO_4$); Mg; Ca	Everywhere $\ll$ 1—2	93; 100; 100; 80
	Sr + Ba; Zn + Cd; Pb; Mn; Co + Ni	Everywhere 1—2	95; 92; 90; 96; 97
Me (III):	Rare-earth elements Bi; Sb ($SbCl_3$)	$\ll$1; ~7; ~15	101; 103; 96
	B ($Na_2B_4O_7$); Al; Cr; Fe	Everywhere $\ll$ 1—2	90; 85; 93; 95
Me (IV):	Ce; Th; U (UCl_4)	~20, ~43, ~43	87; 55; 54
	Zr; Sn ($SnCl_4$); V ($VOSO_4$)	Everywhere $\ll$ 1—2	92; 90; 100
Me (V):	P (Na_2HPO_4)	$\ll$ 1	86
Me (VI):	U; Mo [$(NH_4)_6Mo_7O_{24}$]	~7; $\ll$ 1	94; 90

Since Pu(IV) cations hydrolyze even in acid solutions, complexing of plutonium also occurs in acid solutions.

To effect the coprecipitation, we add, to 200 ml of acid solution containing Pu(IV), 100 mg of a complex-forming reagent in the form of an aqueous solution, bring the pH to the value necessary for complex formation, let the solution stand for 10-20 min, and then introduce, while mixing, 5-7 ml of a 1% solution of methyl violet or methylene blue. The precipitates are then gently dried and ashed as the temperature is slowly raised to ~500°C.

When the Pu(IV) is diluted $1:2\cdot10^9$ (or 0.1 g in 200 ml) and the pH≃1-4, plutonium is coprecipitated at 95-100%, if the reagents used are arsenazo, stilbazo, chromotrope 2B, or others of the type. A coprecipitation of plutonium more complete than that obtained by the nitrate technique, albeit less selective, may be effected from more dilute solutions. Pu(IV) is separated from only those elements whose cations hydrolyze with much greater difficulty than the Pu(IV) cations; i.e., from the alkali metals, doubly charged cations, including U(VI), and several trivalent elements, including the rare earths.

At pH=~5-7, the same method may be used to coprecipitate Pu(III) from highly dilute solutions. In that case, the selectivity of the coprecipitation is inferior to that achieved in the coprecipitation of Pu(IV).

LITERATURE CITED

1. V. I. Kuznetsov, Session of the USSR Academy of Sciences on the Peaceful Uses of Atomic Energy (panel of the Division of Chemical Sciences) [in Russian] (Izd. AN SSSR, 1955) p. 301; Zhur. Anal. Khim. 9, 199 (1954).*
2. V. Kuznetsov, The Application of Radioactive Isotopes for Developing New Methods in Analytical Chemistry. Organic Coprecipitants. International Conference on Radioisotopes in Scientific Research. (Paris, 1957).
3. V. I. Kuznetsov, L. G. Loginova and G. V. Myasoedova, Zhur. Anal. Khim. 13, 453 (1958).*
4. J. Brothers, R. Hart, and W. Mathers, J. Inorg. and Nucl. Chem. 7, 85 (1958).
5. D. Carswell and J. Lawrance. J. Inorg. and Nucl. Chem. 11, 69 (1959).

*Original Russian pagination. See C. B. translation.

* * *

CONTRIBUTION TO THE PROBLEM OF ELECTRON INJECTION TO A BETATRON

V. P. Yashukov

Translated from Atomnaya Énergiya, Vol. 8, No. 2, pp. 150-151, February, 1960
Original article submitted March 16, 1959

Despite the large number of papers which have appeared on the problem of electron capture in betatron operation, no quantitative theory has yet been elaborated to explain theprocess. As well, neither has progress of any kind been registered in increasing the intensity of γ-radiation in betatrons.

The question of the effect exerted by the injection pulse shape on intensity has been probed by various authors [1-5]. No clear answer to the question has been forthcoming as yet, however, in view of the contradictory results reported.

The effect of the injection pulse shape of maximum γ-intensity was verified, under conditions otherwise optimal, on the synchrotron of the Leningrad Physics and Engineering Institute, a 100 Mev machine with betatron injection. A square-wave generator producing rectangular pulses of 2-10 μsec duration, a sinusoidal-wave generator producing pulses of basewidth 1.2 and 12 μsec, a pulse generator producing pulses of 2 μsec duration with a variable leading edge in the capture region (this waveform is obtained by superposing a pulse close to sinusoidal in shape on a rectangular pulse), and a pulse-train generator generating pulses of about 8 μsec width and three pulses per train were used in the investigation.

All of the measurements were conducted with the synchrotron tuned to optimum performance conditions and with injection voltage at 30 kv. The intensity of γ-radiation was measured with a "Cactus" instrument. The sensor employed was a one-liter ionization chamber positioned at 2m from the target.

Peak intensity remained practically unaffected by any change in waveform in the case of a single injection. Peak intensity was in all cases reached in the region of the pulse top or in the region of the angle between the leading edge and the flat top of the rectangular pulse. The γ-radiation was lower at other portions of the injection pulse. No greater intensity was successfully obtained either with a pulse of variable leading edge in the capture region, or with a pulse of gently sloping leading edge and steep trailing edge [3] (such a pulse was obtained by varying the ratio of the amplitudes of the rectangular and sinusoidal pulses in the generator used to generate pulses with variable leading edges). It should be emphasized that the injection emission current must be varied as a function of injection pulse width to obtain peak intensity (e.g., the mean emission current for a pulse width of 12 μsec is 100 μa, and 28 μa for a pulse width of 1.2 μsec). The pulse repetition rate was 50 cps.

In our experiments, oscillograms of the current at the instant of beam capture were used to arrive at the deduction that the optimum number of particles circulating in the chamber during a single revolution reaches 10-25% of the theoretically predicted limiting charge.

The impossibility of increasing γ-radiation intensity by means of injection pulses of different waveform, and the variation in injection current as a function of pulse duration point to some collective interaction between the particles at the time of beam capture. The proper choice of injection waveform in operational service should therefore be arrived at with due consideration for simplicity in generator design and stability of particle acceptance. From this standpoint, preference might be given to an injection pulse of sinusoidal form with base-width of 8-10 μsec.

The number of particles reaching the target at the end of an acceleration cycle is two orders of magnitude less, at least, than the predicted limiting charge value per cycle. This value was arrived at on the basis of data from calorimetric measurements of the γ-ray flux [6] and calculations based on an earlier contribution [7].

The material accumulated permits us to draw an inference as to the possibility of increasing γ-radiation intensity both by approximating the optimum number of particles per single revolution to the predicted limiting value, and by retaining a large number of particles in their orbits after the beam has been captured. What is involved is the creation of new injection conditions, or a repetition of the old conditions in a single cycle [8,9].

Data presented in an earlier paper [9] are available on the adding of γ-radiation intensity from two injection pulses during a single acceleration cycle. The supposition of linearity in the adding of the intensities was checked in three injection pulses. To reduce the slope of the rise of the magnetic field, the permanent magnetization was increased at the time of injection. While a peak intensity of γ-radiation equal to 25 relative units was obtained in working with a single injection pulse at an injection voltage amplitude of 32 kv, work with three injection voltage pulses in a single cycle with pulse amplitudes of 24, 28, and 32 kv resulted in an intensity equal to 48 relative units, i.e., almost twice as high. The intensity of γ-radiation from each pulse was 10, 15, and 25 relative units, respectively.

Peak intensity for repeated injection was obtained in the region of the tops of the pulses.

The intervals between pulses may be assigned arbitrarily with no important effect on γ-radiation intensity resulting. That this is true may be seen from the fact that the particle oscillations diminishes rapidly (in less than 1 μsec) owing to collective interaction.

Now, taking into account the linear increase in intensity of γ-radiation with an increase in injection voltage, it would appear feasible to initiate the injection from a voltage yielding an intensity 20% of that corresponding to peak injection voltage. Supposing that the linear relationship observed in the adding of the intensities of γ-radiation upon repeated injection remain valid, a substantial increase (by a factor of four to six) in γ-radiation intensity in betatrons is within reach. At a slower rate of change in the magnetic field, or with the use of time-invariant magnetic fields, there exists the distinct possibility of an even greater increase in intensity of γ-radiation obtainable in betatrons.

LITERATURE CITED

1. E. Greanias and E. Wukasch, Phys. Rev. 70, 797 (1946).
2. R. Wideroe, J. Appl. Phys. 22, 362 (1951).
3. V. N. Logunov, E. P. Ovchinnikov and V. D. Rusanov, Zhur. Tekh. Fiz. 27, 5, 1135 (1957).
4. I. P. Chuchalin, Izvestiya Tomsk. Politekhn. Inst. 87, 256 (1957).
5. D. Kerst, G. Adams, H. Koch and C. Robinson, Phys. Rev. 78, 297 (1950).
6. S. P. Kruglov, Zhur. Tekh. Fiz. 28, 10, 2311 (1958).
7. J. Lawson, Nucleonics, 10, 11 61 (1952).
8. B. N. Rodimov, Izvest. VUZ. MVOSSSR., Fizika 1, 84 (1957).
9. V. P. Yashukov, Zhur. Tekhn. Fiz. 28, 6,1363 (1958).

* * *

SOME DATA ON THE DISTRIBUTION OF RADIATIONS EMANATING FROM THE SYNCHROCYCLOTRON OF THE JOINT INSTITUTE FOR NUCLEAR RESEARCH*

M. M. Komochkov, and V. N. Mekhedov

Translated from Atomnaya Énergiya, Vol. 8, No. 2, pp. 152-153, February, 1960
Original article submitted April 20, 1959

Measurements were carried out while the machine was being operated to generate neutrons by bombarding a beryllium target with protons ranging up to 680 Mev, with a particle beam current of 0.2-0.3 μa in the neighborhood of the peripheral orbits. Radiation detectors were placed in the orbital plane of the accelerated protons. One of these was a rate meter.

The detector used to record neutrons of energies above 50 Mev was an ionization chamber which recorded pulses from fragments of bismuth fission. With a view to eliminating any possible electric and magnetic field effects on the recording equipment, the latter was positioned 10-13 m from the target. The chamber with the bismuth was shielded by a lead layer 15-20 cm thick to prevent recording of fast neutrons. The chamber background, i.e., the count from aluminum plates not coated with bismuth, was 1.5%. Carbon detectors were also used in performing measurements. This type of detector, possessing a recording threshold in the neighborhood of 20 Mev, allowed the particle flux to be determined at such points where recording by fission chambers was impossible, owing to the effects of the electromagnetic fields associated with the accelerator on fission chambers.

The results of the measurements obtained by means of the chambers with bismuth and the carbon detectors placed around the circumference of the of the synchrocyclotron are indicated in the accompanying diagram. Numbers appearing near measuring positions denote: number of the position as numerator; particle flux in relative units as the denominator.

Measurements conducted with an air ionization chamber and carbon detectors essentially confirmed the results appearing in the diagram. Only at positions 2,3, and 21, where the flux of scattered protons emerging

* A description of the accelerator shielding may be found in earlier work [1, 2].

from the synchrocyclotron are appreciable, was any significant increase noted in the readings on the detectors.

Data obtained by means of the three enumerated forms of detectors provide evidence of the presence of a sharply directed cone of radiation in the angular distribution. For neutrons of energy $E_n > 50$ Mev, this cone is of regular and almost symmetrical shape. The half-width of the angular distribution of the cone of neutrons is $29 \pm 1°$.

It is obvious from the diagram that the background of neutrons of $E_n > 50$ Mev, flying in different directions, does not amount to more than 11% of the peak flux value. Special measurements served to show that the neutrons flying off in directions opposed to the direction of peak flux were formed predominantly outside the target.

The flux of neutrons emerging from the beryllium target was evaluated by means of the carbon detectors. The measurement positions were located at a distance of 14 meters from the target in the collimated beam. The flux of neutrons of energy $E_n > 20$ Mev was $(3-7)\cdot 10^4$ neutrons/cm^2 sec. The neutron flux at $E_n > 50$ Mev, found by integrating the angular distribution, is $\sim 4\cdot 10^{10}$ neutrons/sec. The flux of neutrons attributable to scattered protons is $\sim 3\cdot 10^{10}$ neutrons/sec. There is thus about one neutron of energy >50 Mev for every ten protons in the circulating beam outside the synchrocyclotron chamber.

Photographic plates, type K-200, were used as a neutron detector to sense neutrons of energy $E_n > 50$ Mev, in view of the low intensity of radiation beyond the shielding walls. The neutron flux was estimated from the number of stars having two or more rays. Conversion of the data to absolute units was performed on the basis of calibrated measurements of the number of stars on a photographic plate exposed to a neutron beam with known flux. The neutron spectrum at all measurement positions was assumed approximately uniform. The plates were exposed for 200 hr . It was shown that, under the conditions of the experiment, regression of the tracks in the photographic emulsion was negligibly small.

Neutrons of energy $E_n > 0.5$ Mev were recorded by a scintillation counter, in which a wafer composed of a mixture of plexiglas and zinc sulfide functioned as detector.

The distribution of the radiations in the rooms of the accelerator building used by personnel (laboratories 1,2,3) are indicated on the right half of the accompanying diagram. The following notation is used: the numerator gives the number of the measurement position, the first number in the denominator gives the neutron flux for

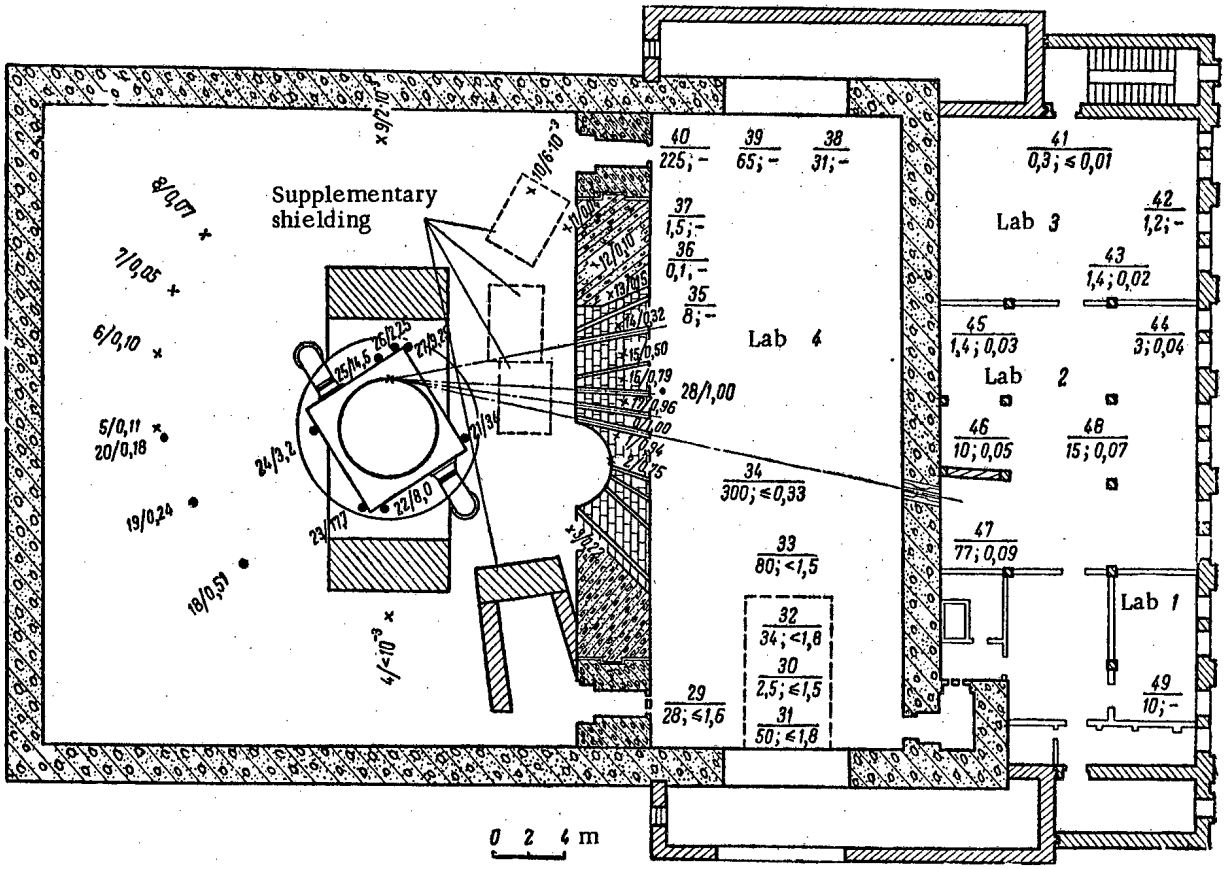

Distribution of radiations about the 6-meter synchrocyclotron: ×-measurements by fission chambers with bismuth; ●-measurements by carbon detectors.

neutrons of energy $E_n > 0.5$ Mev and the second number in the denominator gives the γ-radiation dose rate in $\mu r/sec$.

The neutron flux for neutrons of energy $E_n > 50$ Mev in laboratory 4 while the collimators of the neutron beams near points 28 and 35 are open was ~5 neutrons/$/cm^2 \cdot sec$ at a distance of ~20 cm from the neutron beam. Measurement instrumentation was placed in this laboratory. There were no personnel present either here or in the synchrocyclotron room, while the experiment was in progress.

In laboratories 1, 2, and 3, where the recording equipment was located and where workers associated with the experiment were present while the accelerator was in operation, radiation levels were ascertained for the most unfavorable case: that of penetration of 2 neutron beams with total flux of $\sim 10^7$ neutrons/sec through the laboratory. Neutron fluxes at the spots where the experimental researchers were working ranged from 0.1 to 1 of the maximum allowable dose. For the conditions under which the accelerator was operated, where the neutron beam was not directed through laboratory 2, the neutron fluxes for neutrons of energy $E_n > 0.5$ Mev dropped to as low as ≤ 0.2 neutrons/cm^2 sec in those quarters.

The presence of a rather high level of neutrons was detected outside the accelerator building, when measurements were taken there. At points where the thickness of the shielding walls do not exceed 2 m, neutron levels for $E_n > 50$ Mev were 15-45 neutrons/cm^2 sec, and ranged from 500 to 750 neutrons/cm^2 sec for neutrons at $E_n > 0.5$ Mev.

Comparison of the neutron fluxes at $E_n > 50$ Mev in front of and on the outside of the 2m thick wall enabled us to establish the half-value thickness of the concrete for neutrons at those energies: it was found to be 41-43 cm. The neutron intensity distribution outside the building, with respect to height, was almost symmetrical about the orbital plane of the beam of particles, this plane being located at a height of 5 to 7 m from ground level.

On the roof of the accelerator building, neutron flux at $E_n > 50$ Mev was ≤ 0.2 neutrons/cm^2 sec, and at $E_n > 0.5$ Mev was 20-40 neutrons/cm^2 sec.

Now in summing up the results of the measurements performed, it is safe to assert that the accelerator shielding is perfectly adequate to protect the health and safety of the personnel, for lowering the background levels of scattered radiation, and suitable to accomodate various types of experiments with beam particles. More compact variants in the arrangement of the shielding walls, capable of achieving the desired effect with reduced expenditure of materials, are to be recommended for the building of similar accelerator-housing facilities in the future.

The authors wish to express their thanks to V. P. Dzhelepov for his kind assistance and unflagging interest in the work, and for his valued advice.

LITERATURE CITED

1. D. V. Efremov, M. G. Meshcheryakov, A. L. Mints, V. P. Dzhelepov, P. P. Ivanov, V. S. Katyshev †, E. G. Komar, I. F. Malyshev, N. L. Monoszon, I. Kh. Nevazhskii, B. M. Polyakov and A. V. Chestnoi, Atomnaya Énergiya 4, 5 (1956). ‡
2. V. P. Dzhelepov, V. P. Dmitrievskii, V. S. Katyshev, † M. S. Kozodaev, M. G. Meshcheryakov, K. I. Tarakanov and A. V. Chestnoi, Atomnaya Énergiya 4, 13 (1956)†

† Deceased

‡ Original Russian pagination. See C. B. translation.

* * *

DOSE FIELD OF A LINEAR SOURCE

V. S. Grammatikati, U. Ya. Margulis, and V. G. Khrushchev

Translated from Atomnaya Énergiya, Vol. 8, No. 2, pp. 154-155, February, 1960
Original article submitted May 4, 1959

A rod-shaped source, which proves particularly feasible in the design of movable γ facilities, has been successfully used for several types of industrial and experimental radiation facilities. This has stimulated interest in an approximate, but satisfactorily accurate method for computing the dose field of such a source.

It is known that a dose rate P_A at a point A enclosed within an irradiated object at a depth h is established by a linear source of length L (Fig. 1) in correspondence to the formula

$$P_A = \frac{k_\gamma m}{H} \int_0^{\varphi_0} B e^{-\mu h \sec \varphi} \, d\varphi, \qquad (1)$$

where φ_0 is arctan h/H; H is the distance from point A to the source; k_γ is the γ constant of the isotope; m is the linear activity of the source in mC/cm (where m is

expressed in terms of mg equiv Ra, so that k_γ =8.4 r/hr=0.14 r/min); B is the Fano dose build-up factor, taking into account the contribution of multiple scattering in the process of attenuation of the radiation as it traverses the material [1,2]; μ is the linear coefficient of attenuation for a narrow pencil of γ rays.

Making use of the analytic expression of the build-up factor

$$B = A_1 e^{-\alpha_1 \mu h} + A_2 e^{-\alpha_2 \mu h}, \qquad (2)$$

the dose rate P_A will be expressed in the form of a sum of Sievert integrals which may be found from a Table[3]:

$$P_A = \frac{k_\gamma m}{H}\left[A_1 \int_0^{\varphi_0} e^{-\mu h(\alpha_1+1)\sec\varphi} d\varphi + A_2 \int_0^{\varphi_0} e^{-\mu h(\alpha_2+1)\sec\varphi} d\varphi\right]. \qquad (3)$$

Here $A_2=1-A_1$; α_1 and α_2 are constants whose values for different absorbers and different radiation energies are cited in the literature [4,5].

Formula (3) is valid for the case of infinite geometry and, to a sufficient degree of accuracy (~10%), holds for barrier geometry.

Computation of the dose field has been carried out for Co^{60} radiations, Co^{60} being widely used at present as radiation source in irradiation facilities. Water was selected as absorbing medium. The following vlaues were assumed for the constants in our calculations: coefficient of attenuantion for a narrow pencil of γ rays from Co^{60} traversing water μ=0.063 cm^{-1}; α_1=−0.095; α_2=0.060; A_1=8.88; A_2= =1−A_1=−7.88.

Figure 2 shows a family of curves allowing us to compute the dose rate (in r/min)at several distances H from a linear source and at different depths h within the irradiated object, which is of density ρ=1 g/cm^3. The relative distance H/L is laid off on the abscissa, while the quantity ϵ is plotted on the ordinate:

$$\varepsilon = \frac{k_\gamma L}{H}\left[A_1 \int_0^{\varphi_0} e^{-\mu h(\alpha_1+1)\sec\varphi} d\varphi + A_2 \int_0^{\varphi_0} e^{-\mu h(\alpha_2+1)\sec\varphi} d\varphi\right]. \qquad (4)$$

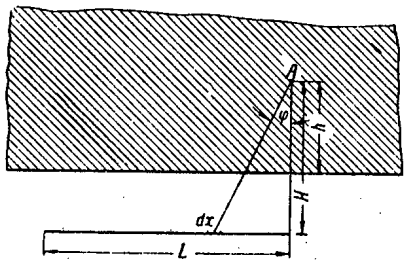

Fig. 1. Diagram for computing the dose rate from a linear source.

Accordingly,

$$P_A = \frac{m}{L}\varepsilon. \qquad (5)$$

The dose rate in air P_0 at point A, for a predetermined H/L, is found along the curve h=0 (cf. Fig. 2). An analysis of the curves for the change in relative value of the dose rate P_h/P_0 in a medium, for different H/L, shows that the dose rate in water may be expressed accurately to an accuracy of 10-15% by means of the following empirical formula:

$$P_A = P_0 \eta e^{-0{,}05(h-\Delta)}, \qquad (6)$$

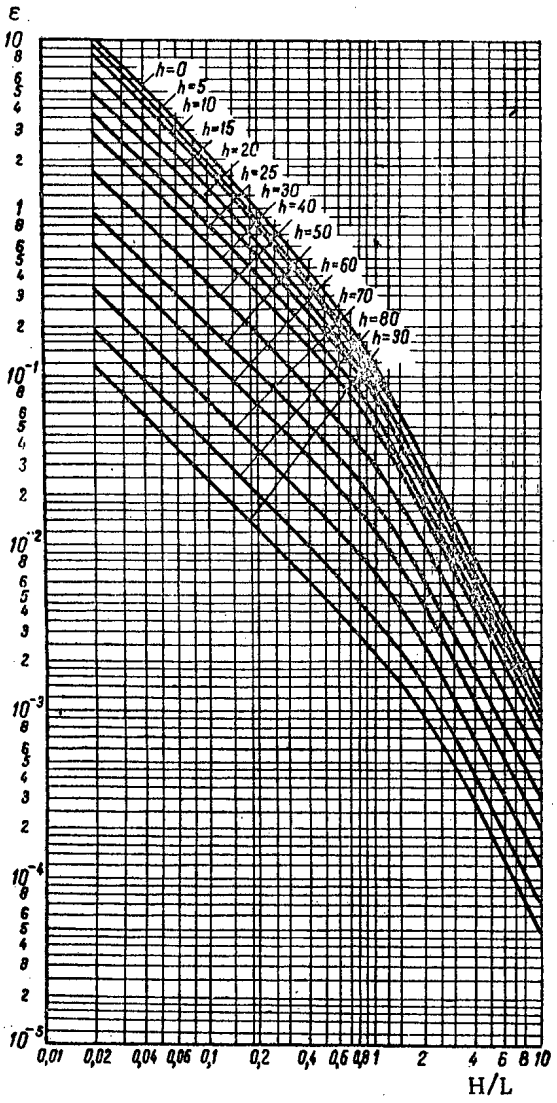

Fig. 2. Nomogram facilitating computation of the dose rate in water, for radiation from a linear source.

Values of Constants in Formulas (6) and (7)

Range of H/L values	η	Δ	σ	Calc. accord. to Eq. (7) for following values of h, cm
0,01—0,1	$(1-2\cdot10^{-3}h)$	5	0	<10
0,2—0,6	1	8	3	<15
0,7—1,0	1	12	3	<20
2,0—10,0	$(1+4\cdot10^{-3}h)$	15	5	<20

where P_0 is the dose rate in air at the given point, η and Δ are constants varying as functions of the relative distance H/L.

The formula cited holds for h $\geq$10 cm at H/L $\leq$ 0.1; for h $\geq$ 15 cm at 0.6 $\geq$H/ L $\geq$0.2 and for h$\geq$20 cm at 10$\geq$H/L$\geq$0.7. For lower values of h

$$P_A = P_0[1-2\cdot10^{-2}(h-\sigma)]. \qquad (7)$$

Values of constants h, Δ,σ are entered in the Table. When the density of the irradiated object is ρ, then the dose rate found from Fig. 2 or from Eqs. (6) and (7) for a given H/L at depth h^1 in the medium will be the same as in water, but h must be taken equal to h^1 .

The curves cited and the empirical formulas make it possible to simplify the calculations of the dose field set up by a linear Co^{60} source in water and in air-equivalent media, retaining reasonable degree of accuracy. They may also be used in calculating the dose fields for sources of other configurations, viewed as a sum of linear sources.

LITERATURE CITED

1. L. Spencer and U. Fano, J. Res. Nat. Bur. Standards 46, 446 (1951),
2. U. Fano, Nucleonics 2, 8, 1 (1953).
3. R. Sievert, Eine Methode zur Messung von Röntgen-Radium und Ultrastrahlen nebst einige Untersuchungen über die Anwendbarkeit derselben in der Physik und der Medizin (Stockholm, 1932).
4. H. Goldstein, Calculation of the Penetration of γ Rays. US AEC, Report NDA-NYO-3075 (1954).
5. Reactor Shielding Handbook. T. Rockwell, ed. (Van Nostrand, New York).

* * *

EXPERIMENTAL INVESTIGATION OF SCINTILLATION COUNTER EFFICIENCY

V. P. Bovin

Translated from Atomnaya Énergiya, Vol. 8, No. 2, pp. 155-158, February, 1960
Original article submitted February 13, 1959

The efficiency of a scintillation counter is defined as the ratio of the number of γ photons recorded to the total number of γ photons corresponding to that energy interval which traversed the volume of the scintillation phosphor.

Several theoretical research efforts [1-5] have addressed themselves to a study of the efficiency of NaI(T1) phosphors with respect to γ radiation, in narrow, broad, and diverging beams. The efficiency of a scintillation counter phosphor depends on the γ-radiation energy, the density, and the mean atomic number of the phosphor, and on the geometry observed in the measurements. The efficiency of cylindrical NaI(T1) crystals irradiated by point sources, isotopes Tl^{204}, Hg^{203}, Sn^{113}, Cs^{137}, Co^{60}, calibrated in an air-equivalent ionization chamber by comparison with a standard radium preparation (0.1 mg) has been subjected to investigation. In that case, efficiency in the general form is expressed, in a spherical system of coordinates, by the relationship

$$\varepsilon = \frac{\int\int\int (1-e^{-\mu x})\sin\theta r^2\, dr\, d\varphi\, d\theta}{\int\int\int \sin\theta r^2\, dr\, d\varphi\, d\theta}, \qquad (1)$$

where μ is the radiation absorption coefficient for absorption within the phosphor, dependent on the energy of radiation; x is the distance traversed by the γ photons inside the phosphor.

Fig. 1 shows the dependence of the efficiency of NaI (T1) crystals, computed using the Monte Carlo technique [5], on energy of radiation upon bombardment by a parallel broad beam of gammas (curves 1 and 3), and upon bombardment by a divergent beam of gammas emitted by a point source placed at a distance of 10 cm from the surface

of the crystal (curves 3 and 4) [3]. For the latter case, Eq. (1) lends itself readily to simplification:

$$\varepsilon = \frac{1}{2\Omega}\int_0^{\theta_0}(1-e^{-\mu x})\sin\theta\, d\theta, \qquad (2)$$

where $\Omega=(1-\cos\theta_0)/2$ is the relative solid angle $\theta_0=\arctan a/h$ (cf. Fig. 1).

It is clear from the characteristics shown that the efficiency of crystals of uniform size is less when emissions from a point source are recorded, because of the lesser mean distance traversed by the radiation within the crystal. The dependence of the efficiency on the distance separating the crystal and the point source of radiation has been investigated both theoretically and experimentally, with results reported in the literature [3,4,6,7]. Calculations demonstrate that, for energies ranging up to 0.1 Mev, efficiency is virtually independent of the distance, while within the range 1-2 Mev it may vary by as much as one and a half to two times, particularly when large crystals are employed. Experimental characteristics obtained for crystals of different sizes show good fit with theoretical predictions. Measurements were carried out with geometry unaltered under conditions allowing for practically 100% recording of photons originating in the crystals (a photomultiplier tube of low noise background and high gain, with good optical contact, optimum discrimination level, etc.).

The use of different filters exerts an important effect on the efficiency of scintillation counters. Figure 2 shows plots of curves of the efficiency of NaI(Tl) crystals with filters placed at the end of the crystal, while Figs. 3,4, and 5 show curves for crystals enclosed in lead, iron, or aluminum filters of different thickness, with radiation acting from the side of the crystal (the source was placed at a distance of 10 cm from the lateral surface of the crystal).

Upon inspecting the diagrams, it becomes evident that the screening action of the iron filters is less thorough than that of lead filters of like thickness (in g/cm^3). The explanation lies in the high efficiency of crystal phosphors

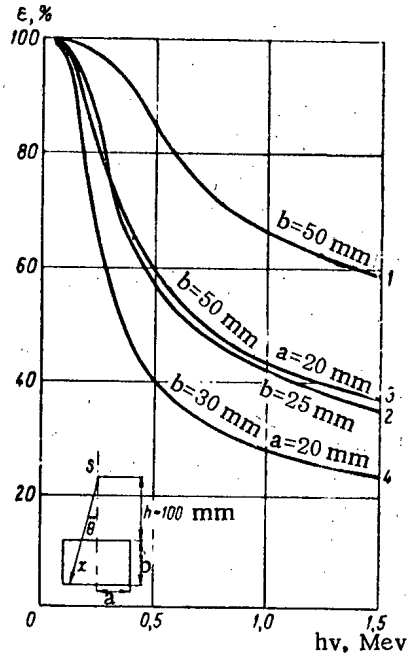

Fig. 1. Predicted curve of dependence of efficiency of NaI(Tl) crystals of different crystal sizes on energy of radiation.

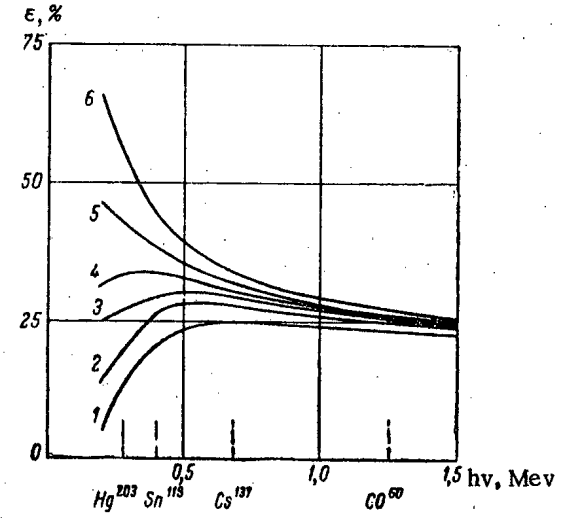

Fig. 2. Curves showing efficiency of NaI(Tl) crystals of 30 mm diameter and 15 mm height, plotted using lead filters of different thicknesses (in mm): 1) 3.0 mm; 2) 2.0; 3) 1.5; 4) 1.0; 5) 0.5; 6) no filter.

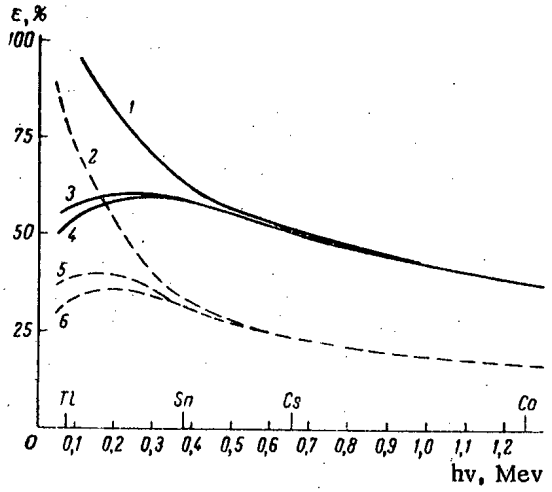

Fig. 3. Curves showing efficiency of NaI(Tl) crystals of different size: 1) 40×50 no filter; 2) 20×20 no filter; 3) 40×50 with lead filter (0.2 mm); 4) 40×50 with filter of aluminum and lead (3 and 0.2 mm); 5) 20×20 with aluminum and lead filter (3 and 0.2 mm); 6) 20×20 with lead filter (0.27 mm).

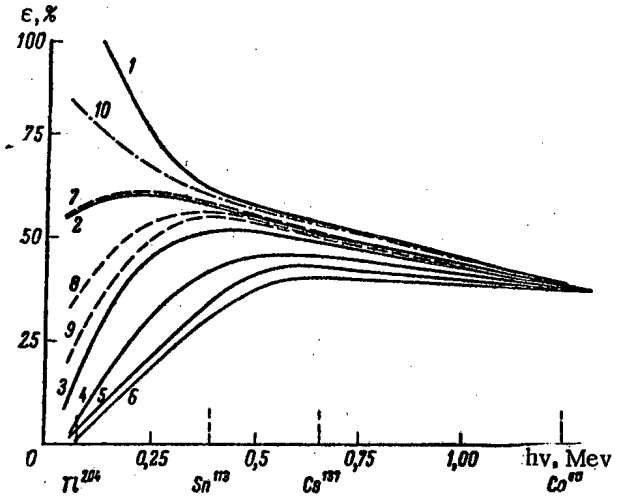

Fig. 4. Plot of dependence of efficiency of a NaI(Tl) crystal, 40×50 mm, on thickness (in mm) and on material used in screening filters: 1) no filter; 2,3,4,5, 6) lead filters, thickness 0.2 mm, 0.5, 1.0, 1.5, 2.0 mm, resp.; 7,8,9) iron filters, 1.0, 2.0, 3.0 mm thick, resp.; 10) aluminum filter (5.0 mm).

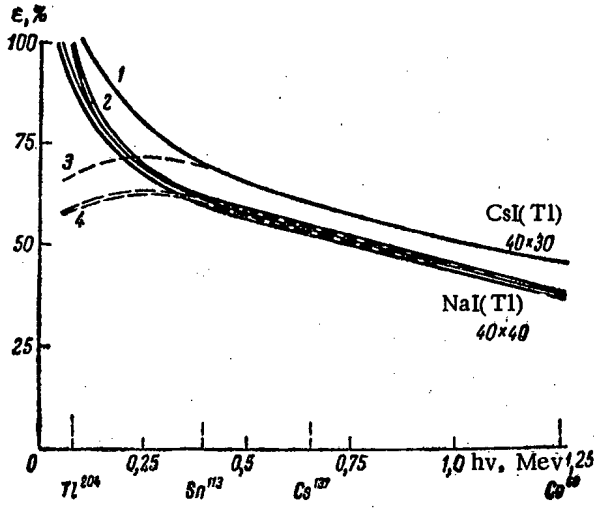

Fig. 5. Curve showing efficiency for NaI(Tl) and CsI(Tl) crystals: 1,2) no filter; 3,4) iron filter, 1 mm diameter.

with respect to soft scattered (Compton) radiation, formed after traversal of the iron filters by radiation, while photoabsorption is the predominant mechanism in lead filters, for energies of radiation up to 0.5 Mev. By means of screened filters of moderate thickness (0.2-0.3 mm lead or 1-1.5 mm iron), it proved possible to achieve some similarity in the efficiency curves for crystals differing in size and type. Figure 5 shows curves for NaI(Tl) and CsI(Tl) crystals, and shows that when lead filters 0.2-0.3

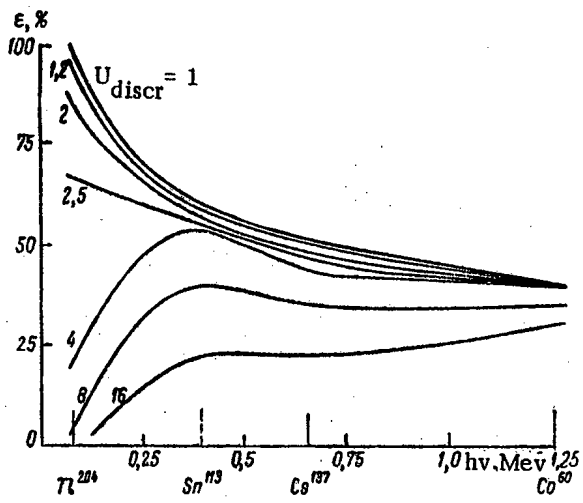

Fig. 6. Plot of scintillation counter efficiency curves for counters using NaI(Tl) crystal 40×50 mm, as a function of the discrimination level of the input signal.

mm thick are used, the efficiency curves become closely similar. Figure 5 also gives the characteristics for five different NaI(Tl) crystals of the same size (± 1 mm). The difference seen in the behavior of the efficiency curves amounts to 5-10%, and this difference may be reduced to 2-3% by using iron filters 1 mm thick.

The differing dependence of scintillation counting efficiency on energy of radiation evinced by different phosphors makes it practically impossible to employ unshielded scintillation counters for quantitative measurements. The similarity observable in the efficiency curves of the scintillation counters greatly facilitates the work of standardization and handling the instruments.

In Fig. 6 we see a plot of curves giving the efficiency of a scintillation counter using NaI(Tl) crystals as a function of the discrimination level of the input signal.

The accompanying diagrams show that the efficiency of a scintillation counter is to a rather large extent determined by the mode of operation of the photomultiplier tube and the sensitivity of the circuit, more so than by any change in the quality or size of the crystals used. For that reason, any comparison of the response (sensitivity) or adjustment of various instruments incorporating scintillation counters should be accompanied by particular attention extended to the judicious choice of mode of operation for the associated circuitry. The purpose of identification of phosphor characteristics will be served reasonably well by shielding the phosphors with lead filters 0.2-0.3 mm thick, or iron filters 1-1.5 mm thick, in some cases using even thicker filters, since the scintillation counter will then become still less sensitive to circuit behavior.

The author avails himself of this opportunity to express his gratitude to V. L. Shashkin for his valuable advice and interest in the research.

LITERATURE CITED

1. Beta and Gamma Spectroscopy, K. Siegbahn, ed. (North Holland Publ. Co., Amsterdam) Chap. 5.
2. M. Berger and J. Dogget, Rev. Scient. Instrum. 27, 269 (1956).
3. A. Stanford and V. Rivers, Rev. Scient. Instrum. 29, 406 (1958).
4. L. Rietjens, G. Arkenbout, G. Wolters, and J. Kluyver, Physica, 21, 1 110 (1955).
5. W. Miller, J. Reynolds, and W. Snow, Rev. Scient. Instrum. 28, 717 (1957).
6. M. Sterk and A. Wapstra, Physica, 19, 669 (1953).
7. W. Hornyak and T. Coor, Phys. Rev. 92, 675 (1953).

* * *

A MOBILE NEUTRON MULTIPLIER UNIT

T. A. Lopovok

Translated from Atomnaya Énergiya; Vol. 8, No. 2, pp. 158-159, February, 1960
Original article submitted July 17, 1959

The techniques of nuclear physics are winning an increasing large number of applications for themselves both in geological research work and in prospecting and exploration work. One of the most effective methods is that of activation analysis.

With a view to developing the method of activation analysis of rocks in the prospecting and exploration of minerals, a method requiring the presence of rather powerful neutron sources, the Atomic Energy Institute of the Academy of Sciences of the USSR, in collaboration with its sister body, the Institute of Petroleum, began work in 1958 on the design and building of a small-size facility known as a neutron multiplier.

The neutron multiplier (Figs. 1-3) is a small-size transportable uranium-water heterogeneous system mounted on a ZIS-151 truck capable of hauling a load of 4 tons.

The maximum multiplication factor of the facility $K_{eff}=0.997$. The primary neutron source, of initial power $\sim 5 \cdot 10^7$ neutrons/sec, is provided by a mixture of polonium and beryllium. The nuclear fuel employed is uranium enriched to 10%, placed in vertically arrayed aluminum tubes each accomodating ~ 7.2 g U^{235}, with ordinary water used as both moderator and reflector. The core of the multiplier unit is of close to cylindrical shape; it measures ~ 45 cm in height and ~ 42 cm in diameter. The optimal lattice pitch is 18 mm, and the core geometry renders the system safe in the event that the truck gets into an accident. The multiplier is charged with ~ 2.8 kg of U^{235} isotope.

The multiplier unit has five experimental channels, each 52 mm in diameter, which are situated within the

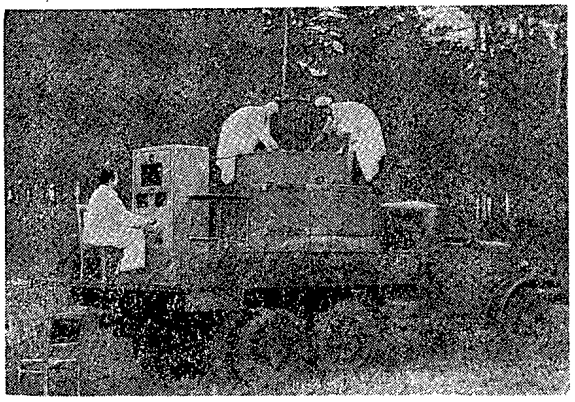

Fig. 1. Neutron multiplier in use under field conditions.

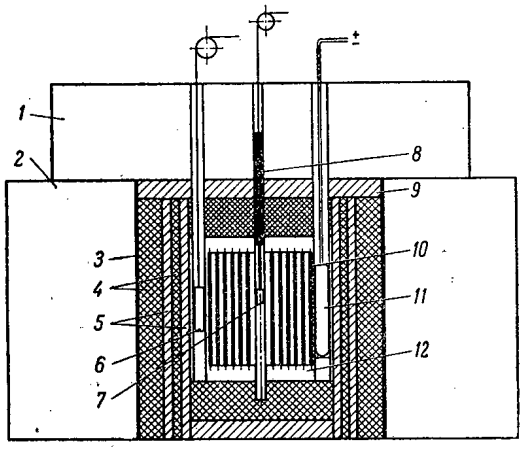

Fig. 2. Layout of multiplier unit: 1) upper shielding tank; 2) lateral shielding tank; 3) boron carbide layer; 4) iron layer; 5) layer of paraffin and boron carbide; 6) test specimen; 7) neutron source; 8) control rod; 9) iron slab; 10) fuel element; 11) ionization chamber; 12) water reflector.

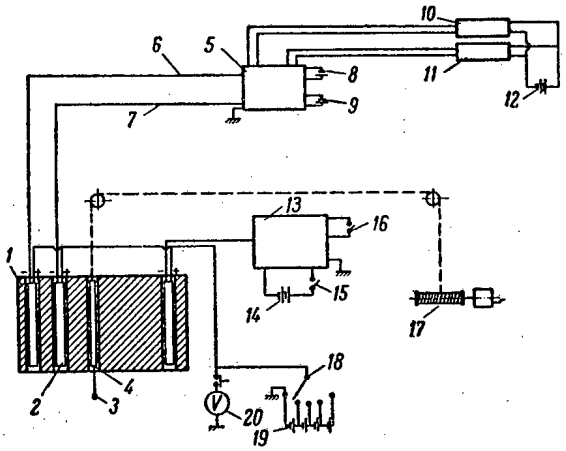

Fig. 3. Control system of multiplier: 1) core; 2) ionization chambers; 3) neutron source; 4) control rod; 5) two-channel dc amplifier; 6) first lead; 7) second lead; 8) channel battery; 9) anode battery; 10) galvanometer No. 1; 11) galvanometer No. 2; 12) signal-light battery; 13) signal unit; 14) signal-unit battery; 15) tumbler switch; 16) check switch; 17) step-down transformer; 18) switch serving ionization chamber batteries; 19) chamber batteries; 20) voltmeter.

reflector. Experiments based on the (n,γ) and (n,p) reactions may be performed simultaneously in both channels. A fast-neutron converter, a thin-walled cylinder made of enriched uranium, is provided, to vary the neutron spectrum in either of the channels. One of the channels is cadmium-plated on the outside. The overall effective volume of the channels is about 2 liters, for a flux of $3\text{-}4\cdot10^6$ neutrons/cm^2·sec in the channels. The multiplier power is controlled by positioning the control rod, which is made of boron carbide, and has the polonium-beryllium source attached to its lower end. When the source is shifted to the center of the core, the control rod is completely withdrawn from the pile; this position corresponds to full power on. At peak power level, the fluxes in the test channels are two orders of magnitude larger than the fluxes obtainable from the source without the use of the multiplier.

The multiplier power is sensed and recorded by two ionization chambers placed in the reflector section and connected up to the circuit containing the galvanometers. The current from the ionization chambers is amplified by a special two-channel dc amplifier with two gain coefficients (200 and 2,000) assuring proportionality between the current at the output and the input signal. Conventional dry cells are used as power supplies for the recording and signal equipment. One interesting feature in the design of the neutron multiplier is that all of the parts and assemblies are portable, the weight of any one unit (including shielding layers) not exceeding 80 kg. This facilitates disassembly and reassembly of the facility under field conditions, should the need arise.

Experience acquired in working with the neutron multiplier, in tests conducted during October 1958 under field conditions, shows that this new facility is a convenient tool for activation analysis work (determination of content of vanadium, indium, chlorine, manganese, aluminum, silicon, sodium, potassium, cobalt, and other elements). However, this by no means exhausts the range of possible applications for the device; it may be employed under any conditions for activation analysis based on activation using short-lived isotopes.

The small size of the facility (~1.5 m high and ~2 m in diameter) and its safe handling, not requiring specially trained personnel to service it, as well as the ease of control, place the successful operation of this facility within the reach of any research institute.

THE PRODUCTION AND USE OF STABLE ISOTOPES IN THE USSR

S. P. Potapov

Translated from Atomnaya Energiya, Vol. 8, No. 2, pp. 160-164, February, 1960

The basic method in the production of enriched stable isotopes for scientific research work is the electromagnetic method. Electromagnetic separation facilities developed in the USSR are capable of producing enriched stable isotopes of most elements in amounts from several milligrams to several kilograms. In those cases where large quantities of particular isotopes are required, a variety of physical-chemical techniques capable of quite large productivity are often resorted to: fractional distillation, chemical exchange, low-temperature distillation, diffusion in a vapor stream, etc. Facilities have been built for separating isotopes of boron, carbon, nitrogen, oxygen, and several other elements by means of those techniques.

The current outstanding task, in line with the development of new trends in the applications of stable isotopes, is to further improve the methods of separating isotopes, with the idea of developing processes suitable for industrial-scale use [1].

The increase in the production and deliveries of stable isotopes for scientific research may be appreciated by examining the following data covering the past several years:*

	1955	1956	1957	1958
Number of isotopes delivered	55	136	170	222
Number of deliveries	130	230	250	350
Quantity of isotopes delivered, g	2500	14000	20000	25000

A listing of enriched stable isotopes made available in quantities larger than a single gram, and their characteristic data, is given in Table 1†.

The most widespread application found for stable isotopes is their use as labeled atoms. Stable "tags" feature several advantages over their radioactive counterparts: research involving their use is free from any time restrictions on that account, and is in fact no different from conventional chemical operations; the absence of radiations makes it unnecessary to build or provide specially equipped radiochemical laboratories. The use of stable isotopes also smooths the way for appreciable improvements in the method of radioactive labeled atoms through the production of "pure" radioisotopes [3] having the required mode of radiation and half-life (Table 3) from the enriched raw material. In addition to improved radiochemical purity, these isotopes also exhibit greater specific activity. In those cases where point sources of radiation with high specific activity are specified, this is of paramount importance.

When stable isotopes are used as labeled atoms, they play an auxiliary role, functioning solely as a means of investigation. Along with the rapid development of work in the study and systematization of the properties of isotopes, the use of stable isotopes in the capacity of materials of varied isotopic composition is occupying a prominent place. The use of such materials is of the greatest practical interest in connection with electron physics equipment and nuclear radiation techniques.

With respect to equipment used in the study of electron physics, differences in the nuclear properties of stable isotopes are used primarily in devising new radiation detectors, e.g., highly sensitive neutron counters which are finding applications not only in research work, but also in the solution of practical problems, particularly in prospecting for minerals [4].

Another, and may we note, most important area in which differences in the nuclear properties of stable isotopes are of great importance is the field of nuclear radiation engineering [1]. Of course, in view of the relative complexity involved in the production of enriched stable isotopes in large yield, it is still early to speak of any widespread industrial use of these substances as materials with varied isotopic composition. However, the present level of production of stable isotopes allows for a detailed study of the opportunities open to their use in that direction, requiring first of all the measurement and systematization of the fundamental nuclear constants of stable isotopes. Accurate knowledge of those constants is important for the elaboration of a quantitative theory of the nucleus, for the design of reactor facilities and for determining which stable isotopes will be promising for industrial-scale use. Up to the present, these constants have been measured primarily in milligram amounts of enriched stable isotopes, al-

* The production and use of hydrogen and uranium isotopes are not included.

† More detailed data on available stable isotopes may be found in a catalog [2].

TABLE 1. Stable Isotopes Supplies in Quantities Larger Than 1 Gram

Isotope	Content in natural mixture, %	Mode of production	Chemical compound	Class*	Content in enriched product, %
B^{10}	18,83	Fractionation	BF_3	IV	85
			H_3BO_3		75
			KBF_4		75
			$CdBF_5$		75
			B (amorphous)		75
B^{11}	81,17	"	B (amorphous)	IV	99
N^{15}	0,38	Chemical exchange	N^{15}, H_4NO_3, and 15 compounds	III	10
O^{18}	0,204	Fractionation	H_2O and other compounds	IV	to 40
K^{39}	93,08	"	KCl	III	99,1
K^{41}	6,91	"	KCl	III	27,2—98,9
Ca^{42}	0,64	Electromagnetic	$CaCO_3$	III	49,8—52,4
Ca^{44}	2,06	Same	$CaCO_3$	III	88,9—93,4
Ca^{46}	0,0033	"	$CaCO_3$	I	4,8
Ca^{48}	0,185	"	$CaCO_3$	II	63,1
Titanium isotopes	—	"	Ti or TiO_2	II—III	—
V^{50}	0,24	"	V_2O_5	I	16,2—28,5
Cr^{50}	4,31	"	Cr_2O_3 or $BaCrO_4$	III	87,7
Cr^{52}	83,76	"	Cr or $Cr_2O_3BaCrO_4$	IV	91,1—99,4
Cr^{53}	9,55	"	Cr_2O_3 or $BaCrO_4$	III	84,3—92,8
Cr^{54}	2,38	"	Cr_2O_3 or $BaCrO_4$	II	60—78
Fe^{54}	5,84	Electromagnetic	Fe_2O_3	III	70,5—84,8
Fe^{58}	0,31	Same	Fe_2O_3	II	25,2—40,1
Ni^{58}	67,76	"	NiO	IV	90,2—97,6
Ni^{60}	26,16	"	NiO	III	92,6—95,4
Ni^{61}	1,25	"	NiO	II	22,8
Ni^{62}	3,66	"	Ni or NiO	III	36,5
Ni^{64}	1,16	"	NiO	II	83
Cu^{65}	30,9	"	Cu	III	94—97,4
Cu^{63}	69,1	"	Cu	III	89,2—96,4
Zn^{64}	48,89	"	Zn or ZnO	III	85—98
Zn^{66}	27,81	"	ZnO	II	89,2—90,4
Zn^{67}	4,11	"	ZnO	II	33,2—40
Zn^{68}	18,56	"	ZnO	II	86—92,3
Zn^{70}	0,62	"	ZnO	II	34,7—44,5
Germanium isotopes	—	"	Ge or GeO_2	II	—
Se^{74}	0,87	"	Se	III	26,2—40,9
Se^{76}	9,02	"	Se	II	62—86,1
Se^{80}	49,82	"	Se	III	92—94
Se^{82}	9,19	"	Se	II	59,2
Rubidium isotopes	9,86	"	RbCl	II	—
Sr^{86}	82,56	"	$SrCl_3$	I	78—86
Sr^{88}	11,23	"	$SrCO_3$	II	98—99,8
Zr^{91}	17,40	"	ZrO_2	II	61,6
Zr^{94}	2,80	"	ZrO_2	III	87,0—94,0
Zr^{96}	—	"	ZrO_2	II	31,0
Molybdenum isotopes		Electromagnetic	Mo or MoO_3	II	—
Ag^{107}	51,35	Same	Ag	I	98
Ag^{109}	48,65	"	Ag	I	99

Isotope	Content in natural mixture %	Mode of production	Chemical compound	Class*	Content in enriched product, %
Cadmium isotopes	—	Electromagnetic	Cd or CdO	II	—
Cd^{114}	28,86	Same	Cd or CdO	III	88,5—94,9
Sn^{112}	0,95	"	Sn	II	60,6—66,2
Sn^{115}	0,34	"	Sn	I	9,6—17,6
Sn^{116}	14,07	"	Sn	I	86—98
Sn^{117}	7,54	"	Sn	I	49—85,6
Sn^{118}	23,98	"	Sn	III	70,8—82,0
Sn^{119}	8,62	"	Sn	I	50,7—74,8
Sn^{120}	33,03	"	Sn	III	86,5
Sn^{122}	4,78	"	Sn	II	73,9
Sn^{124}	6,11	"	Sn	II	76,0
Te^{120}	0,089	"	TeO_2	II	5,9
Te^{126}	18,72	"	TeO_2	III	76,3
Te^{130}	34,46	"	TeO_2	IV	87,8—94,2
W^{182}	26,4	"	W or WO_3	III	71,5—78,9
W^{184}	30,6	"	W or WO_3	II	79,4—89,4
W^{186}	28,4	"	W or WO_3	II	90,0
Tl^{203}	29,50	"	Tl or Tl_2CrO_4	III	76,8—90,2
Tl^{205}	70,50	"	Tl or Tl_2CrO_4	III	94,3—95,6
Pb^{204}	1,48	"	Pb or $PbSO_4$	I	36,6
Pb^{208}	52,3	"	Pb or $PbSO_4$	III	63,6—75,4

* Class signifies the quantitative range within which the stable isotope may be supplied: class I: up to 3 g; class II: up to 30 g; class III: up to 300 g; class IV: up to 1 kg.

TABLE 2. Isotope Targets

Element*	Characteristics of isotope layer		Remarks
	Mode of application**	Thickness, μ	
H	Saturation of zirconium or titanium foil overlaid on metal substrate	0,6—50	Molybdenum or tungsten used as substrate
Li	Vacuum evaporation	***	—
Be	Same	1—2	****
Mg	"	***	—
Al	Electrolytic precipitation	***	—
K	Vacuum evaporation	1—5	****
Ca	Same	1—5	****
Ti	Thermal dissociation of titanium iodide	1—10	****
V	Thermal dissociation of vanadium chloride	***	—
Cr	Thermal dissociation of chromium iodide	1—15	****
Fe	Electrolytic precipitation	4—10	****
Co	Same	1—10	****
Ni	"	1—20	****
Cu	"	1,5—10	****
Zn	"	5—10	****
Ga	"	***	On metal substrate
Ge	Vacuum evaporation	***	—

TABLE 2. (continued)

Element*	Characteristics of isotope layer		Remarks
	Mode of application**	Thickness, μ	
Se	Same	***	—
Rb	»	***	—
Sr	»	***	—
Zr	Thermal dissociation of zirconium iodide	1—10	****
Mo	Thermal dissociation of molybdenum chloride	***	—
Ag	Electrolytic precipitation	5—10	****
Cd	Same	5—10	****
In	» »	***	on metal substrate
Sn	»	***	—
Rare-earth elements	Vacuum evaporation	***	—
Hf	Same	***	—
W	Thermal dissociation of tungsten chloride	***	—
Tl	Electrolytic precipitation	***	on metal substrate
Pb	Same	***	—

*Targets with multiisotope elements may be prepared from the element or its enriched stable isotopes.

**Isotope targets composed of several elements, e.g., B, N, O, noble gases may be prepared by the diffusion method in the electromagnetic separation of stable isotopes

***prepared in experimental order

****the target may be made on a metallic substrate or in the form of free foil. Molybdenum, tungsten, tantalum, and several other products serve as good target materials.

TABLE 3. Radioactive Isotopes Produced from Enriched Raw Material

Radioactive Isotope	Original stable isotope	Natural content, %	Content in enriched product %
P^{33}	S^{32}	0,74	Experiment
Ca^{45}	Ca^{44}	2,06	90—93
Ca^{47}	Ca^{46}	0,0033	4,8
Cr^{51}	Cr^{50}	4,49	90,6—91,8
Fe^{55}	Fe^{54}	5,81	82,3—84,8
Fe^{59}	Fe^{58}	0,34	40
Ni^{59}	Ni^{58}	67,76	90—97,6
Ni^{63}	Ni^{62}	3,66	86,5
Cu^{64}	Cu^{63}	69,09	89,2—96,4
Zn^{65}	Zn^{64}	48,89	85—98
Zn^{69}	Zn^{68}	18,61	86—92,3
As^{74}	Ge^{73}	7,8	Experiment
Se^{75}	Se^{74}	0,87	30
Sr^{85}	Sr^{84}	0,56	31—46
Sr^{89}	Sr^{88}	82—56	99,5
Zr^{95}	Zr^{94}	17—40	87,2—93,8
Sn^{113}	Sn^{112}	0,95	60,6—66,2
Sn^{123}	Sn^{122}	4,71	63,8—77,2
Cd^{115}	Cd^{114}	28,86	88,5—94,9
Te^{127}	Te^{126}	18,72	76,3
J^{131}	Te^{130}	34,49	87,8—94,2
Ba^{131}	Ba^{130}	0,101	Experiment
Ba^{133}	Ba^{132}	0,097	8
Sm^{153}	Sm^{152}	26,63	54,8—84,2
Eu^{155}	Sm^{154}	22,53	94,1
W^{185}	W^{184}	30,6	76,9—96,3
W^{187}	W^{186}	28,4	77,1—92,3
Tl^{204}	Tl^{203}	29,5	84,9—90,2
Pb^{209}	Pb^{208}	52,3	73,2

though samples weighing up to several grams and even tens of grams have been required in some procedures [5]. Therefore, in the case of thermal neutrons, not to speak of intermediate-spectrum and fast neutrons, not all of the fundamental nuclear constants of stable isotopes (total cross sections, resonance level parameters, radiative capture cross sections, etc.) have been measured with adequate precision. Systematic data on stable isotopes with charged particles are not available at all at present.

Other promising research work on the uses of stable isotopes in reactor design should also be taken note of, as for instance on the use of stable isotopes as minor additives or component parts of alloys, illustrated in the case of B^{10}. In reactor design, conventional boron is used as an additive in steels to enhance refractory behavior and at the same time to increase absorption of thermal neutrons. A rather high boron concentration in the steel is desirable if the object is to increase absorbing power, but the boron content must be small (1-2%) to avoid deterioration in engineering properties. This contradiction may be sidetracked by using the light isotope B^{10} [6] as additive, since it has a large (~4000 barns) thermal neutron capture cross section. Other conditions being equal, this property of B^{10} makes it possible to reduce the relative content of the additive required to less than five times.

LITERATURE CITED

1. N. M. Zhavoronkov et al., Khim. Nauka i promyshlennost' 4, 487 (1959); S. Levin and E. von Halle, Paper 719 presented by the USA at the Second International Conference on the Peaceful Uses of Atomic Energy (Geneva, 1958).
2. Catalog of Isotopes, Radiation Sources, and Radioactive Materials (in Russian) (Moscow, Atomizdat, 1959).
3. E. E. Kulish, Proc. of All-Union Conf. on Uses of Radioactive and Stable Isotopes. Production of Isotopes [in Russian] (Izd. AN SSSR, 1958) p. 18.
4. J. Sharp, Atomnaya Tekhnika za Rubekhom, 2, 39 (1959); V. K. Khristianov et al., "Determination of boron content by the neutron method, under field conditions," Geokhimiya 2, 3 (1957).
5. D. J. Hughes, Neutron Cross Sections. BNL-325.
6. Nucl. Sci. and Eng. 4, 3, 357 (1958).

* * *

CONFERENCE ON THE USES OF LARGE RADIATION SOURCES IN INDUSTRY AND PARTICULARLY IN CHEMICAL PROCESSES

V. I. Sinitsy and G. I. Grafov

A conference on the uses of large radiation sources in industry, with emphasis on their applications in chemical processes, was held in Warsaw, September 8-12, 1959, organized by the International Atomic Energy Agency. Over 200 scientists and representatives delegated by industrial organizations of 27 nations participated in the conference. The largest delegations were those from Britain, Poland, USSR, USA, France, and Japan. More than 60 papers were read at the gathering.

Papers dealing with large radiation sources and techniques for using them discussed the design of mobile facilities built for irradiation of potatoes to delay germination, and the engineering data of equipment for radiation polymerization of ethylene on an industrial scale (Canada).

At a panel session discussing "The uses of cobalt-60 and other radiation sources," designs of large facilities incorporating cobalt sources were discussed; also facilities for performing research in the field of the radiation technology of rubber and plastics (Czechoslavakia) with a source of 250 C activity, and a setup engineered by the Japan Atomic Energy Research Institute for the study of the chemical effects of radiation on organic compounds, the radiation effects on high polymers and nonmetallic materials (Japan) using an irradiatior of 10,000 C activity; a cylindrical irradiator unit in this facility is assembled from 110 cobalt slugs, whose activity was accurately established by calorimetric means. Techniques in the design and building of facilities for radiation-chemical experiments were also discussed at this session (Denmark, Hungary, USSR, France).

D. George and D. Gregory (USA) presented a description of the γ facility at the research center of the Atomic Energy Commission of Australia; the radiation source utilized in this device consists of spent fuel elements recovered from the HIFAR experimental reactor. After withdrawal from the reactor, the spent fuel elements are allowed to decay for 40 days in a water-cooled storage chamber. The mean activity of the fuel elements ranges about 10^5 C; they are kept upright in 48 bays along a square grid of pitch 178 mm. A 228 mm diam. thimble surrounded by eight symmetrically arranged fuel-element bays is placed at the center of the facility. The volume available for irradiation has a diameter of 178 mm and is 762 mm high.

A sample to be irradiated is mounted in a shielding plug and inserted into and removed from the thimble by means of a special vertical charging device.

Several tubes are passed through the shielding plug for heating or cooling of the irradiated sample, for temperature readings, removal of reaction products, and other purposes.

Expenditures in outfitting the irradiation chamber directly within the storage room were insignificant, and irradiation costs were practically negligible, since irradiation took place during the time the spent elements were undergoing storage as per regulations.

A report by A. K. Breger et al. (USSR) described the operating principles and gave a picture of the overall characteristics of an indium-gallium radiation circuit developed for application to an IRT type nuclear reactor. Circulation of the substance to be activated in this loop takes place between the zone of activation (inside the reactor) and the irradiator (just outside the reactor). The approach makes possible effective use of short-lived isotopes.

Research conducted in the USA on the utilization of β radiation of fission products was reported on by J. Silverman, who pointed out that this radiation opens up new perspectives for the use of β radiation on an indus-

trial scale, especially for surface modification of plastics and textiles by graft copolymerization. The measurements of absorption of β radiation pointed up the possibility of designing nonpoint sources of rather high radiation efficiency (up to 20% efficiency). According to an analysis of production cost data, β-emitting fission products are competitive with other radiation sources.

A study of the parameters of large slab irradiator units of Co^{60}, Na^{24}, and Cs^{137}, including such constants as source size, activity distribution, geometry of the source-target system, were carried out at Brookhaven National Laboratory to provide data on the size of the specific dose and dose distribution in the target. Several absorbers were considered in the study, at various positions between target and source.

At the panel session devoted to "Studies of fission fragments and recoil energy in chemical processes," questions pertaining to the use of microporous nuclear fuel as a means for utilizing the kinetic energy of decay processes in chemical synthesis processes, the use of decay products in chemical engineering processes, and the use of nitrogen oxidation in reactors were discussed.

H. Heyns and V. Desreux (Belgium) devoted their paper to the use of radiation in chemical industry, dealing with the effects of γ radiation on samples of polyethylacrylate with different molecular weights, both in bulk solid form and dissolved in benzene and carbon tetrachloride. These effects may be detected in concentrated solutions and in the solid material by measurement of viscosity and sedimentation.

The nature of the chemical changes in methacrylamide, the physical-chemical properties of the product, and its infrared spectrum were studied by Polish scientists A. Orszagh and associates at the Institute for Nuclear Research.

In the process of studying the physical properties of polyvinyl chloride with copolymer crosslinking, British scientists (S. Pinner and associates) succeeded in obtaining products with firm linkages, in response to relatively low doses of ionizing radiations on a previously prepared mixture of polyvinyl chloride with diallyl and triallyl ethers. Verification of the physical properties of these products showed that they are not simple graft-copolymers, generally containing long branched chains, but copolymers with chains crosslinked with allyl bonds.

The Japanese scientists S. Onishi and co-workers measured the electron spin resonance spectra of γ-irradiated polymers in a study of the radiation-chemical processes affecting several polymers.

Since electron spin resonance spectra may be quite complex, identification of trapped radicals was found to be difficult in many cases. For such irradiated polymers as nylon, polyethylene, and polyvinyl alcohol, the spectra of the specimens were found to differ from one another.

Radiation polymerization of ethylene in the gaseous phase in solutions of organic substances was studied in research by Soviet scientists S. S. Medvedev, A. D. Abkin, and P. M. Khomikovskii, studying several properties of the polymers formed. It was demonstrated that the polymerization of ethylene in response to nuclear radiations shows promise as a technique both with respect to reaction rate and radiation-chemical yield, and with respect to the engineering properties of the resulting polymer. Radiation polyethylene is superior to polyethylene obtained by other methods in a number of its properties (degree of purity, density, crystallinity). The reaction rate of polymerization for ethylene in solutions of heptane, cyclohexane, methyl alcohol, and acetone, at a pressure of 5 atmos, temperature of 25° C and dose rate of 98 r/sec is 10-15 times faster than in the gaseous phase. The polymers so formed have mean molecular weights ranging from 20,000 to 40,000. The polymerization process in the gaseous phase proceeds during the initial stages at an increasing rate, later tapering off to a constant rate. The polymerization rate is observed to taper off during later stages of the reaction. The radiation-chemical yield at pressure of 300 atmos, temperature of 25°C, and dose rate of 72 r/sec amounts to 4300 to 6500 molecules of ethylene per 100 ev of energy absorbed. When pressure is raised from 100 to 300 atm, the characteristic viscosity of the polymers increases from 1 to 4 (at earlier stages).

G. Oster (USA), in a report entitled "The role of electron excitation in the chemical effects of radiations on plastics," showed that there exists some similarity between many of the chemical results produced by photochemical and ionizing radiation. The differences reside primarily in the different distribution of the products due to chemical effects, for example in the different mutual arrangement of amorphous and crystalline zones.

The study of the effects of radiation on polyvinyl alcohol, carried out by M. Matsumoto of Japan, showed that the process of degradation of the molecular chain in response to a dose of the order of 10^7 r is independent of dose rate. At large doses, the results depend appreciably on dose rate; the introduction of polyvinyl alcohol with the formation of crosslinks is facilitated by increasing the dose rate. Irradiation in the absence of air causes gelation for small dose rates and a lower overall dose, than required in an air medium to produce the same effect. These studies show that oxygen exerts a great effect both in irradiation of the solid material and in irradiation of an aqueous solution of the material.

The problem of radiation-initiated graft polymerization was dealt with in several papers presented by S. Okamura and associates (Japan) on a study of vinyl acetate polymerization in aqueous medium under gamma bombardment. The authors succeeded in obtaining a

highly stable pure cationic emulsion of polyvinyl acetate in an aqueous solution of cationic detergent. Measurement of the rates of cationic and anionic emulsion polymerization of vinyl acetate in response to γ-ray bombardment demonstrated that anionic polymerization proceeds at a more rapid pace than cationic polymerization.

The British scientists F. Dalton and R. Roberts conducted an investigation of graft polymerization of polyacryl nitrile and dimethyl siloxane, initiated by means γ radiation; the dependence of reaction rate on monomer concentration, radiation intensity, and temperature was determined, and a kinetic interpretation of the observed phenomena was given.

Under bombardment by γ rays, nylon fibers began to gel in a nitrogen atmosphere, with degradation of the molecular chain taking place in air. Following irradiation, the nylon fibers were immersed in an aqueous solution of acrylamide and again irradiated. S. Okamura and associates (Japan) observed, upon carrying out that treatment, that graft polymerization took place solely on the surface of the fibers. In studying the effect of concentration of a solution of formamide in methanol (used as a solution for swelling) on increase in weight of the fiber (viscose rayon or artificial silk), they found that maximum grafting took place when a 5% solution was used in preliminary processing.

In an effort to improve the properties of motion picture film and film made from polyvinyl alcohol, the Japanese Association for Polymer Radiation Research undertook investigations on graft copolymerization of various vinyl monomers with motion picture film made from polyvinyl alcohol, under exposure to γ radiation, at their Kyoto and Osaka laboratories. They also found that the effects experienced by methyl methacrylate when grafted with polyvinyl alcohol film are similar to the effects experienced by styrene, while a small amount of water exerts a substantial effect. The efficiency achieved in grafting of methyl methacrylate at any given dose of irradiation is usually higher than the grafting efficiency of styrene.

J. Sutherland and A. Allen (USA) studied radiolysis of pentane occluded within the crystal lattice of dehydrated synthetic zeolites (Linde molecular sieve). The yield of hydrogen (amount of hydrogen forming per unit of energy spent on the entire solid plus pentane) for sodium zeolite varies little as the amount of pentane is varied.

Under exposure to radiation, chlorine dissolved to saturation in one of its liquid derivatives displaces one hydrogen atom in the carbon chain. As in radiolysis, this reaction is of a radical type and assumes the nature of a chain process. Radicals are formed in the radiolytic decomposition of the liquid medium, while chlorine is the causal agent responsible for chain propagation. F. Traynard and P. Verrier (France) found that weak irradiation renders the initial reaction rate proportional to the square root of the radiation dose rate. However, as the latter is increased, this relationship fails, as a rule. At the most, chlorination may be carried out to the extent of displacing five hydrogen atoms in the carbon chain and even to the point of forming the acid chloride of pentachloropropionic acid, which leads to the formation of a whole series of individual and often crystalline substances.

As shown in papers submitted by E. Taylor and associates, reporting on work performed at the Oak Ridge National Laboratory, radiations may be used to effect a drastic modification in the activity of catalysts in heterogeneous catalysis. For instance, under exposure to γ bombardment, the activity of zinc oxide in ethylene hydrogenation processes is lowered, while it is increased in hydrogen-deuterium exchange. Emphasis is laid on the fact that the perspectives of using irradiation to improve catalysts are still basically remote at the present state of the art, since this effect disappears in most instances when the catalyst is heated to those temperatures at which most processes of industrial interest occur.

A. Henglein (USA) stated that nitric oxide acts on organic liquids as a radical scavenger. He succeeded in oxidizing new nitro compounds through reactions of free radicals with nitric oxide. Trichloronitromethane (chloropicrin) was formed from mixtures of CCl_4–NO, and dichloronitromethane, never before synthesized, was formed from mixtures of $CHCl_3$–NO.

F. Balestic and M. Magat (France) determined the factors effecting reaction yield as a result of an investigation of the synthesis of several colorants (particularly Lauth purple) in response to radiation.

A special session of the conference was devoted to the genetics of plants, the suppression of virus activity and sterilization, and to methods for coping with harmful insects.

Studies were carried out at Brookhaven National Laboratory on the effects of radiation on a large number of species and varieties of plants. This research done on varieties of plants exhibiting comparatively high radiosensitivity showed that the range of sensitivity varies by about 1000 times in highly developed plants. These variations are affected by chemical composition, size and amount of chromosomes, and other factors. Modifications were also observed in many species of plants accompanied by pronounced stunting or growth stimulation.

Removal of sources of infection from foodstuffs or drugs, and extraction of vaccines from viruses with antigenicity retained and with the elimination of infectious properties may be achieved by means of ionizing radiantions. E. Pollard and W. Guild (USA) plotted inactivation curves for several plant, animal, and bacterial viruses, and determined the required source activities to obtain different degrees of activation. The authors came to the conclusion that the method of combining

moderate heat processing and γ inactivation makes it possible to produce a vaccine which is antigenically potent while at the same time noninfectious.

A method for sterilization of pharmaceutical preparations, sutures and hospital supplies by ionizing radiations was discussed in a paper submitted by C. Artandi and associates (USA). The advantages of this method lie in the possibility of sterilizing the product while still in the package, in the use of new, cheaper and more convenient packing materials, and in ease of adaptation to a continuous technological process.

Eradication of the screwworm fly by γ sterilization of the males provided the stimulus for research in the USA on the use of such approaches to eliminate other insect pests, such as fruit flies, which jeopardize truck and crop farming.

In reports delivered at the session devoted to the economics of radiation processing, comparisons were made of the use of cobalt radiation sources and spent fuel elements, estimates were made of the costs involved in chlorination of polymers under irradiation, and results of a study of the economic aspects of the use of electron-beam irradiation on a production basis were made available.

A paper by P. Aebersold (USA) was devoted to a review of developments of fundamental forms of industrial radiation applications, and to the program outlined for radiation processing on an industrial scale in the USA; this program envisages, in particular, expansion of research in the field of radiation chemistry and verification of the basic reaction constants in reactions induced by irradiation, as well as development and research work on the design and manufacture of radiation sources, uses of nuclear reactors and fission product applications.

* * *

TASHKENT CONFERENCE ON THE PEACEFUL USES OF ATOMIC ENERGY

A. Kiv and E. Parilis

A conference on the peaceful uses of atomic energy, convened under the auspices of the Academy of Sciences of the Uzbek SSR and the State Science and Engineering Committee of the Council of Ministers of the Uzbek SSR, met September 28 to October 3, 1959, in Tashkent. The conference call was timed for the commissioning of the nuclear reactor of the Nuclear Physics Institute of the Academy of Sciences of the Uzbek SSR, which was started up on September 10, 1959.

About 1,000 persons participated in the conference, these including 400 persons from other republics. About 270 papers were read on nuclear physics and various aspects of the peaceful uses of radioactive isotopes and nuclear radiations. The conference took on the appearance of an all-union congress, judging by the scope of the subject matter, the number of participants, and the composition of delegations from scientific institutions.

A report by the Director of the Nuclear Physics Institute of the Academy of Sciences of the Uzbek SSR, U. A. Arifov, dealing with the perspectives of development envisaged for scientific research at the Institute was delivered at the first plenary session, followed by a report from representatives of the Main Control Board attached to the Council of Ministers of the USSR, P. S. Savitskii and V. I. Sinitsyn, on the opportunities for peaceful uses of atomic energy in the USSR.

S. V. Starodybtsev, Vice President of the Uzbek SSR Academy of Sciences, delivered an extensive review paper at the same session, on investigations of changes in the properties of matter, and intense nuclear radiation fields. The report included a balance sheet of studies in the field of the physics of radiation effects conducted in laboratories of the Uzbek SSR Academy of Sciences.

The rest of the proceedings of the Conference was heard in panel sessions.

Nuclear and radiation physics: 50 papers were delivered. The papers on nuclear physics dealt primarily with nuclear reactions and neutron scattering of neutrons. Some papers were devoted to reactions between α particles and deuterons, as well as radiation from fission fragments.

Some of the papers contained an exposition of studies on photodisintegration of nuclei. Papers were also read on investigations of excited fragments and conversion-electron spectra.

Most of the papers on radiation physics were devoted to changes in the optical, electrical, magnetic, elastic, and adsorptive properties of crystals bombarded by γ rays. Radiolysis of hydrocarbons under γ-ray bombardment was discussed in other papers delivered at this session. A separate panel heard a discussion of the

procedure followed in the investigations, particularly in physical investigations using radioactive isotopes. Mass-spectrometric techniques, the use of nuclear magnetic resonance spectroscopy, applications of radioactive isotopes in nuclear and molecular physics and in electronics, were discussed.

Radioactive isotopes and nuclear radiations in industry and geology: 29 reports and 10 short communications were heard at this panel. Some of the reports at the first session of the panel dealt with applications of radioactive isotopes and nuclear radiations in instrument design and metrological work. Descriptions were given of automatic control devices, level gauges, flowmeters, high-sensitivity radioactive relays. These reports were supplemented by papers delivered at the second session which contained the results obtained by using radiations for measurement of density, moisture, and volume, and in studies of wear on machine parts.

Papers heard at the third session of the panel dealt mostly with γ-radiography and γ-flaw detection of metal parts and reinforced concrete. A report on applications of radioactive isotopes in the cotton textile industry was also delivered.

The fourth session was devoted in its entirety to high-level γ facilities. Problems in the design, construction, use, and economic efficiency of such radiation facilities were discussed. A report on a general-purpose facility using a Co^{60} source of 60,000 gram equivalents Ra activity, in use at the L. Ya. Karpov Research Institute for Physical Chemistry, and a paper on a facility incorporating a Co^{60} source of 160,000 gram equivalents Ra activity, under construction at the Nuclear Physics Institute of the Uzbek SSR Academy of Sciences, were heard with intense interest.

The two remaining sessions were reserved for nuclear geophysics and nuclear geology. The reports given touched on radioactive techniques in the determination of the content of different elements in rock species and studies of moisture transport, density, and moisture of soils. Papers on radiometric methods in petroleum and gas prospecting in various districts, especially in Central Asia, stimulated much interest.

Radioactive isotopes and nuclear radiations in chemistry: 44 papers and 5 communications. The papers ranged over a variety of problems in radiochemistry, radiation chemistry, uses of radioactive isotopes in chemistry, chemical analysis of radioactive isotopes. Radiation-chemical techniques for producing pure substances, studies of chemical reaction kinetics using the effect of nuclear radiations on the physical-chemical and engineering properties of preparations, the use of spectral analysis in the production of radioactive isotopes were discussed. Further discussion centered on problems in γ spectroscopy, production of doubly-labeled compounds, and many other matters. The session set forth a series of problems as the most important problems requiring probing in coming work.

Radioactive isotopes and nuclear radiations in medicine: 60 papers and 2 communications. The use of radioactive iodine in determining the functional state of the thyroid gland and in goiter therapy received the most detailed attention. The formation of iodized substances in the organism when radioactive iodine is used was discussed. Various instances of the use of labeled atoms in the study of turnover processes in the organism were discussed in the reports presented, as well as problems of functional changes in different human and animal organs exposed to nuclear radiations.

Particular emphasis was given to the problem of changes induced in the organism by light doses of x-radiation. Some of the papers undertook an evaluation of the functional state of the vascular system by radioisotope techniques. Problems discussed included shielding of skin against radiation injury, cases of successful cures of radiation sickness, and methods of research on radiation sickness. The efficacy of radioactive cobalt emissions in the therapy of malignant tumors was demonstrated.

Panels devoted to the use of radioactive isotopes and nuclear radiations in studies on animal and plant biology. The subject matter of the 59 reports and 6 communications dwelt primarily on the characteristics of various functional changes occurring in biological objects in response to radiation effects.

The outstanding importance of the initial functional state of the organism for the distribution of the radioactive isotopes employed in a biological experiment was pointed out.

A communication was received on the effect of radioactive isotopes on the immunobiological reactions of the organism, as well as on changes in the response of the nervous system of the progeny to single exposure and partial exposure of pregnant animals.

The turnover of various substances in animals suffering from radiation sickness and healthy animals was discussed.

Research on translocation of mineral substances in plants and the transformation of those substances, as a function of external and internal factors, was discussed. A clinical study of the features of chlorophyll biosynthesis in plants, based on the radioisotope method, was discussed. The specific features of the response of plant tissues to exposure to ionizing radiations were noted. Data provided on the effects attributable to several factors (nutrition, water and light environment) on phosphorus turnover in the cotton plant demonstrated the possibility of varying the content of phosphorus compounds by changing the vegetative conditions of the cotton plant. A communication was read on the use of the radioisotope technique in studying the effects of microfertilizers on the rate of photosynthesis in the white mulberry tree. An analysis was made of the physiological and biochemical effects of ionizing radiations

on plants, as well as other questions related to radiation effects on biological objects.

Radioactive isotopes and nuclear radiations in agriculture: the general trends in the use of ionizing radiation in agriculture were duscussed. The possibility of obtaining new wheat mutants and improving the quality of cotton plants by γ irradiation was indicated. Uptake of phosphorus and sulfur via the roots and via pathways bypassing the roots during the period of fruit-bud formation and translocation of phosphorus and sulfur in the cotton plant were discussed. Results were given on a study of the efficacy of various methods of introducing phosphates into the cotton plant, using labeled atoms. The use of radioactive isotopes to establish the pathways by which plants make use of nutritive substances from subsoil layers proved interesting. The same may be said for the use of stable oxygen and hydrogen isotopes in soil science and agronomical research. The use of labeled atoms in animal husbandry and veterinary science was discussed. A proposal was voiced on working out a standard method of irradiating seeds of agricultural plants prior to sowing, and on the need for introducing statistical techniques into the processing of experimental data in work using nuclear radiations.

The following reports were read at the concluding plenary session: "Production of radioactive isotopes in the USSR" (E. E. Kulish, G. M. Fradkin), "The present status and the perspectives for the use of radioactive isotopes in turnover studies in healthy and pathological states" (Ya. Kh. Turakulov), "A well-logging neutron generator and new techniques for investigating wells" (G. I. Budker). The transactions of the conference will be published in a special edition in 1960.

While the Conference was in session, the city of Tashkent was host to an "Atoms for Peace" exposition organized by the Main Control Board on the Use of Atomic Energy attached to the Council of Ministers of the USSR, the Health Ministry of the USSR, and the Academy of Sciences of the Uzbek SSR.

* * *

STANDARDS

Tm^{170} Gamma Sources

The achievements in flaw detection and materials testing arrived at by the use of gamma-radiation sources based on artificial radioactive isotopes have been given wide publicity. The simplicity, portability, and ease of handling of gamma-ray flaw detection devices have opened up a broad range of applications for them in quality control of castings, weldments, etc.

The sources which have won greatest popularity in such applications are those based on the radioactive isotopes Co^{60}, Cs^{137}, Ir^{192}. These sources emit comparatively hard gamma radiation, and are consequently good for quality control of steel parts of not less than 8-10 mm thickness. For the radioscopy of light metals and alloys, and of thin items made of steel and other heavy metals, the quality of the shots taken with such sources deteriorates in short order. This has opened the way in recent years for broader use of sources based on the isotope Tm^{170}, which can be successfully employed to take excellent shots of steel parts of thickness of the order of 1-2 mm, and of thin sheet of light metals.

The Tm^{170} nuclide has a half-life of 129 days and a fairly simple decay scheme, containing two β-lines with energies 0.968 Mev (76%) and 0.884 Mev (24%), and a single γ-line at 0.084 Mev coinciding with a β-line at 0.089 Mev. There also exist traces of weak positron radiation (not more than 0.01%). However, the over-all decay

Characteristics of Tm^{170} Sources of Soviet Manufacture

Source activity* g-equiv Ra	Radioactive impurities	Source capsule size, mm		Size of active portion of source, mm		Price, rubles
		diameter	height	diameter	height	
0,002	Not detected	4,5±0,5	5±0,5	1,5	1,5	55
0,004		4,5±0,5	5±0,5	1,5	1,5	100
0,02		7,5±0,5	8±0,5	4,5	4,5	200
0,10		7,5±0,5	8±0,5	4,5	4,5	700
0,50		12±0,5	10±0,5	9,0	6,0	2500

* Arrived at by considering external radiation.

scheme is measurably complicated by the presence of intense conversion-electron emission, the composition of which still awaits adequate investigation.

The softness of the gamma emission and the rather large effective activation cross section (~116 barns) creates considerable difficulties in the preparation of Tm^{170} sources.

Experience shows that sources of fairly high activity are required to cut down the exposure time in gamma radiography. The usual approach to improvements in this direction is by increasing the amount of material irradiated, which however fails to yield positive results in the case of interest. The reason is intense self-absorption of gamma radiation by the source material and self-shielding of the source, resulting in absorption of the bulk of the neutrons by the outer layers of the source material, so that the inner layers remain virtually unactivated. Furthermore, an increase in source thickness results in the appearance of intense bremsstrahlung at an effective energy of 300-400 kev, impairing the quality of the shots.

For a predetermined neutron flux, this establishes the only feasible way to produce high-activity sources, namely by lengthening exposure periods.

Thulium oxide containing not less than 95% of the basic substance is used in preparing Tm^{170} sources. Prior to irradiation, the thulium oxide is inserted into double aluminum capsules with tightly crimped lids. The leak-tightness of each capsule is carefully checked. The pile-irradiation time for the capsules at a given neutron flux is determined by the amount of thulium oxide inserted into the pile, and the required source activity. This irradiation period does not exceed three to four months for any of the types of sources fabricated in practice.

At the present time, fabrication of a large number of different types of Tm^{170} sources (cf. accompanying table) has been put on a steady basis in the USSR.

LITERATURE CITED

1. G. Seaborg, I. Perlman, and J. Hollander, Table of Isotopes. Russian edition; (IL, Moscow, 1956).
2. Isotopes, radiation sources, and radioactive materials (catalog) [in Russian]. (Atomizdat, Moscow, 1959).
3. I. P. Selinov, Table of Isotopes. Great Soviet Encyclopedia, [in Russian] (Moscow, 1958). Volume 51.

E. K.

* * *

BRIEF NOTES

USSR. In December 1959, the Physics and Engineering Institute of the Academy of Sciences of the USSR completed construction on a low-power atomic reactor, a water-cooled, water-moderated reactor rated at 10,000 kw, with thermal neutron flux intensity of 10^{14} neutrons/cm^2 sec, and started it up.

The reactor will be used for a broad scope of investigations in the fields of nuclear physics, solid-state physics, radiochemistry, metallurgy, nuclear power, use of radioactive isotopes in industrial applications, and research on a number of problems in the area of biology and agriculture.

China. A small Van de Graaff electron accelerator, built for 2 Mev with a beam current of 100 μa, has been commissioned at Na-Kai University. The machine was placed inside a steel tank under 15 atmos pressure. It is expected that the accelerator will be employed for scientific and industrial research projects.

Yugoslavia. In December 1959, the research reactor at the Boris Kidrič Institute of Nuclear Physics in Vinc (near Belgrade) was started up. The reactor was built with the aid of the Soviet Union.

NEW LITERATURE

V. I. Gol'danskii, A. V. Kutsenko, and M. I. Podgoretskii. Statistika otschetov pri registratsii yadernykh chastits [The statistics of counts in nuclear particle recording]. Moscow, Fizmatgiz, 1959 411 pages; 12 rubles; 25 kopeks.

This book examines the problems of processing the results of measurements expressed in the number of counts recorded by nuclear radiation counters. The related statistical problems are based on discrete distributions. Poisson's law is explained in the first two chapters. The third chapter offers a description of statistical problems encountered in radioactive decay. The fourth chapter takes up the performance of particle counters with dead time. The operation of scalers and coincidence circuits is analyzed in the last two chapters. The book is written for experimental physicists working in the field of nuclear physics and the physics of elementary particles.

B. Price, C. Horton, and K. Spinney. Radiation Shielding. Translated from the English (Pergamon Press, London). (Zashchita ot yadernykh izluchenii) Moscow, Foreign Literature Press, 1959, 490 pages.

This book is the second special edition on nuclear radiation shielding published in Russian translation in the USSR in recent years. The contents of the first such translation, Reactor Shielding Design Manual (Zashchita yadernykh reaktorov, Foreign Literature Press, 1958; edit. T. Rockwell), could be gleaned from the title. The monograph by B. Price et al. takes up not only problems of reactor shielding but also shielding for charged-particle accelerators. The authors devote a good deal of attention to problems involving the passage of radiations through shielding material, where the bulk of the data presented is taken from the records of British and American laboratories. Shielding design problems, especially where concrete and metal wire shielding materials are used, are discussed in no less detail. Graphs, tables, and calculations are liberally appended to the text. The characteristics of new shielding materials specially designed for thermal shielding materials, such as boron steel, boron, boron graphite, are of unquestionable interest.

The book was written by research scientists employed at the British Harwell Atomic Energy Research Establishment.

P. Ageron, M. Gauzit, A. Bonaldi, and T. Reiss. Technologie des Réacteurs Nucléaires. Vol. I. Matériaux. Eyrolles et Gauthier, Villars, 1959, 568 pages.

This French publication constitutes the first volume of a projected five-volume series devoted to nuclear reactor technology. This first volume contains nine chapters: I. Fundamentals of reactor physics; II. Radiation effects on materials; III. Fissionable materials and secondary nuclear fuel; IV. General requirements for nonfissionable nuclear materials; V. Reflectors for slow reactors. Moderators; VI. Coolants; VII. Neutron absorbers; VIII. Shielding materials; IX. Structural materials.

The contents of the chapters are basically a compilation of American and British work published up to 1958, plus some lesser known French work. In contrast to previous works on the subject, the description of properties of materials is unified with a systematic approach to materials requirements as pertains to nuclear physics. The book also contains some useful reference material. However, the book is based primarily on obsolete material, with much new and important data conspicuous by its absence. This volume would therefore be of scant interest to specialists working in atomic industry.

ARTICLES FROM THE PERIODICAL LITERATURE

I. Nuclear Power Physics

Vestnik Leningrad. univ. 16, seriya fiz. i khim, No. 3 (1959)

Yu. M. Kagan and V. I. Perel', pp. 49-50. On the effect of finite lifetime on the shape of ion lines in a positive discharge column.

Vestnik Moskv. univ., seriya matem., mekh., astron., fiz., khim., No. 2 (1959)

Yu. I. Remnev, pp. 43-47. Symmetric deformation of a sphere in the presence of cubic dilatation (in neutron irradiation).

V. N. Tsytovich, pp. 135-141. On the effect of the resonance properties of a plasma on the propagation of electroacoustic waves.

Doklady akad. nauk SSSR, 127, No. 6 (1959)

D. V. Sharikadze, pp. 1183-1186. Self-similar flow and point explosion in magnetic gas dynamics, for infinite gas conductivity.

Doklady akad. nauk SSSR, 128, No. 4 (1959)

V. I. Kogan, pp. 702-705. On the role of impurity emission in the energy balance of a plasma pinch.

Doklady akad. nauk SSSR, 128, No. 5 (1959)

B. M. Gokhberg et al., pp. 911-912. Effective fission cross section of Th^{229}.

Zhur. tekhn. fiz., XXIX, No. 11 (1959)

Yu. V. Vandakurov, pp. 1312-1316. On possible equilibrium configurations of a thin annular plasma conductor immersed in a magnetic field.

A. N. Lebedev, pp. 1339-1345. Contribution to the theory of particle injection in cyclic accelerators at high currents.

D. P. Ivanov and Yu. S. Korobochko, pp. 1414-1415. Contribution to the problem of the effectiveness of some portions of the injection pulse in betatron capture of electrons.

Zhur. eksptl. i teoret. fiz. 37, No. 4 (10), (1959)

L. I. Guseva et al., pp. 973-977. Production cross section of Cm^{240} in the irradiation of Th^{232} by C^{12} and C^{13} ions.

V. D. Shafranov, pp. 1088-1095. On the equilibrium of a plasma torus in a magnetic field.

B. B. Kadomtsev, pp. 1096-1101. On convective instability of a plasma pinch.

V. D. Kirillov, pp. 1142-1144. Energy losses due to radiation in a gas discharge plasma.

N. A. Perfilov and Z. I. Solov'eva, pp. 1157-1159. Angular distribution of long-range α-particles associated with fission.

G. S. Golitsyn, pp. 1062-1067. Some problems of dynamics and heating of a conductive medium in a magnetic field.

Izvestiya akad. nauk Arm. SSR, seriya fiz.-matem. nauk 12, No. 3 (1959)

M. L. Ter-Mikaelyan, pp. 95-99. Radiation of a relativistic electron moving on a circular path in a plasma.

Izvestiya akad. nauk Latv. SSR, No. 6 (1959)

R. Ya. Damburg and V. Ya. Kravchenko, pp. 87-92. Excitation of magnetohydrodynamic waves in a plasma by a moving charge.

Trudy fiz. inst. akad. nauk SSSR, 11 (1959)

M. V. Kazarnovskii, pp. 176-223. Theory of a nonstationary elastic slowing down of neutrons in a heavy medium.

Atomkernenergie 4, No. 10 (1959)

O. Allkofer, pp. 389-395. A new pulse height analyzer for cosmic radiation.

Brit. J. Appl. Phys. 10, No. 9 (1959)

---, pp. 383-391. Review of papers presented at the high-vacuum symposium (London, April, 1959).

Helv. phys. acta 32, No. 5 (1959)

K. Meyer et al., pp. 423-444. Absolute intensity measurements of radioactive emissions, using the coincidence technique.

J. Appl. Phys. 30, No. 10 (1959)

R. Hill and S. Tetenbaum, pp. 1610-1611. Harmonic generation in a cyclotron resonant plasma.

Nucl. Instrum. and Methods 5, No. 3 (1959)

D. Robertson and D. Elliott, pp. 133-141. Magnetic losses in cores of different geometries.

W. Parker, pp. 142-147. Equipment for vacuum deposition of radioactive substances.

J. Rosenblatt, pp. 152-155. Design of alternating-gradient quadrupole lenses.

J. Thirion and J. Saudinos, pp. 165-169. Magnets for focusing and analysis of particles, in the Saclay cyclotron.

S. Bjornholm et al., pp. 196-198. A method of fabricating cyclotron targets of rare-earth oxides by electrophoresis.

Nucl. Instrum. and Methods 5, No. 4 (1959)

D. Chick et al., pp. 205-210. A Van de Graaff accelerator tube of very low retrograde electron current.

M. Barbier and A. Schoch, pp. 211-233. A study of two-dimensional linear oscillations with the aid of an electromechanical model applied to particle motion in cyclic accelerators.

W. Brown, pp. 234-241. Use of a Van de Graaff electron generator in semiconductor research.

C. Vincent et al., pp. 254-258. Modification of the nuclear resonance technique to measure inhomogeneous magnetic fields.

D. Luckey, pp. 266-268. Use of an electrostatic generator as an injector for an electron synchrotron.

Nucl. Sci. and Engng. 6, No. 2 (1959)

G. de Saussure and E. Silver, pp. 159-160. Measurement of the temperature dependence of the transport mean free path of thermal neutrons in beryllium.

F. Valente and R. Sullivan, p. 162. Age of neutrons from a Pu-Be source in water.

R. Vernon, p. 163. Effective resonance integral for uranium carbide.

Nuovo Cimento, Vol. 14, No. 1 (1959)

G. Cortini et al., pp. 54-61. Photoneutrons ejected from aluminum.

Phil. Mag. 4, No. 44 (1959)

E. Silk and R. Barnes, pp. 970-972. Study of fission fragment tracks with the electron microscope.

II. Nuclear Power Engineering

Elektrichestvo, No. 10 (1959)

V. L. Bershadskii et al., pp. 50-56. Electrical power machinery of the propeller propulsion system on the atomic icebreaker "Lenin."

Atomkernenergie 4, No. 10 (1959)

A. Kirchenmayer, pp. 395-397. A method for calculating the thermal utilization factor in heterogeneous reactors.

A. Kirchenmayer, pp. 397-398. The use of thermal neutrons from a heterogeneous reactor, in the light of two-group diffusion theory.

H. Baehr and W. Strewe, pp. 398-402. Calculation of coolant temperature in reactor channels.

A. Weber, pp. 417-418. The Belgian nuclear center.

W. Braunbek, pp. 418-420. Measurement techniques in nuclear physics.

Chem. and Process Engng. 40, No. 9 (1959)

J. Baxter, pp. 327-329. Nuclear power in Australia.

Chem. and Process Engng. 40, No. 10 (1959)

B. Harbourne, pp. 347-351. Sodium as reactor coolant.

J. Appl. Phys. 30, No. 10 (1959)

H. Smets, p. 1623. On Welton's stability criterion for nuclear reactors.

J. Brit. Nucl. Energy Conf. 4, No. 3 (1959)

H. Rose and J. Syrett, pp. 179-183. Variations in reactivity with reactor period.

S. Lewis, pp. 184-188. Theory of fuel cycling with continuous loading and unloading of fuel elements.

J. Balfour et al., pp. 189-197. Effect of fuel cycling on perturbations of axial reactor flow.

P. French and C. Lowtian, pp. 198-202. Optimization of fuel cycling. I.

P. Grant et al., pp. 203-209. Optimization of fuel cycling. II.

J. Stewart and N. Franklin, pp. 210-216. Performance problems associated with fuel cycling.

A. Harwood et al., pp. 234-249. Design of electromechanical equipment for power reactors.

J. Brit. Nucl. Energy Conf. 4, No. 4 (1959)

N. Mackay and E. Hardwick, pp. 263-281. Electrical equipment of the Calder Hall nuclear power station.

J. Binns and W. Outram, pp. 282-300. Electrification of plants of the Industrial Group of the United Kingdom Atomic Energy Authority.

D. Watt, pp. 301-311. Design of electromagnetic pumps for liquid metals.

J. Cockcroft, pp. 348-357. Recent developments in nuclear engineering.

Nucl. Engng. 4, No. 42 (1959)

---, pp. 383-385. Fuel element with transverse coolant flow.

G. Gunnill and G. Kinchin, pp. 386-393. The "Zenith" high-temperature zero-power reactor.

D. Barnard et al., pp. 394- 399. Investigation of heat transfer by a gas.

P. Robinson and J. Taylor, pp. 400-403. Thermal instability from graphite oxidation.

A. Miller, pp. 404-405. Monitoring humidity in the design of steam raising units.

P. Froggatt, pp. 406-407. Filters for reactor gas channels.

---, p. 411. The Westinghouse Corp. nuclear power station.

E. Gorlett and E. Hawthorne, p. 412. An organic-moderated reactor for cargo ships.

Nucl. Instrum. and Methods 5, No. 4 (1959)

G. Neyret and J. Parain, pp. 259-265. Correcting circuits for the "Saturn" synchrotron.

Nucl. Sci. and Engng. 6, No. 3 (1959)

C. Maynard, pp. 174-186. Rod transparency theory and transparency factors for slab geometry.

L. Holway, pp. 191-201. Use of perturbation theory to solve reactor diffusion equations.

L. Tonks, pp. 202-213. Theoretical fundamentals of the method of "absorption area"; use of this technique to evaluate the efficiency of uniformly spaced control elements.

J. Hanna et al., pp. 214-221. Elastic response to internal blast loading of containment shell models.

J. Wilkins, pp. 229-232. Minimum total mass of a reactor.

W. Kimel et al., pp. 233-237. Determination of time behavior of neutron density and reactivity in the "Argonaut" reactor.

T. Harris, pp. 238-244. Study of coolant expansion in pressurized-water power reactors, resulting from loss-of-coolant accident.

V. Schrock and L. Grossman, pp. 245-250. Local pressure gradients in evaporation with forced convection.

Ch. Kelber and Ph. Kier, p. 251. Some remarks on Bell's approximation to the resonance integral.

J. Davis et al., pp. 251-252. Solution of P_3-equations in the one-dimensional and two-dimensional cases.

C. Truman, pp. 252-253. Use of nondimensional variables in reactor kinetic equations.

G. Melese, pp. 253-254. Fission counter sample disk holder and slide.

Nukleonik 1, No. 8 (1959)

R. Schulten et al., pp. 277-286. Physics of the "Brown Boveri-Krupp consortium" high-temperature reactor.

E. Kern, pp. 286-290. Determination of temperature of a neutron gas.

A. Kirchenmayer, pp. 290-295. Determination of steady-state distribution of neutron flow by analog simulation.

A. Ziegler, pp. 295-305. Fine structure of a heterogeneous reactor.

III. Nuclear Fuels and Materials

Doklady akad. nauk SSSR 128, No. 3 (1959)

T. G. Aminov et al., pp. 533-535. Magnetic susceptibility of some oxalate complexes of tetravalent uranium.

Zhur. prikladnoi khim. 32, No. 9 (1959)

A. T. Davydov and Yu. A. Tolmacheva, pp. 1979-1984. Comparative characteristics of some anion exchangers.

Zavodskaya laboratoriya 25, No. 10 (1959)

V. F. Luk'yanov et al., pp. 1155-1157. Photometric assay of thorium in zircons, using the new arsenazo III reagent.

Zapisi Vsesoyuz. mineralog. obsh., Part 88, No. 5 (1959)

G. Yu. Epshtein, pp. 564-570. On molybdates of uranium, moluranite, in iriginite.

Zapisi Kirgiz. otdel. Vsesoyuz. mineralog. obsh., No. 1 (1959)

S. D. Turovskii, pp. 5-11. Contribution to thorium geochemistry.

P. I. Chalov et al., pp. 113-124. Estimate of the comparative migrating power of $UX_1(Th^{234})$ in the hypergenetic zone of uranium deposits.

Izvestiya akad. nauk SSSR, seriya fiz. 23, No. 9 (1959).

N. P. Ivanov, pp. 1154-1156. Spectral assay of uranium by isotope dilution techniques.

Radiokhimiya 1, No. 4 (1959)

A. I. Moskvin, pp. 430-434. Investigation of complexing of plutonium and americium (III) in aqueous solutions by the solubility and ion exchange techniques.

M. N. Yakovleva and M. A. Shurshalina, pp. 445-449. On a field technique for determining the forms of uranium migration in natural waters.

V. P. Shvedov and Sh. A. Musaev, pp. 465-474. Coprecipitation of La^{140}, Pm^{147}, and Y^{91} with iodates of tetravalent cerium.

E. S. Pal'shin and Yu. A. Zolotov, pp. 482-487. Extraction technique for isolating neptunium-239 from irradiated uranium.

K. F. Lazarev and S. M. Grashchenko, pp. 493-496. On the concentration of radioelements from large volumes of natural water.

Trudy Sverdlovsk. gorn. inst., No. 34 (1959)

A. S. Vershinin, pp. 165-172. Radioactive equilibrium in uranium minerals as an indicator of their time of formation and of migration direction of radioactive elements.

A. S. Vershinin, pp. 172-182. Field techniques for quantitative assay of radioactivity of ore deposits by radiometric techniques.

Khim. nauka i prom. 4, No. 4 (1959)

N. P. Rudenko, pp. 441-448. Methods for isolating carrier-free radioactive isotopes.

Yu. B. Gerlit et al., pp. 465-472. The chemistry of the new elements: technetium, promethium, astatine, and francium.

Ya. M. Varshavskii and S. E. Vaisberg, pp. 498-509. Current techniques in heavy water production.

P. I. Dolin, pp. 516-521. Effect of ionizing radiations on aqueous solutions of inorganic compounds.

B. K. Preobrazhenskii, pp. 521-526. Applications of ion exchange chromatography for the separation of transuranium and radioactive rare-earth elements.

V. I. Baranov and T. V. Malysheva, pp. 526-530. Current radiometric methods.

Amer. Ceram. Soc. Bull. 38, No. 10 (1959)

B. Schaner, pp. 494-498. Fabrication of UO_2 pellets for fuel elements.

Atomkernenergie 4, No. 10 (1959)

R. Reiter and H. Ziehr, pp. 409-415. Results of measurements of air radioactivity in the region of development of uraniferrous brown coal.

Atomwirtschaft 4, No. 10 (1959)

R. Gain, pp. 435-439. Testing of reactor materials by pile-irradiation fast reactors.

Canad. Mining J. 80, No. 10 (1959)

F. Joubin, pp. 110-114. Development of the uranium industry in Canada.

Chem. and Process Engng. 40, No. 9 (1959)

D. Harries, pp. 313-316, 319. Production of zirconium and its alloys. I.

Chem. and Process Engng. 40, No. 10 (1959)

D. Harries, pp. 363-368. Production of zirconium and its alloys. II.

J. Appl. Phys. 30, No. 10 (1959)

C. Houska and B. Averbach, pp. 1525-1531. Neutron irradiation effects in a copper-aluminum alloy.

J. Brit. Nucl. Energy Conf. 3, No. 4 (1959)

D. Hull and I. Mogford, pp. 230-233. Effect of a brittle shell on the transition of unirradiated and irradiated steel from the brittle to the plastic state, in impact strength testing.

P. Cotterill and H. Axon, pp. 250-251. Composition of the alloy Bi–U in the range 0-35 at. % U.

J. Brit. Nucl. Energy Conf. 4, No. 4 (1959)

K. Meredith and M. Waldron, pp. 328-334. Nonmetallic impurities in uranium metal.

J. Stephenson, pp. 335-341. Vacuum casting of uranium.

P. Pfeil et al., pp. 342-347. The uranium-niobium system in the solid state.

J. Inorg. and Nucl. Chem. 10, No. 3/4 (1959)

C. Hardy and D. Scargill, pp. 323-327. Investigation of mono- and dibutyl phosphoric acids. I. Separation of mono- and dibutylphosphoric acids by selective extraction and paper chromatography.

J. Inorg. and Nucl. Chem. 11, No. 2 (1959)

T. Sato et al., pp. 84-90. Neutron irradiation of various phosphates in a vacuum.

B. Weinstock et al., pp. 104-114. Vapor pressures of NpF_6 and PuF_6. Thermodynamic calculations for UF_6, NpF_6, and PuF_6.

C. Hardy and D. Scargill, pp. 128-143. Investigation of mono- and dibutyl phosphoric acids. II. Solubility and distribution of mono- and dibutyl phosphoric acids between aqueous solutions and a series of organic solvents.

D. Cohen et al., pp. 159-161. Half-life of Np^{239}.

J. Duncan, pp. 161-163. Determination the solubility product by means of radiometric titration; a new method.

Mining Congress J. 45, No. 7 (1959)

W. Lennemann and F. McGinley, pp. 59-63. Development of processes for reprocessing uranium ores.

Mining Congress J. 45, No. 8 (1959)

A. Quine, pp. 79-81. Uranium mining in Wyoming.

G. Sidhu and E. Oberbillig, pp. 82-83. Flotation of monazite.

Mining Congress J. 45, No. 10 (1959)

J. Borden, pp. 94-96. Uranium mining on the Colorado plateau.

Mining Engng. 11, No. 7 (1959)

W. Overstreet et al., pp. 705-714. Thorium and uranium reserves in monazite placer deposits in the Western Piedmont (USA).

Nucl. Sci. and Engng. 6, No. 3 (1959)

L. Prus et al., pp. 167-173. Dispersion of enriched boron in titanium.

S. Zegler and M. Nevitt, pp. 222-228. Some properties of uranium-fissium alloys.

IV. Nuclear Radiation Shielding

Vestnik akad. med. nauk SSSR, No. 9 (1959)

A. V. Lebedinskii and Yu. I. Moskalev, pp. 3-16. On some problems of current radiobiology.

Okhrana truda i sots. strakhovanie, No. 10 (1959)

S. Gurvits and E. Chitov, pp. 65-66. Determination of radioactive contamination of air.

Atomkernenergie 4, No. 10 (1959)

H. Wilski, pp. 402-403. A new method of dosage measurement in the megarad range.

K. Sommermeyer and H. Opitz, pp. 404-408. Beta dosimetry in shielding.

Mining Congress J. 45, No. 10 (1959)

R. Musgrove, pp. 48-50. Measurement and monitoring of radiation in uranium plants.

Nucl. Sci. and Engng. 6, No. 3 (1959)

N. Ketzlach, pp. 187-190. Study of safety conditions in storage of fuel elements in iron shipping containers.

Nukleonik 1, No. 8 (1959)

G. Hermann et al., pp. 305-314. Critical remarks on the discussion of the problem of radioactive contamination.

W. Kern, pp. 314- 319. Measurement of radioactivity of air using an electric filter.

A. Dannecker et al., pp. 319-324. Measurement of low-level alpha and beta radioactivity in water.

V. Radioactive and Stable Isotopes, Uses of Nuclear Radiation

Avtomobil. prom., No. 9 (1959)

D. I. Vysotskii et al., pp. 24-26. A laboratory on wheels for studying wear on automobile parts by means of radioactive isotopes.

Bumazhn. prom., No. 9 (1959) [Paper and Pulp Ind.]

A. A. Gusev, pp. 9-12. Determination of the amount of condensate in drying calandria of paper and pulp making machines, using radioactive tracers.

Vodosnabzhenie i san. tekhnika, No. 10 (1959) [Water Works and Sewage]

A. A. Gusev, pp. 37-38. Radioactive tracer for sanitation equipment.

Gaz. prom., No. 10 (1959)

D. Yu. Gamburg, pp. 17-20. Use of heat from nuclear reactors to produce synthesis gas and hydrogen.

Doklady akad. nauk SSSR 128, No. 4 (1959)

B. I. Bruk, pp. 709-712. Application of C^{14} isotope to determination the solubility of carbon in alpha-iron.

Izvestiya vyssh. ucheb. zaved. Pishchev. tekhnologiya, No. 4 (1959) [Food Technology]

N. V. Romenskii and A. D. Chmyr', pp. 29-31. Effect of Co^{60} gammas on fatty substances in corn during storage.

Izvestiya vyssh. ucheb. zaved. Pishchev. tekhnolog. legkoi prom., No. 4 (1959) [Light Industry]

V. N. Borodina et al., pp. 85-93. Effect of ionizing radiation on the structural and mechanical properties of polyvinyl chloride.

Izvestiya Sibir. otdel. akad. nauk SSSR, No. 3 (1959)

V. K. Mel'nikov, pp. 112-113. Radioactive phosphorus as a tracer in studying the physiological state of wood plants.

Pochvovedenie No. 10 (1959) [Soil Science]

M. V. Preobrazhenskaya, pp. 105-109. Results of using gammas to study the dynamics of soil moisture reserves in the Pakhta-Aral sovkhov.

Razvedka i okhrána nedr, No. 9 (1959)

E. M. Filippov and G. A. Kuznetsov, pp. 38,40. Determination of densities of rock and ore in outcroppings and mine workings, using the method of scattered gamma radiation.

Stroit. i dorozh. mashinostroenie, No. 10 (1959) [Highway and Civil Engng.-Machinery]

M. I. Smorodinov, pp. 28-29. Tracer studies of wear on stone cutting tools.

Trudy Arkt. i Antarkt. nauchno-issled. inst. 225 (1959).

N. N. Aleksandrov, pp. 113-122. Tracer applications in the determination of atmosphere turbulence.

Trudy Tsentr. nauchno-issled. inst. rechnogo flota, No. 41 (1959) [Proc. of River Transport. Res. Inst.]

D. G. Tochil'nikov, pp. 56-73. Calculation of radioactivation of specimens and parts in electrolytic steeling.

Khim. nauka i prom. 4, No. 4 (1959)

A. K. Lavrukhina, pp. 472-478. Radioactive isotopes in the earth's crust.

Elektrichestvo, No. 10 (1959)

N. G. Drozdov and V. N. Egorov, pp. 63-67. On the problem of neutralization of charges of static electricity, by radioactive radiations.

Atomwirtschaft 4, No. 10 (1959)

H. Götte, pp. 408-413. Uses of radioactive isotopes in industry, medicine, and agriculture.

E. Pohland and K. Frenzen, pp. 415-426. Uses of radioactive isotopes in West German industry.

L. Dolle, pp. 426-429. Study of radiations, and nuclear engineering.

K. Peter, pp. 439-443. Charged-particle accelerator for industry.

S. Jefferson, pp. 444-447. High-level radiation sources in industry.

D. Trageser, pp. 447-449. Techniques of electron-irradiation of wires and cabling.

J. Brit. Nucl. Energy Conf. 3, No. 4 (1959)

S. Burgess and A. Green, pp. 217-229. Uses of radioactive isotopes for the study of the performance of facilities used to process sewage water.

Nucl. Engng. 4, No. 42 (1959)

R. Roberts, pp. 408-409. High-level radiations sources for industry.

Nuova Technika, No. 10 (1959)

A. Krcma, pp. 509-511. Uses of atomic energy in the textile industry.

Research, Vol. 12, No. 10/11 (1959)

B. Giletti and R. Lambert, pp. 368-373. Uses of radioactive isotopes for determining age of geological and archeological processes.

F. Hurley, pp. 417-423. Industrial separation of uranium isotopes.

A MESSAGE FROM THE CENTRAL COMMITTEE OF THE COMMUNIST PARTY OF THE SOVIET UNION AND THE COUNCIL OF MINISTERS OF THE USSR

The Central Committee of the Communist Party of the Soviet Union and the Council of Ministers of the USSR announce, with profound sorrow, the sudden death on February 7, 1960, in the 58th year of his life, of the country's outstanding scientist and physicist, member of the Presidium of the Academy of Sciences of the USSR, director of the Atomic Energy Institute of the Academy of Sciences of the USSR, member of the Communitst Party of the Soviet Union, deputy to the Supreme Soviet of the USSR, three times decorated as Hero of Socialist Labor, Academician Igor' Vasil'evich Kurchatov.

CENTRAL COMMITTEE

CPSU

COUNCIL OF MINISTERS

USSR

ACADEMICIAN IGOR' VASIL'EVICH KURCHATOV

Academician Igor' Vasil'evich Kurchatov, leading Soviet scientist, Communist, thrice named as Hero of Socialist Labor, deputy to the Supreme Soviet of the USSR, member of the Presidium of the Academy of Sciences of the USSR, director of the Atomic Energy Institute of the Academy of Sciences of the USSR, died suddenly in the 58th year of his life, on February 7, 1960, in Moscow.

In his person, our country and the world scientific community have lost one of the most prominent scientists and physicists of our time, a man who was working on the solution of problems of wide scope in harnessing the inexhaustible reserves of energy within the atom, for the benefit of mankind.

I. V. Kurchatov was born on January 12, 1903, in the village Simskii Zavod of the Ufa district, in the household of a land surveyor. In 1923, he completed the physics and mathematics curriculum of the University of Crimea. He manifested exceptional interest in scientific work during those years. From 1925 on, he began work at the Leningrad Physics and Engineering Institute.

While still a young scientist, I. V. Kurchatov achieved remarkable successes in research on dielectrics, on which little research had been done up to that time. At that young age, he laid some of the foundations for the theory and initiated work on an encompassing experimental study of a new category of materials, the ferroelectric materials, which have since assumed great practical significance.

In subsequent years, I. V. Kurchatov became engaged in research on the physics of the atomic nucleus. In 1935, he discovered the extremely important phenomenon of nuclear isomerism.

In 1940, investigations leading to the remarkable discovery of spontaneous fission on the part of uranium nuclei were completed under the guidance and on the initiative of I. V. Kurchatov.

During the Great Patriotic War, I. V. Kurchatov placed all of his efforts and knowledge at the service of strengthening the defensive might of our Motherland.

For his outstanding scientific services, the Academy of Sciences of the USSR elected I. V. Kurchatov as an Acting Member of the Academy in 1943.

In his later work, all of his activities were related to problems involving the harnessing of atomic energy, and to the end of his life he unstintingly directed this work in the Soviet Union. Under his able scientific leadership and with his direct participation, atomic studies were begun in our country and raised to a new high in the investigation of the atomic nucleus, work was developed on controlled thermonuclear fusion, ways were explored for employing atomic energy in various branches of the national economy. I. V. Kurchatov educated countless cadres of scientists and engineers in this new field of nuclear science. Academician Kurchatov was not only a great scientist, but a most prominent activist in public affairs, a passionate fighter for peace. He was elected on more than one occasion to the post of deputy to the Supreme Soviet of the USSR. His contributions at the XX and XXI Congresses of the Communist Party of the Soviet Union and at the sessions of the Supreme Soviet of the USSR for the prohibition of nuclear weapons, for the use of atomic energy for peaceful purposes, for peace throughout the world were acknowledged by the Soviet people with great satisfaction.

Taking the floor at the January 15, 1960 session of the Supreme Soviet of the USSR, Igor' Vasil'evich stated: "I am happy that I was born in Russia and could devote my life to the atomic science developing in the great country of the Soviets. I profoundly believe and firmly know that our people, our government will devote the achievements in this science solely to the good of mankind."

The brilliant capabilities of the scientist, his enormous energy, his outstanding organizing ability, and his exceptional efficiency were happily combined in I. V. Kurchatov with rare spiritual qualities. He won the sincere respect and warm love of all those who were fortunate enough to have the opportunity to work alongside him and under his guidance.

Igor' Vasil'evich was a responsive and sensitive person, with a relationship of real concern and attentiveness toward his companions in work. I. V. Kurchatov's straightforward and buoyant personality, his unflagging and lively interest in his work inspired all those around him to creative work in the name of Soviet science and our Motherland.

For his outstanding services to the Motherland, I. V. Kurchatov was awarded on three occasions with the honors of Hero of Socialist Labor, the Lenin and Stalin prizes, and was decorated with five Orders of Lenin, two Orders of the Toiler of the Red Banner, and other medals.

The whole glorious life of this true son of the Communist Party, Academician Igor' Vasil'evich Kurchatov, serves as a shining example of selfless and unrestrained service to one's Motherland. Our people will cherish his memory forever.

Presidium of the Academy of Sciences of the USSR

Main Control Board on the Uses of Atomic Energy, attached to the Council of Ministers of the USSR

Division of Physical and Mathematical Sciences of the Academy of Sciences of the USSR
Division of Technical Sciences of the Academy of Sciences of the USSR
Atomic Energy Institute of the Academy of Sciences of the USSR
Leningrad Physics and Engineering Institute of the Academy of Sciences of the USSR

A MESSAGE FROM THE ACADEMY OF SCIENCES OF THE USSR

The Academy of Sciences of the USSR announces, with profound grief, the sudden death on February 7, 1960, in the 58th year of his life, of the three-time Hero of Socialist Labor, Academician IGOR' VASIL'EVICH KURCHATOV, the outstanding physicist and scientist, leading activist in public affairs, member of the Presidium of the Academy of Sciences of the USSR, deputy of the Supreme Soviet of the USSR, director of the Atomic Energy Institute of the Academy of Sciences of the USSR, recipient of the Lenin Prize, four-time recipient of the Stalin prize. The Academy takes this occasion to express its condolences to the family of the deceased.

THE MAIN CONTROL BOARD ON THE USES OF ATOMIC ENERGY, attached to the Council of Ministers of the USSR, expresses, in the name of all workers in atomic industry and scientific institutions, its profound grief motivated by the untimely end of the outstanding Soviet physicist, Academician IGOR' VASIL'EVICH KURCHATOV.

Igor' Vasil'evich Kurchatov was the scientific leader in charge of the building of atomic industry and nuclear engineering in our country.

The untimely demise of I. V. Kurchatov is a heavy loss for nuclear science.

We take this occasion to express our profound condolences to the family of the deceased.

Main Control Board on the Uses of Atomic Energy, attached to the Council of Ministers of the USSR

MIKHAIL MIKHAILOVICH KONSTANTINOV

Translated from Atomnaya Énergiya, Vol. 8, No. 2,
February, 1959

On January 19, 1960 Mikhail Mikhailovich Konstantinov, Candidate of Geological and Mineralogical Sciences, who served as an author, reviewer and scientific editor on the editorial board of the journal Atomnaya Énergiya and Atomizdat since their foundation, died after a long and serious illness.

Mikhail Mikhailovich Konstantinov was born at Irkutsk in 1907, his family being professional revolutionaries who had been imprisoned for their beliefs. In 1921 he joined the Komsomols and entered the Party in 1930.

In 1931 Mikhail Mikhailovich completed his studies at the Moscow Geological Prospecting Institute and was directed by the Central Committee of the Party to work in The Supreme Economic Council, USSR.

Mikhail Mikhailovich was one of the organizers of the rare-metal industry in the Soviet Union. He worked as the chief engineer of the Trust and as its director and chief geologist; he took part in prospecting operations for rare-metal ores in Yakutiya, Transbaikal, the Caucasus and the Far East. Many newly discovered deposits are associated with his name.

Mikhail Mikhailovich devoted the latter part of his life to scientific work. More than 40 scientific investigations were described in his writings, 16 of these appearing in print.

Mikhail Mikhailovich had a well deserved reputation in scientific circles. All his scientific colleagues sincerely mourn his early death.

SOVIET

research in

ANALYTICAL CHEMISTRY

OF URANIUM

A collection of ten papers from the Consultants Bureau translations of the Soviet Journal of Analytical Chemistry and the famous "Doklady" of the Academy of Sciences (1949-58)... This collection will acquaint the analytical chemist working in this field with Soviet techniques for the determination of uranium in solutions, in ores and the products of their treatments, and in accessory minerals, plus methods for the determination of impurities in uranium.

heavy paper covers illustrated $10.00

CONTENTS

c/b CONSULTANTS BUREAU
227 WEST 17TH STREET, NEW YORK 11, N. Y.

Declassified and Approved For Release 2013/02/19 : CIA-RDP10-02196R000100050002-7

Now available . . . an insight into the Soviet problems and achievements in . . .

PRODUCTION of ISOTOPES

The eighteen papers which comprise this volume were originally read at the All-Union Scientific and Technical Conference on the Application of Radioactive Isotopes, Moscow, 1957. The reports consider the problems and achievements of Soviet scientists in the production of radioactive isotopes by irradiation of targets in Soviet reactors and cyclotrons. Not only is this work of significance to producers of isotopes, but many of the papers will prove useful to isotope users as well.

The Development of Isotope Production in the USSR.
Certain Aspects of the Production of Radioactive Isotopes in a Nuclear Reactor.
Production of Radioactive Isotopes in a 10-Mev Deuteron Cyclotron.
Determination of Product Yields in Nuclear Reactions.
Spectrochemical Methods of Analyzing High-Purity Materials Used in Reactor Construction and for the Production of Radioisotopes.
Quantitative Spectral Determination of Impurities in Radioactive Preparations.
The Production of Alpha-, Beta-, and Gamma-Sources Using Oxide Films on Aluminum and Its Alloys.
Stable Isotopes Enriched by the Electromagnetic Method.
Ultrahigh-Temperature Ion Source for Electromagnetic Separation of Isotopes of Elements in the Platinum Group.
Inhomogeneous-Field Mass-Spectrometer for Analysis of Light-Element Isotopes.
The Relative Abundance of Palladium and Germanium Isotopes.
Some Problems in the Theory of Isotope Separation.
Separation of Isotopes of Light Elements by Diffusion in Vapors.
A Diffusion Column for the Separation of Isotopes.
A Fractionating Column for Preparing BF_3 Enriched in the Isotope B^{10}.
An Investigation of the Separation of the Stable Isotopes of Light Elements.
The Separation of Carbon Isotopes.
Low-Temperature Methods for Separating Helium Isotopes ($He^3 - He^4$).

1959 durable paper covers 136 pp. $50.00

CONSULTANTS BUREAU
227 WEST 17TH STREET, NEW YORK 11, N. Y.

Declassified and Approved For Release 2013/02/19 : CIA-RDP10-02196R000100050002-7